2019

Structural Determinants of High Potency MDPV Inhibition of the Dopamine Transporter

Tyler Steele

Structural Determinants of High Potency MDPV Inhibition of the Dopamine Transporter

A dissertation submitted in partial fulfillment of the requirements for the degree of Doctor of Philosophy in Neuroscience at Virginia Commonwealth University School of Medicine.

by

Tyler W.E. Steele
B.S. Biochemistry and Molecular Biology, University of Richmond, 2010

Director: José-Miguel Eltit, Ph.D., Assistant Professor
Department of Physiology and Biophysics

Virginia Commonwealth University
Richmond, Virginia
July, 2019

DEDICATION

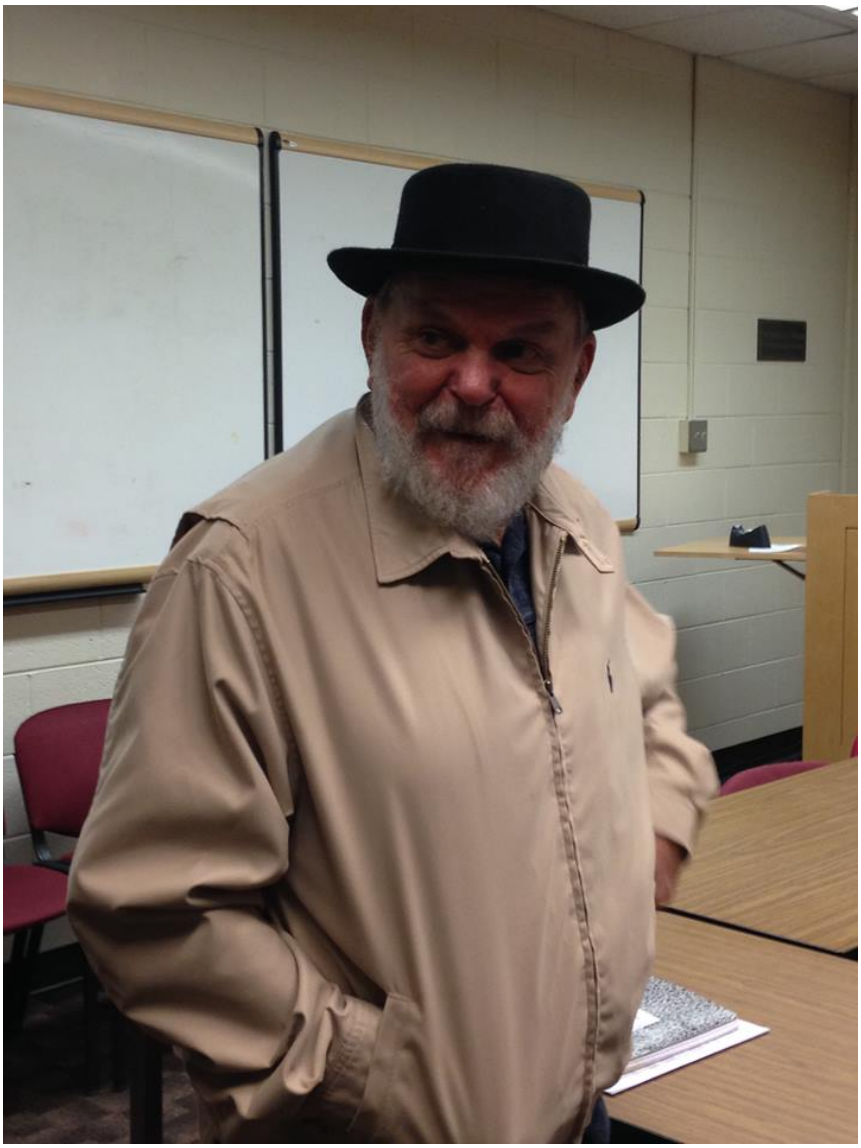

In loving memory, I dedicate this work to my friend and mentor Louis J. De Felice, Ph.D.

Across the horizons of time, forward and back, I look to the side, to the now, where you still guide me.

ACKNOWLEDGEMENTS

I would like to acknowledge all of the people that made this possible over the years through their help and support. Most prominently, I thank my scientific mentors. These include my father Dr. Michael Steele who introduced me to research as a teenager, Dr. Carol Parish who mentored me in research during my undergraduate days at the University of Richmond, Dr. Montserrat Samso who introduced me to new avenues of research as a post baccalaureate research tech, Dr. Louis De Felice who encouraged me to enroll at VCU and advised me for the majority of my graduate years, and finally, Dr. Jose Eltit, who took over for Lou after his passing and helped me get across the finish line. I have learned a great deal about science and research and taken so from each of these outstanding, though quite different and unique mentors. Furthermore, I thank my committee members (Dr. I Scott Ramsey, Dr. Diomedes Logothetis, Dr. Douglas Sweet, and Dr. Hamid Akbarali) for their guidance in the development of my project. Additionally, I thank De Felice Lab and Eltit Lab members past and present for their comradery, support and encouragement over the years.

I would also like to thank my parents, Mike and Margaret, and brother and sister, Mike Jr. and Emily, for all of their love and reinforcement throughout this process. Without their unending support, I would surely not have made it. Similarly, to all of the friends and family over the years who have shared a drink or a conversation, I thank you for your time. That list could occupy volumes. Finally, I thank my girlfriend and partner, Rebecca Gage, who brought me light in the darkest of my days.

Table of Contents

ABSTRACT

Monoamine transporters (MATs) are a unique group of neurotransmitter transporters that include the dopamine (DA), serotonin (5-HT), and norepinephrine (NE) transporters (DAT, SERT, and NET, respectively). At synapses in the brain, these proteins work to transport neurotransmitters back into cells after vesicular release. Because they play critical roles in regulating levels of neurotransmitters, MATs are a target for a number of licit and illicit compounds. Therapeutic agents for depressive conditions such as selective serotonin reuptake inhibitors (SSRIs) inhibit reuptake of 5-HT by hSERT and thereby augment 5-HT levels in the synapse. Alternatively, molecules such as amphetamine (AMPH) and cocaine augment dopamine at the terminals of dopaminergic neurons and are frequently used illicitly. The significance of this work lies in the fact that these transporters share affinity for certain ligands to varying degrees – they are promiscuous for monoamines – but the structural features within the transporters that govern the observed selectivity for these ligands has not been completely determined, despite the determination of a number of MAT crystal structures in recent years.

One such ligand is methylenedioxypyrovalerone (MDPV), which was frequently found in “bath salts” preparations that were available in convenience stores and were sold with labelling indicating that they were “not for human consumption” to circumvent drug laws. MDPV is a MAT blocker that is highly selective for human DAT (hDAT) and is orders of magnitude more potent there than at hSERT. SERT:DAT selectivity is one metric that correlates well with the abuse liability of psychostimulants, with higher affinity at DAT and lower affinity at SERT resulting in a higher associated abuse liability. MDPV

has accordingly been found to have a high abuse liability and is able to augment DA levels in the nucleus accumbens of rats for hours. In electrophysiological studies of *Xenopus laevis* oocytes expressing DAT, MDPV was observed to be highly "sticky", and remained bound to the transporter despite many minutes of washout, which corresponds with its long duration of action in rats.

In this work we use a comparative 2D and 3D structural approach to compare hDAT, hSERT, and the *Drosophila melanogaster* dopamine transporter (dDAT) in the S1 binding site to determine residues there that contribute to MDPV's high affinity binding at hDAT. dDAT is of particular interest for these purposes because along with hSERT, it has been crystalized with a number of ligands and co-transported ions. Additionally, dDAT displays a unique hybrid pharmacology wherein it prefers substrates that also have good affinity for hDAT, while it binds tightly to blockers of hSERT that have low potency at hDAT. After finding that MDPV is weak at dDAT, we deductively determined a short list of candidate mutations by identifying residues near or adjacent to the S1 site that were homologous between hSERT and dDAT but unique in hDAT. Initially we docked MDPV into crystal structures of dDAT and homology models of hDAT to determine possible molecular interactions between MDPV and the candidate mutations, or residues in close proximity to them. Multiple binding modes were determined for MDPV in the S1 site of both constructs, suggesting several roles that the target residues play in hDAT S1 recognition of MDPV.

We then made chimeric mutations in dDAT using site-directed mutagenesis. We hypothesized that the residues in the S1 site that are unique to hDAT but shared by

dDAT and hSERT play critical roles in the high affinity hDAT-MDPV interaction. To test our mutants, we employed a recently developed assay that exploits intracellular calcium as a reporter for MAT function. We expressed our mutant constructs in Flp-In TRex HEK-293 cells stably transfected with dDAT mutants and transiently expressing voltage-gated Ca^{2+} channels. Depolarizing currents associated with MAT transport cause Ca^{2+} channel opening, which in turn causes a rise in intracellular Ca^{2+}. Alone, each of the four candidate mutations we tested produced only marginal increases in MDPV potency at dDAT. However, combinations of the four showed marked increases in MDPV potency, with the quadruple combination displaying a ~100 fold increase in potency over wild-type dDAT, nearly matching the high potency seen in hDAT. Importantly, this chimeric dDAT construct maintained dDAT's typical affinity for dopamine. These results correspond with previous findings that suggest that the structural basis for MAT selectivity for transported substrates may lie outside the S1, while the actions at of inhibitors at MATs are dominated by the environment of the S1 site. Furthermore, when considered alongside the results from our docking studies, these findings suggest the possibility of multimodal inhibitor binding in the S1 site.

INTRODUCTION

1.1 Monoamine Transporters and Human Health

Monoamine transporters (MATs) play significant and essential roles in maintaining the homeostasis of biogenic amines in the central nervous system (CNS). Accordingly, their dysfunction and dysregulation are implicated in a number of disease states and they are the target for a number of therapeutic small molecules. Additionally, MATs are the target for compounds that are taken illicitly, which can lead to addiction. This section will highlight a few of the ways these proteins and the neurotransmitters they traffic are linked to human health.

Serotonin (5-HT) is implicated in the regulation of the behaviors of mood, emotion, sleep, appetite, aggression and sexual behavior.[1,2] Early investigations of tryptophan, a 5-HT precursor, implicated 5-HT as playing a role in depression, while errant serotonergic signaling has since been connected to number of other disease states including obsessive compulsive disorder (OCD), autism, and bipolar disorder.[3−5] The serotonin transporter (SERT) is a target for reuptake inhibitors that modulate levels of synaptic 5-HT, such as fluoxetine, a selective serotonin reuptake inhibitor (SSRI).[6] Genetic variations and polymorphisms of SERT that have been linked to diseases and have been found to result in altered SERT function. For example, the uncommon I425V polymorphism in SERT is linked to OCD, and was found to result in constitutively active SERT with increased transport.[7,8] This would presumably lead to decreased synaptic levels of 5-HT. Another example of a SERT polymorphism is in the promotor region of

the SERT gene, and results in reduced SERT expression and is linked to major depression.[9,10]

Dopamine (DA) is an important player in the processes of attention, motivation, working memory, reward and voluntary movement.[11] DA is known to play roles in addiction, Huntington's disease, depression, attention deficit hyperactivity-disorder (ADHD), and Parkinson's disease.[12,13] A hallmark of abused substances is the elevation of DA that they cause in the mesolimbic system.[14,15] The dopamine transporter (DAT) is a known target for a number of psychostimulant drugs which act at DAT to increase synaptic levels of DA, such as amphetamine and cocaine.[16,17] Genetic variations in DAT have been linked to ADHD and to patient response levels to ADHD medications such as methylphenidate.[18,19] Specifically, the A559V coding variant of DAT was found in two male children diagnosed with ADHD and was shown to evoke more DA efflux than wild type DAT.[20] Methylphenidate and amphetamine were found to block efflux in this transporter variant, in contrast to their actions in wild type DAT.

Norepinephrine (NE) is involved in sleep and mood regulation and alertness and arousal.[21] Multiple reports have identified elevated or altered plasma NE levels in affective disorders such as psychotic depression as well as post-traumatic stress disorder.[22−24] The norepinephrine transporter (NET), which is responsible for the reuptake of NE, is the target of reuptake inhibitors that block reuptake of NE. Despite multiple studies, though, there is little evidence that polymorphisms of NET are associated with psychiatric illness.[21] However, a polymorphism in exon 9 of the NET

gene is linked to orthostatic intolerance (OI). This results in an altered transporter (A457P) that has 98% decreased uptake activity.[25]

In summary, MATs play critical roles in human health by tuning synaptic monoamine neurotransmitter levels. Targeted therapies for the symptoms of certain disease states aim small molecules at MATs, while illicit molecules that also interact with MATs can lead to addiction. Additionally, genetic variants and dysfunctional expression of MATs can lead to certain diseases. But what exactly are these proteins? How do they function mechanistically, how do they interact with small molecules at the membrane, and what is their structure? The following sections will aim to answer these questions and introduce some of the techniques by which they are studied as they relate to the current research described here.

1.2 Monoamine Transporters

Monoamine transporters (MATs) belong to the solute carrier (SLC) gene family. The growing family of SLC transporters currently contains >400 secondary active transporters and facilitated transporters.[26] MATs specifically belong to the SLC6 gene family, which is itself contained within the amino-acid-polyamine-organocation (APC) superfamily. The SLC6 family is comprised of 20 sodium and chloride-dependent transporters that are neurotransmitter/sodium symporters (NSS). SLC6 transporters include the γ–aminobutyric acid (GABA), glycine, proline, and taurine transporters as well as the biogenic amine or monoamine transporters, the dopamine (DA), serotonin (5-HT), and norepinephrine (NE) transporters (DAT, SERT, and NET, respectively). MATs in humans are encoded by the SLC6A2 (hNET), SLC6A3 (hDAT), and SLC6A4 (hSERT) genes.[11] The hSERT gene is found on chromosome 17q11, and contains 13 exons spanning 24kb.[27] Chromosome 5p15.3 contains the 15 exon hDAT gene, which spans 65kb.[28] The 14 exon gene encoding hNET is localized to chromosome 16q12.2 and is around 45kb long.[29] Neither hDAT or hSERT were found to have splice variants, though hNET has three carboxy termini variants, of which only two are functional.[30]

At synapses in the central nervous system (CNS), these transporters work to move released neurotransmitters back into neurons after vesicular release (**Fig 1**). When an action potential causes vesicular fusion and release into the synaptic cleft, receptors on post synaptic cells bind the released neurotransmitter and propagate the signal. To cease this signal, monoamine transporters act like vacuums on the

presynaptic cell and work to traffic the released dopamine into the cell to be recycled as they are loaded back into vesicular stores.[11] Each MAT is the primary transporter for its cognate neurotransmitter, though it has been demonstrated that NET can transport DA in regions of the brain with low DAT expression.[31] DAT has been found in ventral tegmental area, and the substantia nigra; NET has been found in the found in the locus coeruleus; SERT has been found in raphe nuclei.[32]

It has been demonstrated that MATs play an essential role in regulating the homeostasis of the CNS. DAT for example was determined to be responsible for the reuptake of dopamine after release at dopaminergic synapses and is the target for abused compounds such as amphetamine (AMPH) and cocaine. Mice that have DAT knocked out (DAT-KO) were shown to display spontaneous hyperlocomotion and were insensitive to amphetamine or cocaine.[33] Furthermore, in striatal slices from DAT-KO mice, DA was found to persist for 300 times as long as in slices from wild-type mice.[34] Interestingly DAT-KO mice have lower overall levels of DA production, indicating that presynaptic DA homeostasis is regulated by DAT via recycling of DA.[35] As might be expected, investigations of SERT knockout mice (SERT-KO) were also performed. Similarly to DAT-KO mice, SERT-KO mice were found to have decreased levels of 5-HT overall, but increased extracellular levels of 5-HT.[36] While S(+)AMPH produced hyperlocomotion in these mice to similar levels as in wild-type mice, 3,4-methylenedioxymethamphetamine (MDMA), a well-known SERT dependent 5-HT releaser[37], did not produce enhancements in locomotor activity in SERT-KO mice, whereas it did in wild-type mice. Subsequent studies of SERT-KO mice found that these

mice displayed altered serotonin levels throughout their lives, increased anxiety, a depressive-like phenotype, and higher rates of serotonin syndrome behaviors upon administration of 5-HTP over SERT(+/+) mice.[38] Finally, NET knockout (NET-KO) mice were also found to have decreased tissue levels but increased extracellular levels of NE.[39] Interestingly, these mice showed increased locomotor sensitivity to the psychostimulants AMPH and cocaine, but behaved like wild type mice that had been treated with antidepressants that bind to net in “behavioral despair” tests.

In summary, the SLC6A(2-4), genes encode the monoamine transporters, NET, DAT and SERT. These proteins play pivotal roles in the maintenance of synaptic and presynaptic NE, DA, and 5-HT homeostasis. Their function in the CNS – to move released neurotransmitters back into presynaptic cells — serves two important roles: to terminate the signal propagated by these molecules as well as to recycle them for future use. How MATs function mechanistically to accomplish this is the subject of the next section

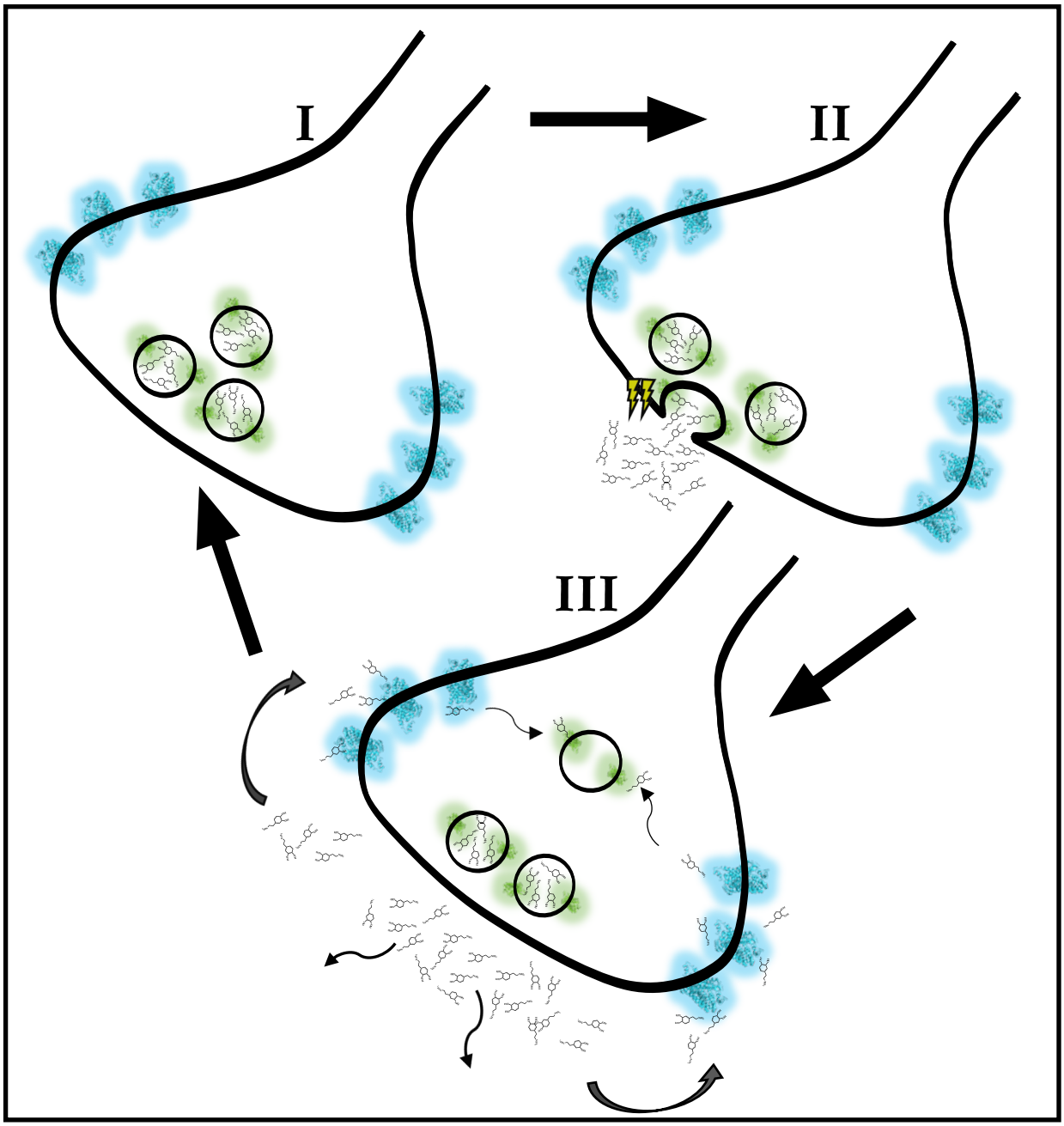

Fig 1. Monoamine Transporters Remove Neurotransmitters from the Synapse. As seen in this cartoon diagram for the dopamine transporter (blue), resting vesicular pools of neurotransmitters such as dopamine (**I**)**,** are released into the synapse when action potentials cause vesicular fusion (**II**). Some neurotransmitters will diffuse away or bind

to postsynaptic receptors (**III**— small arrows at bottom), while many will be transported back into the cell for recycling by the vesicular monoamine transporter (green).

1.3 Mechanisms of Monoamine Transporter Function

Monoamine transporters are thought to function by two primary mechanisms. While these mechanisms are typically described separately and in contrast to one another, they are not necessarily mutually exclusive. These mechanisms are the alternating access model and an ion channel-like mechanism of transport.

The alternating access model of membrane pump function was first put forth by Oleg Jardetsky in the 1960s.[40] While the "chemically activated pump" was the object of initial focus, he proposed other sources of pump activation, such as electrical or pressure mediated activation. As depicted in **Figure 2**, the transporters start in an outward-open conformation, and upon substrate and ion binding undergo a conformational change to an inward-facing conformation that allows the substrate access to the inside of the cell. In the last step, the transporter moves back to its initial, outward-facing conformation. In this model of transport, the neurotransmitter and its co-transported ions bind in a stoichiometrically-fixed fashion. For SERT, this stoichiometry was initially thought to be fixed at $1Na^+$, $1Cl^-$, and 1 5-HT^+ with intracellular $1K^+$ or H^+ accompanying SERT's return to the outward-open, initial state of the transport cycle.[41–44] This results in a non-electrogenic stoichiometric turnover of zero charges per transported 5-HT. The stoichiometries of the DAT and NET transport cycles were determined to be 2:1:1 and 1:1:1 respectively (Na^+:Cl^-:DA^+/NE^+), with no intracellular K^+ or H^+ involvement in the return of the transporter to the outward facing conformation.[44,45]

The transport cycles for DAT and NET were therefore initially thought to be electrogenic, in contrast with SERT's transport cycle.

These early studies of MATs primarily evaluated radiolabeled neurotransmitter uptake at a variety of ionic conditions to determine the ionic dependencies of uptake as well as turnover rate. Subsequent studies of MATs using alternative methods however, upended the notion that transporters function in a stoichiometrically-fixed alternating access mechanism. SERT, NET, and DAT, were all found generate currents that exceed what would be predicted from the alternating access model when expressed in *Xenopus laevis* oocytes and HEK-293 cells and studied using voltage-clamp techniques.[46−48] This led to the proposition that MATs may function more similarly to ion channels, wherein the downward flow of ions along their electrochemical gradients drive transport.[45,49,50] In the ion channel-like description of MAT function, the stoichiometry of ligands to ions is not fixed. Indeed, the ratio of MAT transport to MAT-generated current has been found to diverge under different conditions and gives rise to "uncoupled" or non-stoichiometrically fixed currents.[47,48,51−54] Unlike the alternating access model, a single file channel description of ion and neurotransmitter transport allows for "slippage" of the stoichiometric coupling of the ligand and co-transported ions.[15] It is also worth noting that these studies found that in human MATs, there is a constitutively active leak current that is present in the absence of activation by MAT substrates, and this current is blocked by MAT inhibitors that also inhibit transport. It was later found that the second Na^+ binding site is responsible for this leak current.[55] It is important to note that consequences one might imagine to follow from transporter induced currents that are

much larger than expected have also been observed. For example, DAT currents were found to depolarize *C. elegans* dopaminergic neurons.[56] Additionally, increases in excitability of rat midbrain neurons were found to arise from DAT conductances.[57] These findings led to the proposition that MATs may function akin to ionotropic receptors.[58,59]

Recently, kinetic models have attempted to rescue the alternating access model from an ion channel-like description of function.[60−62] Indeed, the currents predicted from these models do reproduce the currents that are found experimentally under a variety of conditions, and these models do not include any “pure” ion channel states. However, the assumptions underlying determinate transporter states with fixed stoichiometries have been challenged for MATs as well as glucose transporters.[63−65] The alternative mechanism offered is one in which a string of sites coordinates ligands and co-transported molecules along the transport coordinate across the membrane, similar to ion coordination sites in ion-channels. Furthermore, frictional interactions at a stricture or occluded central binding site in the transporters where all chemical species interact drive the observed transport stoichiometries, which can vary depending on experimental conditions.

Though the exact mechanism that governs the function of monoamine transporters eludes, MAT induced currents do indeed depolarize cell membranes in expression systems such as HEK-293 cells. This fact is the basis of the work described here, wherein the coupling of this depolarization to the activation of Ca^{2+} channels can be used as a reporter of MAT function and MAT interactions with small molecules.[66] A

more detailed description of the MAT/Ca^{2+} and other methods for investigating MAT-ligand interactions will follow in the next section.

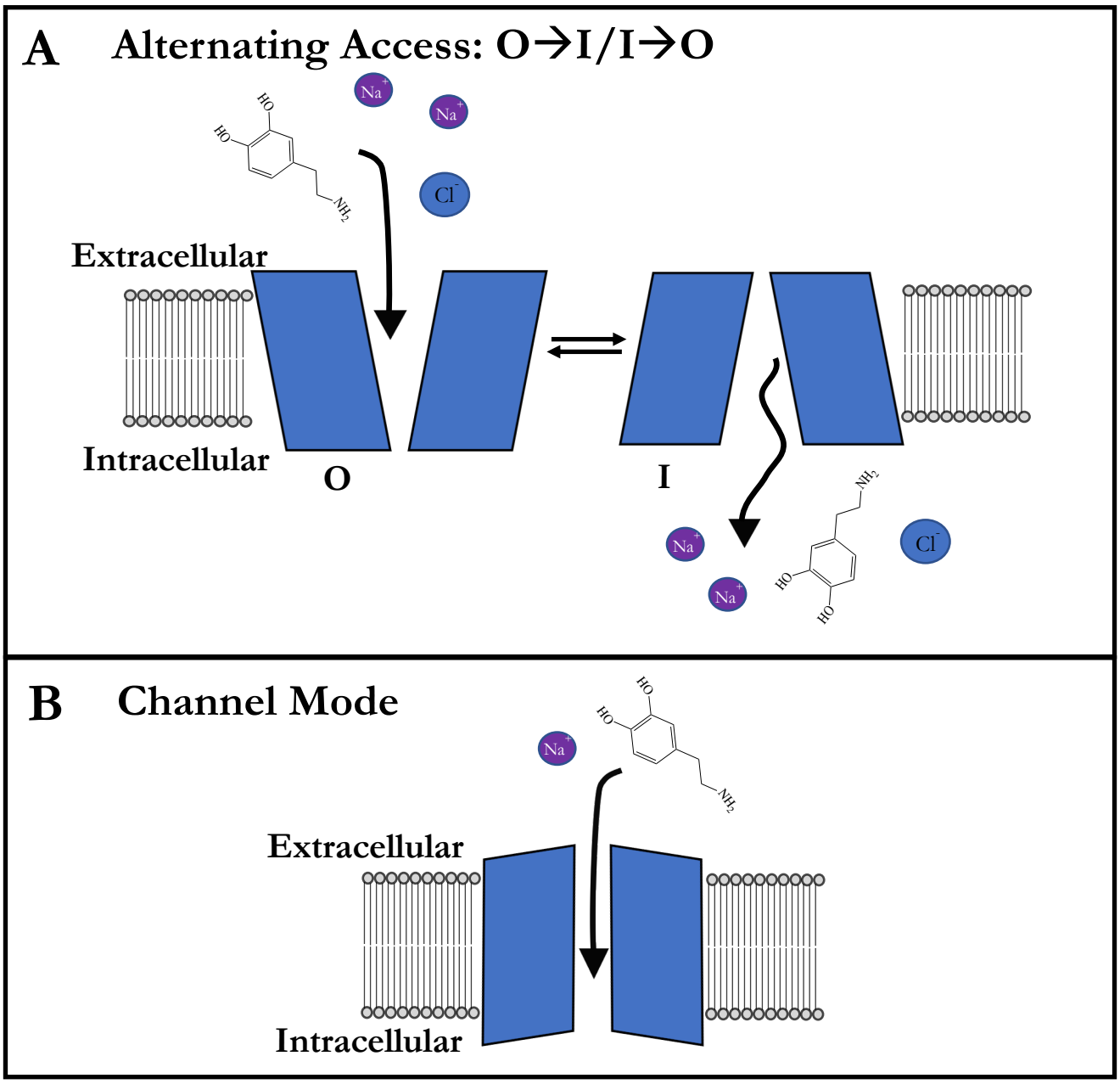

Figure 2. The Alternating Access and Ion Channel-like Modes of Monoamine Transporter Function. Basic representations of the A) Alternating Access B) Ion Channel like mechanisms of monoamine transporter function. In A), the transport cycle for the dopamine transporter is shown as an example. In B), only one Na^+ is depicted, though multiple may cross the membrane per dopamine transported.

1.4 Investigating Substrates and Blockers of Monoamine Transporters

Molecules that act at monoamine transporters can be broken down into two general categories: substrates (releasing agents) and blockers (reuptake inhibitors).[67] Substrates are molecules that are transported or trafficked into cells similarly to endogenous neurotransmitters. Once inside, these releasing agents disrupt vesicular stores of neurotransmitters and increase the cytosolic concentration, which in turn causes efflux of neurotransmitter via reverse transport at MATs.[37,68,69] While it is true that the presence of a competitive agonist or substrate will compete with endogenous neurotransmitters for uptake and could thereby increase synaptic levels of neurotransmitter, exogenous substrates are thought to increase neurotransmitters at the synapse primarily through reverse transport.[62] Conversely, blockers such as cocaine act as a stopper in a vacuum line and inhibit the ability of transporters to move substrates across the cell membrane.[70,71] Both of these types of ligands work to augment neurotransmitter levels at the synapse (**Figure 3**).

To investigate ligands that interact with MATs and probe their mode of action, researchers have employed a number of techniques. One of these involves the preparation of membranes from rat brains into synaptosomes, which can be used to evaluate both substrates and blockers of MATs. Synaptosome preps are particularly useful because they allow for the investigation of both uptake inhibition and substrate induced release or efflux, depending on how the synaptosomes are used.[72,73] For both “modes” of synaptosome investigation, synaptosomes are created using centrifugation

in sucrose gradients on homogenized brain tissue. For the study of ligand interactions with DAT, rat caudate is isolated and homogenized, whereas for ligand interactions with NET and SERT, whole rat brains with cerebellum and caudate removed are used. For the study of each MAT, selective blockers of each of the other two MATs are employed. This ensures that a ligand's ability to interfere with uptake or to provoke release at a given MAT is isolated to only the MAT of interest. For example, NET and SERT blockers would be used when testing AMPH's ability to inhibit DA uptake at DAT. For both uptake inhibition and substrate-induced release assays using synaptosomes, radiolabeled cognate neurotransmitters are used for each MAT. This was subsequently changed to [^{3}H]MPP$^+$ for NET and DAT studies because [^{3}H]MPP$^+$ gave a better signal-to-noise ratio than did either [^{3}H]NE or [^{3}H]DA.[74,75] In the synaptosome release assay, synaptosomes are pre-loaded with the radiolabeled ligand and exposed to the test compound for a period, washed and filtered. The amount of radiolabeled ligand released from the synaptosomes is then counted using a scintillation counter. Conversely, in the uptake inhibition mode, the ability of synaptosomes to uptake the radioligand is competed with a test compound, and after wash and filtration, retained radioligand is counted in a beta counter. In the uptake assay, both reuptake inhibitors (blockers) and releasing agents (substrates) will inhibit uptake of the of the radioligand. In the synaptosome release mode, only substrates that can be taken up by the MAT of interest will induce appreciable efflux. An interesting result from studies using synaptosomes was the identification of "partial releasers", certain compounds are not fully efficacious in causing release.[76] It is speculated that these compounds bind to

transporters but do not completely generate conformational changes in MATs that are necessary for reverse transport.

Synaptosome assays have been immensely helpful in understanding the interactions between MATs and the ligands that bind to and modulate them. Another useful technique used in understanding drug interactions with MATs is to inject *Xenopus llaevis* oocytes with cRNA for a given transporter and use the machinery of the oocyte to express the transporter on the cell surface. When these oocytes are electrically clamped using two-electrode voltage clamp (TEVC) the effect of substrates and blockers can be clearly ascertained.[53,77] One notable limitation of this approach is that human NET (hNET) does not express at the plasma membrane of frog oocytes.[78] However, for human DAT and SERT (hDAT and hSERT) this technique provides valuable information about the currents induced by ligands that bind to MATs. As mentioned earlier in Section 1.3, MATs display an endogenous and constitutively activate leak current that is blocked by reuptake inhibitors. Additionally, substrates illicit inward currents. These facts make both substrates and inhibitors readily identifiable by the type of electrophysiological trace that they produce.[79] As one might expect, MATs can also be expressed stably in human cells (e.g. HEK-293 cells) and studied using patch clamp.[47,60] While electrophysiological approaches offer unparalleled kinetic information about MAT function, it is possible though difficult to assess dose-response relationships of MAT ligands because of the low-throughput nature of these techniques. However, as compared with the synaptosome-based uptake and release assays, it is

much less laborious to identify compounds as either a substrate or a blocker with electrophysiological approaches.

In recent years, a new approach has been developed that uses intracellular Ca^{2+} as a reporter for MAT function. In this approach, HEK-293 cells stably expressing a MAT of interest are transiently transfected with voltage-gated Ca^{2+} channel subunits. Substrate induced membrane depolarizations activate these channels causing an intracellular rise in Ca^{2+} which can be monitored using fluorescent calcium dyes.[80] Initially the coupling between MAT activity and Ca^{2+} channel activation was observed in skeletal muscle cells that were engineered to express hSERT.[81] This activation was present only in cells expressing hSERT that also expressed $Ca_V1.1$, the voltage sensing component of excitation-contraction coupling in these cells. Furthermore, it was shown that HEK-293 stably expressing hSERT and exposed to MDMA or 5-HT were able to produce intracellular Ca^{2+} signals when transiently expressing the L-type Ca^{2+} channel $Ca_V1.3$ but not the N-type $Ca_V2.2$. This seminal work provided evidence that MATs may activate Ca^{2+} channels in excitable cells, where they are known to modulate excitability and Ca^{2+} levels. In a subsequent study, it was demonstrated that hDAT mediated depolarizations could activate $Ca_V1.2$ and $Ca_V1.3$ in HEK-293 cells stably expressing hDAT and transiently expressing Ca^{2+} channels.[66] In this work, it was unequivocally demonstrated that this assay could be used to determine dose-response relationships for MAT activation by substrates such as AMPH and DA in agreement with previous work. Ca^{2+} signals in response to DA and AMPH were not observed in cells that lacked hDAT, or that had been exposed to isradipine, a known Ca^{2+} channel blocker.

Furthermore, DA induced signals were blockable with the potent hDAT inhibitor MDPV. Other studies have further demonstrated that this approach is a new and powerful method for studying MAT activation and inhibition by small molecules.[78,82,83] While MAT blockers produce no directly observable effect in these engineered systems, they can be tested for their ability to diminish Ca^{2+} channel activation by a known substrate. Interestingly, while the determined potency values for compounds in the Ca^{2+} assay do not match the nominal values determined by the synaptosome-based approach for uptake and release, there is a strong correlation between values determined for multiple ligands by both methods (**Figure 4**).[80] The MAT/Ca^{2+} channel assay does not measure release via substrates, but is less labor intensive than synaptosome preparations for uptake and release assays. Compared to direct electrophysiological techniques, the MAT/Ca^{2+} channel assay is much higher throughput, but given the coupling to channels, is not ideal for studying MAT kinetics. (A more thorough review detailing the development and use of the MAT/Ca^{2+} can be found in reference 80.)

In summary, a number of methods are used to investigate how ligands interact at MATs. These approaches aim to determine molecules' potency and efficacy in eliciting and blocking currents, competing for uptake, and causing release via reverse transport. In essence, these experiments endeavor to answer whether ligands that have affinity at MATs are substrates (releasers) or blockers (uptake inhibitors), and how well they accomplish these roles. A new and novel approach, The MAT/Ca^{2+} assay, has been developed which has a number of advantages over older methods, but gives information that correlates well with results determined by those more established

techniques. This technique is the primary method in the work presented in this manuscript, which aims in part to extend the applicability of the MAT/Ca^{2+} assay to answer more detailed questions about MAT-ligand interactions. The next section will focus more specifically on a group of compounds that act on MATs and their place in the phenomenon of emerging “new psychoactive substances.”

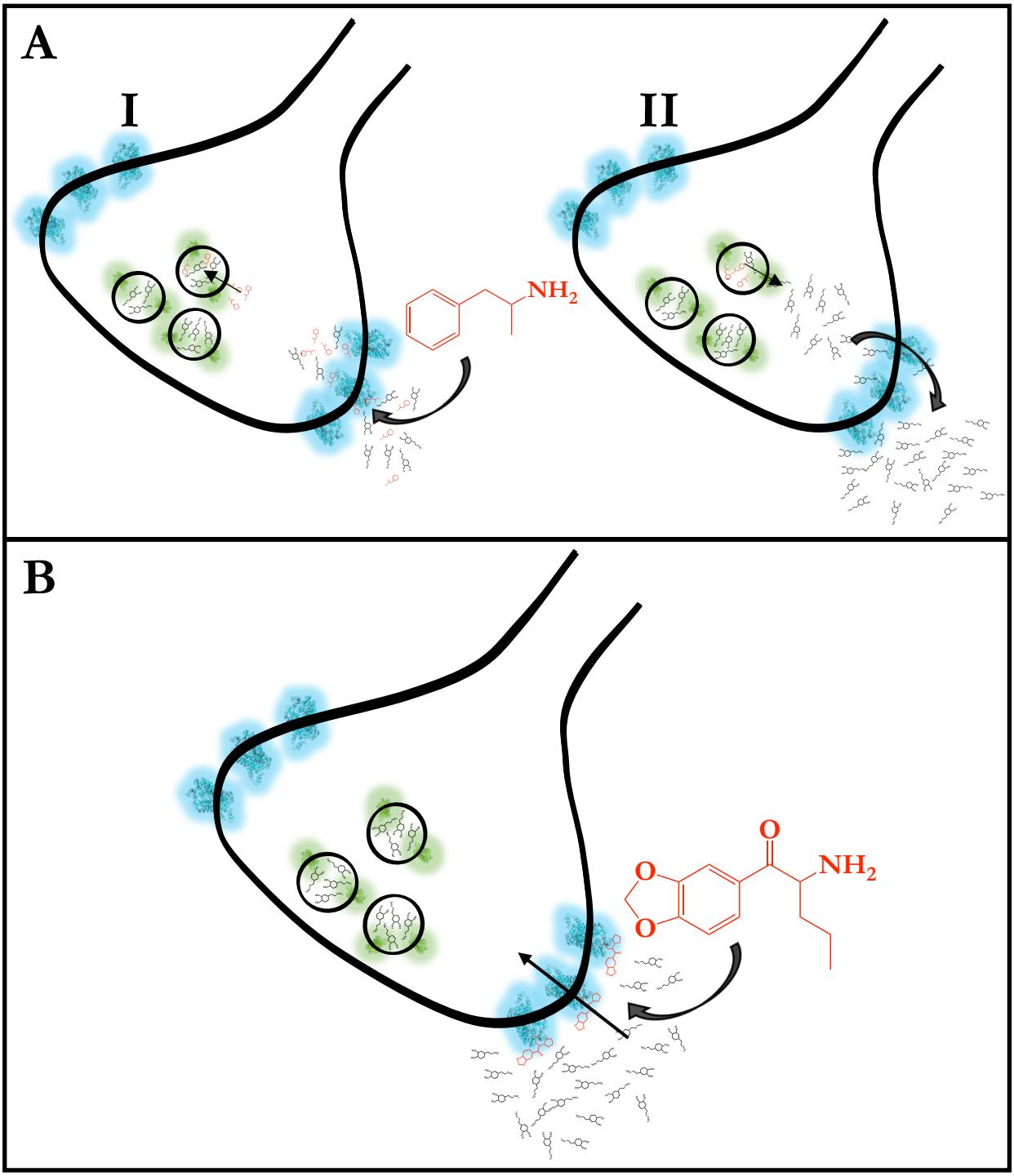

Figure 3. Substrates and Blockers Have Distinct Modes of Action. A) Substrates such as amphetamine (red) are transported into axonal termini via MATs (blue) where they can compete with endogenous neurotransmitters for uptake (I). Once inside the

cell they are transported into vesicles by vesicular transporters (green) where they disrupt vesicular stores. This disruption results in vesicular depletion of neurotransmitters whose concentration rises in the cytosol (II). This induces the reverse transport mode, and neurotransmitters are transported outside the cell. B) Blockers or reuptake inhibitors such as MDPV (red) work by inhibiting uptake at MATs (blue) and monoamine transporters are unable to reuptake neurotransmitters.

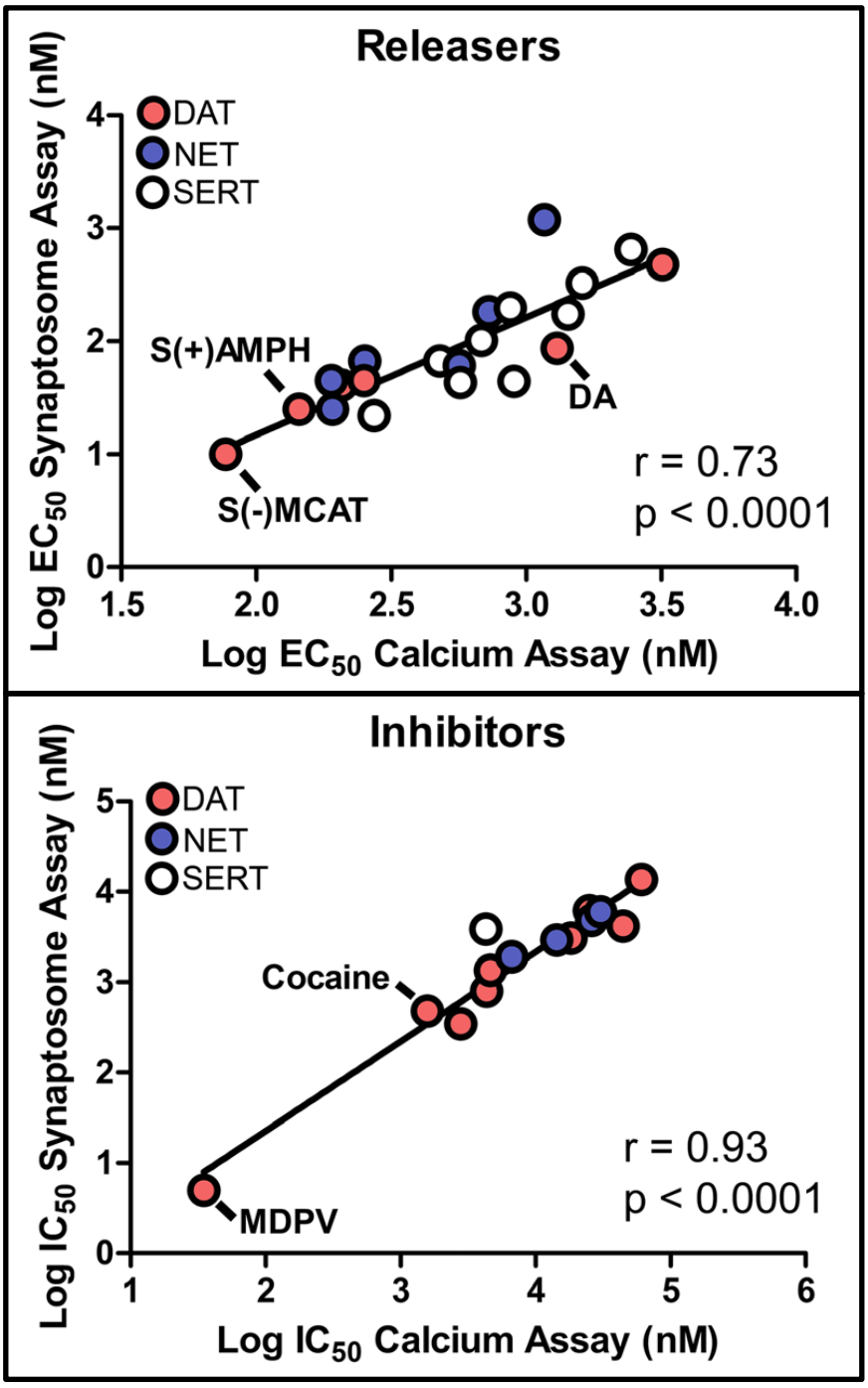

Figure 4. The Monoamine Transporter/Ca^{2+} Assay Correlates with Established Synaptosome Release and Uptake Assays. Linear correlations for a number of compounds between release EC_{50} or uptake inhibition IC_{50} values from synaptosomes and EC_{50} values for eliciting or IC_{50} values for inhibiting MAT induced Ca^{2+} signals.

Compounds were tested at NET, DAT, or SERT (blue, red, and white). Adapted from Steele and Eltit 2018.[80]

1.5 "Bath Salts" Are New Psychoactive Substances That Contain Synthetic Cathinones

For centuries and perhaps longer, humans have consumed molecules related to phenethylamine (PEA) that are found in plants for their psychostimulant effects. In the East, shrubs in the genus *Ephedra* and in the Horn of Africa and Middle East *khat* trees (*Catha edulis)* contain ephedrine and cathinone, respectively.[84] Their leaves are commonly ingested by mastication or imbibed in teas. These molecules belong to a broad and loosely-defined class of psychostimulants known as "amphetamines" and contain an α-methyl modification to the PEA core.[62] Amphetamine (AMPH), the quintessential member of this group, and a number of other prominent analogues are pictured in **Figure 5**. AMPH is taken both licitly as a therapeutic agent (Adderall) and illicitly by recreational users and drug abusers. N-methyl substituted AMPH, methamphetamine (METH) is prescribed legally as well (Desoxyn), but is principally known to the public as a drug of abuse.[85] Contrary to popular belief, METH does not differ from AMPH in its potency or abuse liability, and has similar pharmacokinetic and pharmacodynamic properties to AMPH.[86] Despite the fallacious nature of this widely maintained notion, some differences between the effects of AMPH and METH have been reported.[87-89] These molecules are canonical dopamine transporter (DAT) substrates, and are thought to work by promoting reverse transport of dopamine (DA) at DAT, as described in Section 1.4.

A large number of AMPH analogues exist and monoamine transporters (MATs) vary in their selectivity for amphetamine analogues depending on the position and identity of molecular substitutions on the basic AMPH scaffold. Cathinones, a specific subgroup within the broad amphetamine class, differ from classical amphetamines by the addition of a ketone at the *β*-carbon of AMPH (**Figure 5**). Synthetic cathinones are of particular interest because of their unique role in the ongoing worldwide emergence of "new psychoactive substances" (NPS). NPS are compounds which are produced clandestinely and designed in such a way as to skirt the law.[90] Analogues to molecules that have already been legally scheduled but produce similar effects can thereby be distributed without the risk of repercussions that that can result from trafficking in scheduled substances. These compounds can be easily sold as "research chemicals" on the internet, for example, which an information highway that fast tracks the exchange of information between clandestine chemists, and grants them access to a wide variety of medical and chemical literature that can direct their syntheses. While NPS can be developed to produce effects similar to a variety of classes of abused substances, the majority produced in recent years are related to synthetic cathinones and synthetic cannabinoids.[91] These substances entail a particularly difficult public health problem as the effects of these analogues and the preparations that they are distributed in can be cause an array of negative health effects including death.[92] Additionally, some are metabolized differently than the compound they are designed to mimic and are therefore not detected by conventional toxicology screens. The phenomenon of NPS is not "new", nor are all the compounds deemed NPS necessarily unknown to humans

before they are found forensically in illicit preparations. In the 1990s, Alexander Shulgin and his wife Ann authored two books, *PiHKAL* and *TiHKAL*, in which they described their synthesis and experiences with myriad psychedelic substituted phenethylamines and tryptamines.[93,94] Among others, this spurned interest in the 2C class of ring-substituted phenethylamines, which it should be noted are not considered amphetamines due to their lack of a substitution on the *α*-carbon.[85] Indeed, resurgent 2Cs are identified as NPS today if they are not scheduled.[95] Similarly, 3,4-methylenedioxymethamphetamine (MDMA), known colloquially as "ecstasy", was synthesized and known to humankind for decades before it emerged as a party drug and was scheduled in the 1980s.[96] Today, it's potential as a therapeutic agent for certain psychiatric disorders is limited by the strict regulations that preclude it's study. It seems that NPS are part of a continual and ongoing tug-of-war between state interests that seek to formally schedule abused compounds and clandestine chemists and distributors that seek to profit by strategically circumventing the law. But how do synthetic cathinones fit into this milieu and why are they of scientific interest?

As part of the NPS phenomenon, preparations of compounds that mimic the effects of amphetamines and cocaine started emerging in gas stations and head shops in the late 2000s and early 2010s. Sold as "bath salts", marketed as "legal highs", and labeled as "not for human consumption", these products rapidly became available in the US and Europe and were found to contain synthetic cathinones.[92,97] The three most prevalent bath salts compounds found in these preparations were reported as methylenedioxymethcathinone (MDMC) or methylone, methylenedioxypyrovalerone

(MDPV) and 4-methylmethcathinone (MEPH) or mephedrone (**Figure 5**).[98,99] These compounds were all previously synthesized licitly by researchers, but unknown to be widely abused agents. Along with related molecules, these cathinones could be found alone or in combination in a single formulation. As described above, the NPS phenomenon is a veritable political and public health Lernaean Hydra; however, the scientific study of these compounds and their actions have yielded fascinating insights. For example, MDPV and mephedrone were determined to have opposite effects at DAT expressed in *Xenopus* oocytes and studied by two-electrode voltage clamp: mephedrone is a substrate and MDPV is a potent blocker.[77] Furthermore, the rapid substrate action of mephedrone, a releasing agent, followed by the slower kinetics of MDPV inhibition imply a synergistic effect at DAT; DA release by mephedrone would be followed and augmented by blockade of DAT by MDPV.[79] These effects would occur to varying degrees, depending on the identity of compounds found in specific bath salts formulations. These studies also determined that MDPV is a potent inhibitor of DAT, with a ~30 fold higher potency over the canonical DAT blocker cocaine in uptake studies of DAT expressing HEK-293 cells. These findings were replicated soon thereafter in synaptosome uptake studies, but MDPV was found to be ~50 times more potent than cocaine in that assay.[100] Interestingly, this study also showed that MDPV is highly selective for DAT over SERT, with a >800 fold stronger IC_{50} for uptake inhibition in synaptosomes, with considerable potency at NET as well.

While the three primary bath salts have been scheduled (2011), analogues have predictably turned up in street preparations. Ideally, research efforts would evaluate

these compounds individually for abuse liability, pharmacokinetic properties, and the chronic effects of abuse.[93] Given the whack-a-mole nature of NPS cycles, however, alternative strategies that study how the molecular substitutions to synthetic cathinones contribute to their actions at MATs may be preferential. As a first step, they can direct researchers to important compounds that merit further study. Structure activity relationship (SAR) and quantitative SAR (QSAR) studies aim to determine what molecular moieties are important for a given effect and how the moiety physically accomplishes this effect.[101] One SAR study of synthetic cathinones investigated the "deconstruction" of MDPV by systematically removing each substitution that MDPV contains on its amphetamine scaffold.[102] The compounds resulting from each modification were tested separately for their ability to inhibit radiolabeled DA uptake by HEK-293 cells as well as for their effects on DA induced electrophysiological signals in DAT expressing *Xenopus* oocytes using two-electrode voltage clamp. It was determined that the methylenedioxy ring contributed minimally to MDPV's potency, indicating that α-pyrrolidinovalerophenone (*α*-PVP, or "flakka"), should behave similarly to MDPV in other studies. The removal of the carbonyl caused a considerable drop in potency, while shortening the alkyl side chain or reducing the tertiary amine of the pyrrolidine ring to a primary amine caused precipitous drops in potency (**Figure 6**). The authors noted that many of these analogues were already beginning to be found in street preparations, underscoring the value of SAR studies in understanding emerging bath salt type NPS. Subsequently, synaptosome uptake studies recapitulated some of these findings.[103] Later, a QSAR study of α-PVP analogues using rat synaptosomes found strong

correlations between the potency to inhibit DAT uptake and the volume of the *α*-substituent and overall lipophilicity of the molecules.[104]

These studies show how SAR and QSAR approaches have elucidated the molecular determinants of the potency of synthetic cathinone DAT inhibitors, but later studies also revealed fascinating insights into synthetic cathinone actions at SERT as well. For example, it was found that 4-para substituted methcathinone analogues have differential selectivity for DAT and SERT (**Figure 6**).[105] Specifically, the potency for producing release at DAT or SERT in synaptosomes was tested and correlated with steric bulk at the 4-para position. It was determined that compounds with bulkier substituents were better releasers at SERT, while methcathinones with smaller substituents at this position preferred DAT. Mephedrone, the 4-para-methcathinone analogue found in bath salts, was determined to be only slightly more selective for DAT than for SERT. Another SAR study found that the methylone analogues butylone and pentylone, which are closely related to MDMA, also differentially affect SERT and DAT (**Figure 6**).[106] In synaptosome uptake assays, butylone and pentylone are potent inhibitors of DAT, but inhibit uptake at SERT weakly. Recall that both substrates and inhibitors can inhibit uptake at MATs, but only substrates produce appreciable release from synaptosomes. When synaptosomes were prepared in the “release mode,” pentylone and butylone were found to be releasers at SERT, but not at DAT. Additionally, in hSERT expressing HEK-293 cells under voltage clamp, both compounds produced inward currents, but they did not in HEK-239 cells expressing DAT. Therefore, these compounds were found to be substrates/releasers at SERT and blockers/uptake

inhibitors at DAT. An interesting caveat was that only partial release by pentylone at SERT was observed. Also, at DAT, pentylone was more potent than butylone, which fits with the conclusions of studies of MDPV and α-PVP analogues wherein the volume of the *α*-substituent was found to be positively correlated with the potency of a compound to inhibit uptake.[102,104] Another recently published study demonstrated the differential action on DAT and SERT of a series of N-alkyl substituted 4-methylamphetamine (4-MA).[78] All of the compounds are SERT substrates, while the majority are DAT blockers. Another fascinating finding was that increasing the length of the 4-MA substituent from a methyl to an ethyl switched the compound from a substrate to a blocker at DAT. This also fits with the study of MDPV deconstruction, wherein removing the pyrrolidine ring greatly decreased potency.[104]

In conclusion, psychostimulant class NPS are part of the storied history of illicit drug development across the globe. As clandestine chemists churn out these molecules, medical and scientific researchers hastily endeavor to understand their action, assess the risk that they pose, and evaluate their potential as therapeutic agents. Meanwhile, governments seek to schedule them, a process that can paradoxically hinder researchers' efforts.[107] Psychostimulant class NPS such as bath salts typically contain synthetic cathinones, which are themselves a subclass of amphetamines. Among them, MDPV, the subject of the new work described here, is a potent and highly selective DAT inhibitor that contains certain moieties contributing to its high potency. SAR studies have identified molecular substituents important in MAT recognition of and affinity for synthetic cathinones, while QSAR studies have revealed

the physical reasons why these molecular substituents contribute to their determined actions. A common thread runs through these studies: monoamine transporters are promiscuous proteins that share affinity for a number of compounds. However, in certain cases, MATs get selfish and prefer to keep certain molecules to themselves. Beyond the particularly salient question of how this happens in terms of protein-drug interactions, there is an important consequence that results from this evolutionary reality. Namely, the ability of monoaminergic drugs such as synthetic cathinones to differentially affect SERT versus DAT serves as a good predictor of their abuse liability. Accordingly, determining the SERT:DAT selectivity of psychostimulant class NPS is a central pillar in the broad program of NPS investigations. The next section will explore why a compound's SERT:DAT selectivity is thought to drive its abuse liability and summarize recent work that aims to differentiate compounds along this activity axis.

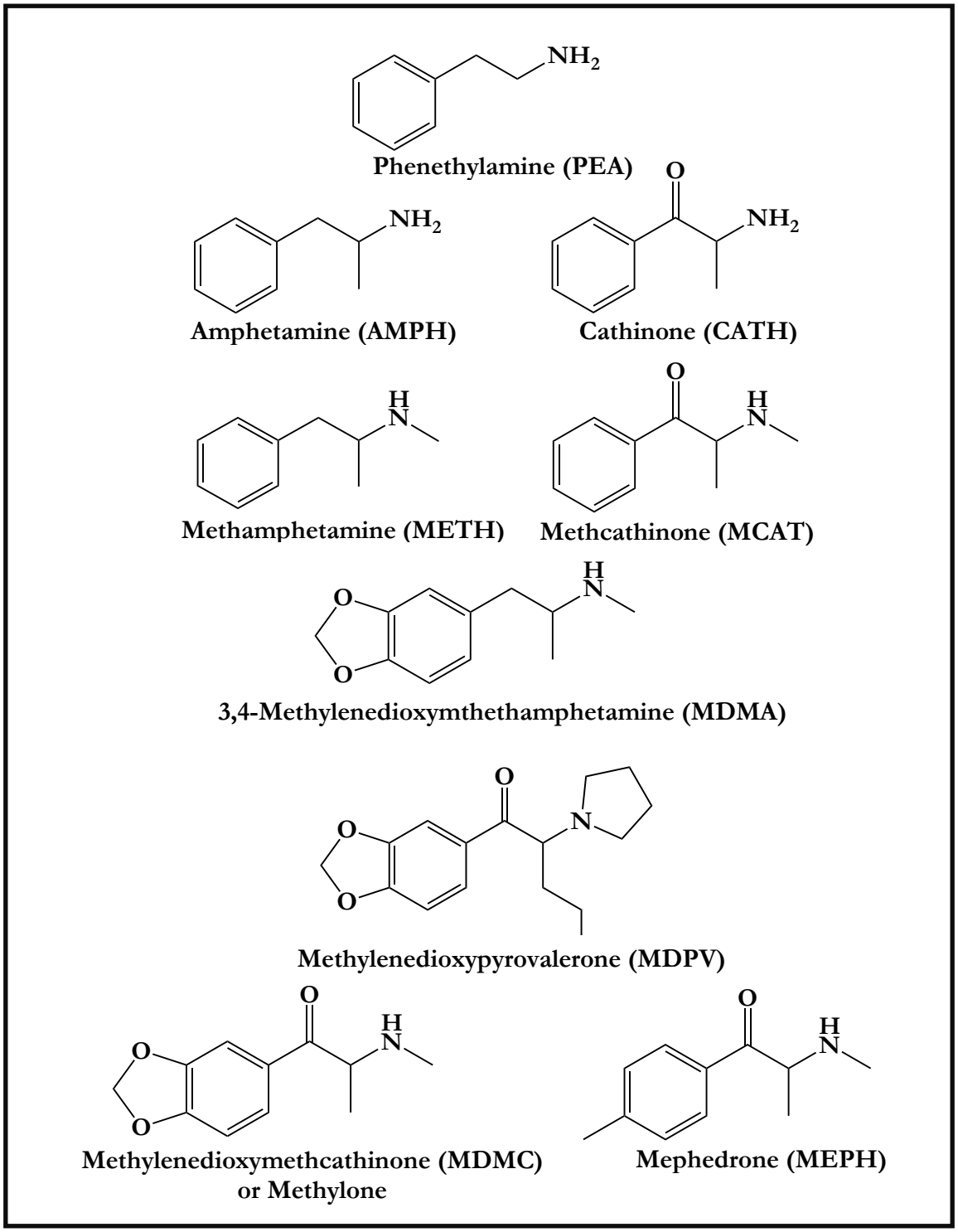

Figure 5. Phenethylamines: Amphetamine and Its Analogues. The PEA scaffold is the molecular foundation of amphetamine and its analogues. AMPH and METH are depicted beside their cathinone counterparts CATH and MCAT, which contain a

characteristic *β*-ketone. The nonselective monoamine transporter substrate MDMA can be seen in the middle. The three most prominent bath salts components, methylone, MEPH, and MDPV are depicted at the bottom.

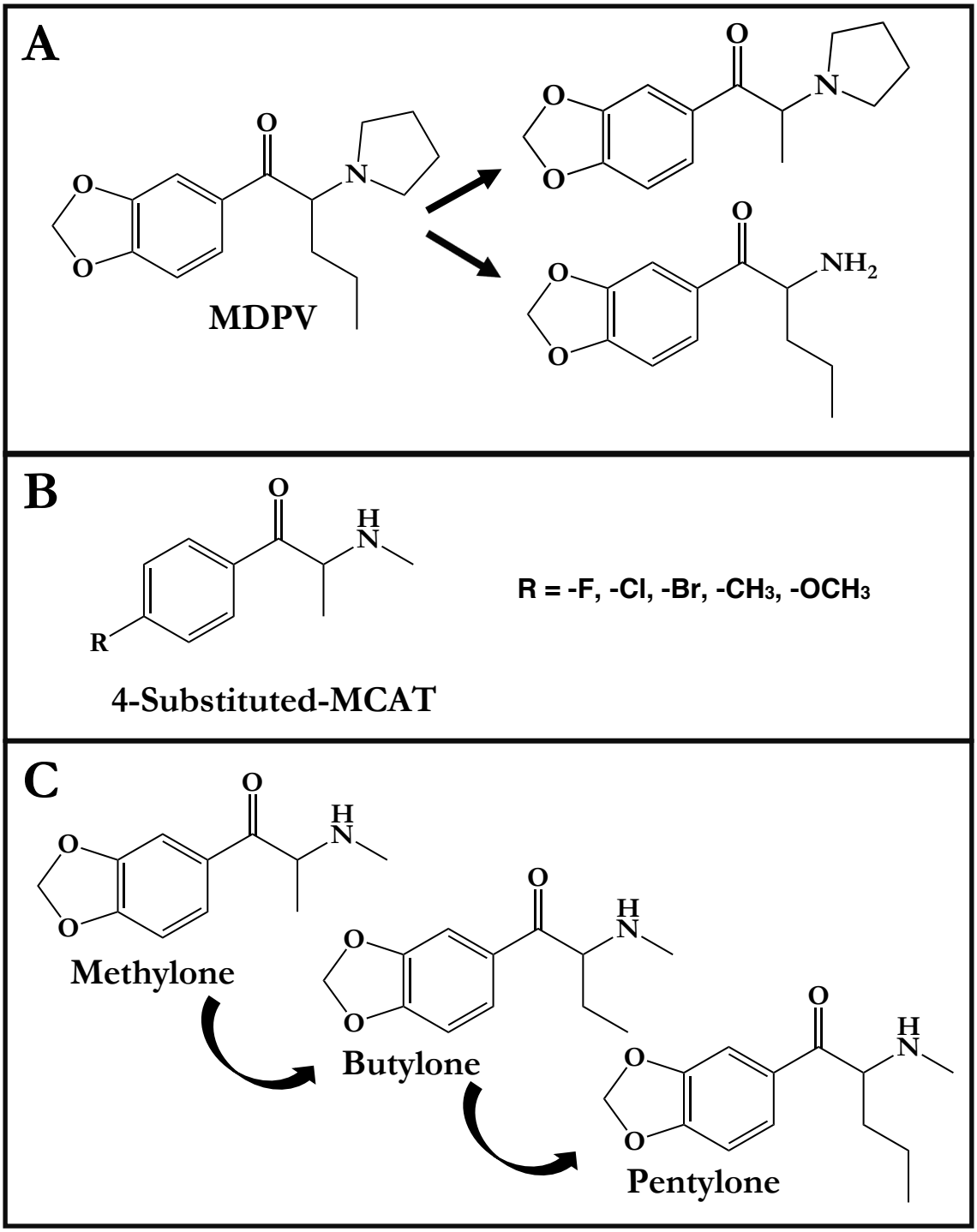

Figure 6. SAR and QSAR of Synthetic Cathinones. Panel A) MDPV was deconstructed into multiple analogues, two of which are depicted at the right.[102] These two analogues resulted in precipitous losses of potency for uptake inhibition at DAT. Panel B) A series of MCAT derivatives with increasing steric volume at the 4-para

position were tested at DAT and SERT.[105] As steric bulk was increased, the molecules became more SERT selective. Panel C) Extension of the α-alkyl chain of methylone yields butylone and pentylone, both of which are substrates at SERT but blockers at DAT.[106]

1.6 Abuse Liability of Monoamine Transporter Substrates and Blockers

Drug addiction is the loss of control over drug intake despite negative outcomes and results from changes to normal functioning of certain brain regions.[108] Dopaminergic neurotransmission from the ventral tegmental area (VTA) in the midbrain to the nucleus accumbens (NAc) in the ventral striatum constitutes the primary reward pathway of the brain and is associated with positive reinforcement. This pathway is called the mesolimbic pathway and is centrally involved in the development of addiction. Raphe nuclei in the brain stem contain serotoninergic neurons that also project to the NAc. Drugs that act on serotonin and dopamine transporters (SERT and DAT), are therefore thought to modulate the activity of these brain regions, as SERT and DAT are expressed on the neurons that comprise them. In the 1950s, James Olds and Peter Milner discovered that electrodes implanted into the brains of rats in the medial forebrain bundle produced positively reinforcing, or rewarding effects.[16,109] This region contains the aforementioned reward centers. Furthermore, by attaching the electrodes to levers that could be controlled by the rats they could assess rats' drive to self-stimulate this region electrically and intracranial self-stimulation (ICSS) was born.

Since its development, ICSS has been instrumental in determining the abuse liability of addictive compounds.[110] In a modern experimental set up, rats are trained to lever press across a variety of stimulation frequencies. Lower frequencies of electrical stimulation maintain lower rates of lever pressing, while higher rates of electrical

stimulation maintain higher pressing rates.[111] Certain compounds facilitate ICSS at low frequencies of stimulation, that is they increase the rate of lever pressing at these lower frequencies. Conversely, certain compounds decrease or depress rates of responses at the higher end of stimulation frequencies. Compounds of the former category are said to have abuse liability, while those in the latter are said to be abuse limiting. The use of ICSS in assessing the abuse liability or abuse limiting effects of compounds is well established and corresponds with other methods animal models of drug addiction.

ICSS has been used to assess the abuse liability of compounds that work at the monoamine transporters SERT and DAT. In a recent study in rats, it was shown that DAT selective compounds produce facilitation at low frequencies, in keeping with previous findings that DAT selective drugs have high abuse liability.[112] Furthermore, SERT selective compounds, such as the 5-HT releaser fenfluramine, depress rates of response at high frequencies of stimulation. Interestingly, co-administration of fenfluramine with the DAT selective releaser 3-fluroamphetamine nullified the facilitation observed for administration of 3-fluroamphetamine alone. In addition, the nonselective releaser 3,4-methylenedioxymethamphetamine (MDMA) produced both facilitation of response rates at low frequencies and depression of response rates at high frequencies of stimulation.[112] SERT:DAT selectivity, determined as the ratio of the potencies of a given compound to produce release at DAT and SERT in synaptosomes, was positively correlated with maximal facilitation in ICSS. Furthermore, maximal facilitation in ICSS was positively correlated with the self-administration of these compounds by rhesus monkeys, which is thought to be a good predictor of abuse liability in humans.[112] Taken

collectively, these findings show that not only do DAT selective compounds result in ICSS facilitation and SERT selective compounds result in ICSS depression, but also that the rate depressing effects of SERT selective compounds can overcome the facilitation caused by DAT selective compounds. The strong correlations observed between ICSS facilitation in rats and both *in vitro* SERT:DAT selectivity and self-administration by rhesus monkeys imply a correspondence continuum: *in vitro* SERT:DAT selectivity is a decent predictor of abuse liability in humans.

Subsequent studies have reproduced the correlations between *in vitro* findings of SERT:DAT selectivity and ICSS. For example, one study investigated 4-para substituted methcathinone analogues and found that bulkier substitutions at this position tipped the balance of SERT:DAT selectivity to the SERT side of the selectivity seesaw *in vitro*, as described in the previous section.[105] This same study investigated the ability of these compounds to facilitate ICSS and found that again, SERT selective compounds did not produce facilitation but depressed response rates, while the compounds with smaller 4-substitients were better facilitators of ICSS and better DAT substrates *in vitro*. An interesting follow up study was also conducted on these compounds *in vivo* using microdialysis to measure their ability to augment neurotransmitter (DA and 5-HT) levels in the rat nucleus accumbens.[113] The *in vitro* SERT:DAT selectivity, changes to baseline ICSS, and volume of the 4-para substituent as determined in the former study were all significantly correlated to the *in vivo* SERT:DAT selectivity measured by microdialysis. This study adds an *in vivo* predictive metric of abuse liability for these compounds that does not involve behavior. Another study using ICSS to assess the ability of bath salts

components to facilitate response rates found that MDPV is not only a potent facilitator of ICSS, but it also has a long duration of action, with facilitating effects observed 24 hours after its administration.[114] This seems congruent with the finding that MDPV is recalcitrant to buffer wash out in electrophysiological studies of DAT, as opposed to the short-acting DAT blocker cocaine.[79] A recently published investigation of the effects of racemic N-alkyl substituted 4-methylamphetamine analogues at MATs found that these compounds were substrates at SERT *in vitro*, and accordingly produced rate limiting effects on rat ICSS responses.[78] A follow up study investigated the stereoselectivity of MATs for these compounds again comparing *in vitro* results in both the synaptosome and MAT/Ca^{2+} assays to changes in baseline ICSS in rats and found similar results.[82]

These studies provide substantial support for the idea that SERT:DAT selectivity is a determining factor in the associated abuse liability of compounds that act at MATs. ICSS in rats is one behavioral method wherein the abuse liability of compounds can be assessed *in vivo*. ICSS is a good predictor of the abuse liability in monkeys, and by extension, humans. As discussed in the previous section, synthetic cathinones found in bath salts contain structural tweaks that determine their differential affinity for MATs; these substitutions therefore govern the degree of their associated abuse liability. In this and the previous section, some of the SAR and QSAR of related synthetic cathinones have been highlighted. MDPV is a long acting, potent, and selective DAT reuptake inhibitor found in bath salts, which accordingly produces long-lasting ICSS facilitation. Structural changes to MDPV have revealed the essential substitutions to its amphetamine scaffold that contribute to its potency at DAT. But what drives the

seemingly picky nature of monoamine transporters for high affinity ligands from the structural perspective of the transporters themselves? Why, for example, do SERT and DAT hem and haw for MDMA, while DAT pines for the structurally related MDPV and SERT shuns it? These are difficult questions to answer, and a detailed structural understanding of MAT-ligand interactions is a vigorous area of interest for researchers. However, these efforts have been aided tremendously by structural studies of MATs that have provided fundamental insights. Through X-ray crystallography and mutagenesis, the structure-function relationship of monoamine transporters is coming into clearer view. The next section will briefly describe these studies and their findings, with particular emphasis on the *Drosophila melanogaster* dopamine transporter, dDAT, and its involvement in a watershed decade of MAT structural insights.

1.7 Structure of Monoamine Transporters

In 2005, the crystal structure of LeuT, the leucine transporter from *Aquifex aeolicus* leucine was first reported.[115] This bacterial orthologue of SLC6A transporters offered the first snapshot of SLC6A structure, but is not highly homologous to these transporters. For example, LeuT shares ~25% overall sequence homology with the human dopamine transporter (hDAT), though in the transmembrane (TM) domains the homology is somewhat higher (~50%).[116] This initial structure confirmed previously predicted structural features of these transporters. For example, when the norepinephrine transporter (NET) was initially cloned, it was predicted to have a 12 or 13 transmembrane domain topology with intracellular amino and carboxy termini.[117] The serotonin transporter (SERT) was suspected to have a similar topology from site directed chemical labelling studies.[118] Subsequent LeuT structures shed light on the mechanism of tricyclic antidepressant blockade of transporter uptake.[119,120] In these structures, the tricyclic antidepressants clomipramine and desipramine were both found to bind to an extracellular facing vestibule in LeuT. These molecules act as non-competitive inhibitors of LeuT as the canonical binding site sits lower and toward the intracellular face of the transporter. In another study, the competitive inhibitor tryptophan was found in the canonical site of LeuT.[121] These structural studies also elucidated the location of the Na^+ binding sites positioned along TM helices 1, 6, and 8. Though these initial LeuT structures offered new insight into SLC6A structure, LeuT differs from SLC6A transporters in a number of ways. For example, LeuT has no observed chloride

dependence for substrate uptake whereas SLC6A transporters do; accordingly, no chloride binding site was revealed by these reports.[116] Additionally, no uncoupled current mode could be deduced from these structures. Interestingly, while the tricyclic antidepressant, non-competitive inhibitors of LeuT were shown to bind to a vestibule above the canonical substrate binding site, it was shown that in LeuT based SERT and DAT homology models that the competitive inhibitors citalopram and cocaine bind in the canonical binding site.[122,123] Therefore LeuT structures offered essential insights, but due to its low degree of homology, left some structural questions unanswered.

A further improvement in the understanding of SLC6A structure came when the *Drosophila melanogaster* dopamine transporter (dDAT) was crystalized in 2013. This report found the tricyclic competitive inhibitor nortriptyline bound in the canonical central binding site, with the transporter in an "outward-open" conformation.[124] Around the same time, a study of LeuBAT, a chimera of LeuT with some residues mutated to SLC6A residues in the central binding site, found that competitive inhibitors also bound in the central site.[125] This central site is known as the S1 site and this initial dDAT structure firmly established the importance of this structural feature in inhibitor binding (**Figure 7**). Additionally, this structure included a chloride bound near the two Na^+ sites. However, the construct used in this crystallographic study was a non-functional mutant with no measurable uptake activity. The protein had five point mutations to thermo-stabilize the construct, as well as a sizeable deletion in the EL2 loop and N and C-terminal truncations.

An improvement came in 2015, when a new dDAT construct was crystalized along with a range of molecules including dopamine (DA), 3,4-dichlorophenethylamine (DCP), cocaine (COC), amphetamine (AMPH), and methamphetamine (METH).[126] These structures revealed a number of important insights and differences. In the DCP bound structure, for example, Phe319 was found be moved over the central binding site in an occluded state of the transporter. This occluded state had previously been seen in LeuT structures bound to substrates.[115,119] However, this was in contrast to the binding modes for dopamine as well as the previously published nortriptyline bound structure in which Phe319 is moved away from the S1 site in an outward-open conformation of the transporter.[124,126] Additionally, amphetamine and methamphetamine bound in slightly shifted positions relative to one another, but similar to DA, both bound to the S1 site in an outward-open conformation. Finally, the tropane-based inhibitor cocaine bound in an outward-open conformation, as was previously seen with nortriptyline, with Phe319 shifted away from the S1 site. Interestingly, however, Phe325 which sits toward the intracellular side of the S1 was slightly shifted in the nortriptyline-bound structure to accommodate the 3 ringed anchor of the tricyclic molecule.[124,126] The authors surmise that their substrate-bound structures, along with the previous LeuT-substrate crystals, capture the proteins at different stages of the conformational cycle that proceeds from the outward-open to the occluded state. The inhibitor bound structures all have the protein in an outward-open conformation, with Phe319 moved away from the S1 site. This is thought to be a hallmark of inhibitor action, in which inhibitors as a wedge in the S1 and prohibit conformational rearrangement to the occluded state.[126] Taken together,

these structures point to the flexible nature of the 6a-6b helices which rearrange to accommodate a variety of ligands that act as both substrates and inhibitors. Phe319, which sits on helix 6a and Phe325, which sits on helix 6b, are both highly conserved residues in monoamine transporters, and are focal points in this conformational rearrangement.[126] These two phenylanilines are illustrated in **Figure 8**.

Recently, human SERT (hSERT) crystal structures were reported with a number of inhibitors in the outward-open conformation of the transporter.[127] In addition to binding to the central S1 site, citalopram was also found to bind in an allosteric site that sits above the S1 site in the extracellular vestibule above the extracellular gate of the transporter. In these structures, Phe335, which is equivalent to Phe319 in dDAT is moved out and away from the S1 as in the dDAT inhibitor bound, outward-open structures. Additionally, Phe441, which is equivalent to Phe325 in dDAT is seen coordinating the hydrophobic side chains of citalopram and paroxetine. Along with Ile172, Phe341 form a hydrophobic face along the side of the S1 site. Previously both residues had been shown to be important for strong interactions between hSERT and inhibitors by uptake studies in which these residues were mutated.[128,129] The hSERT crystal structures were recapitulated earlier this year by cryo-electron microscopy (cryo-EM).[130] This study investigated the structures of hSERT bound to ibogaine in outward-open, occluded, and inward-open conformations. Phe335 moved progressively into the S1 site as the transporter-ibogaine complex went from outward-open, to occluded, and finally to inward-open states, blocking ibogaine's exit from the central pocket.

Some limitations apply to the crystal structure studies, such as the fact that truncations and thermostabilizing mutations were made, and antibodies were used to form crystals.[124,126,127] Similarly, in the cryo-EM structures, the best determined resolutions were around 4.1 Å, and some docking and molecular dynamics simulations were used to verify ibogaine binding poses.[130] Despite these caveats, however, these results taken together point to the important nature of Phe319 and Phe 325 in dDAT (hSERT equivalents: Phe335 and Phe341) in molecular rearrangements in the transport cycle (dDAT:319/hSERT:335) and in coordinating inhibitors in the S1 via hydrophobic interactions (dDAT:325/hSERT:341). These snapshots of proteins in complex provide unparalleled information about interactions with small molecule binding partners. To date, however no crystals or cryo-EM structures exist for human DAT (hDAT) either alone or in complex with small molecules.

It is also important to note that while dDAT was crystalized with molecules traditionally associated with modulating hDAT function, the report originally detailing the cloning and pharmacological profiling of dDAT indicated that dDAT is somewhat of a "hybrid" transporter.[131] dDAT seemingly prefers inhibitors that also inhibit hSERT with high potency, such as tricyclic antidepressants. These molecules have weak inhibitory effects at hDAT. Additionally, the hDAT selective inhibitor buproprion has low potency at both hSERT and dDAT. One notable exception to this trend is that citalopram is highly SERT selective, and is not potent at either hDAT and dDAT in inhibiting uptake.[131] Conversely, substrate type molecules, such as AMPH and DA are well tolerated by dDAT, while hSERT has little affinity for them. This raises the possibility that while

conserved residues that have been observed interacting directly with small ligands in the S1 site in dDAT and hSERT crystal structures are important for overall recognition of these molecules, they do not govern how transporters preferentially select for these molecules.

As discussed previously, 3,4-methylenedioxypyrovalerone (MDPV) is a highly selective hDAT inhibitor that has little affinity for hSERT (See Introduction sections 1.5 & 1.6). No structures for hDAT have been reported, but based on the dDAT and hSERT structures, it would seem that potent DAT inhibitors would also bind in the S1 site. The work presented here aimed to determine the structural elements that make hDAT selective for MDPV, with an emphasis on the S1 site. The following section will detail the hypothesis and specific aims of this study.

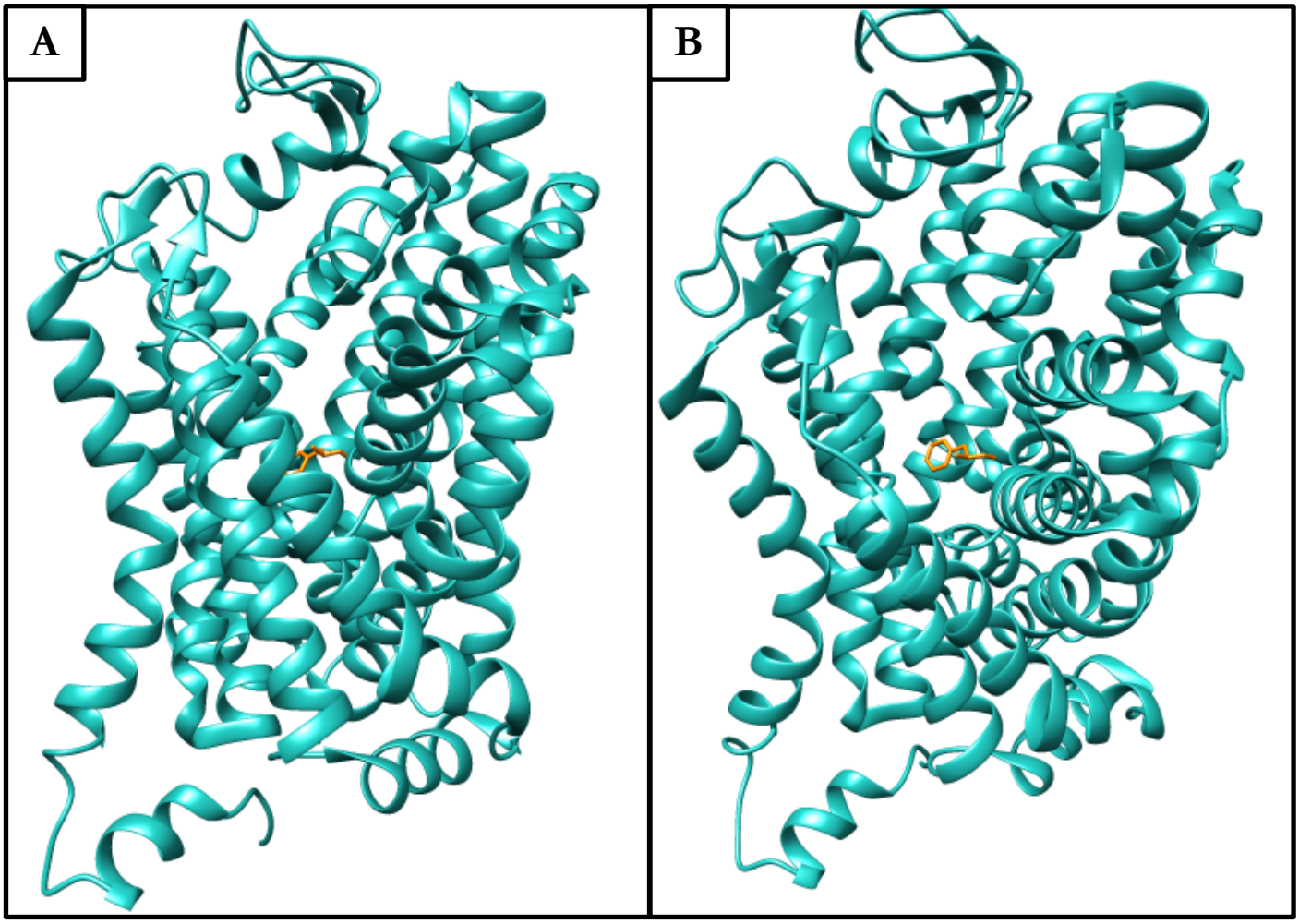

Figure 7. General Structure of dDAT with Methamphetamine Bound to the S1 Site. Panel A) The dDAT crystal structure is shown in blue (pdb:4XP6) with methamphetamine bound at the S1 site (colored orange). The S1 site is in the center of the dDAT, which is comprised of 12 transmembrane helices. Panel B) Same as Panel A but slightly tilted toward the viewer about the x axis to reveal the extracellular vestibule that sits above the S1 site.

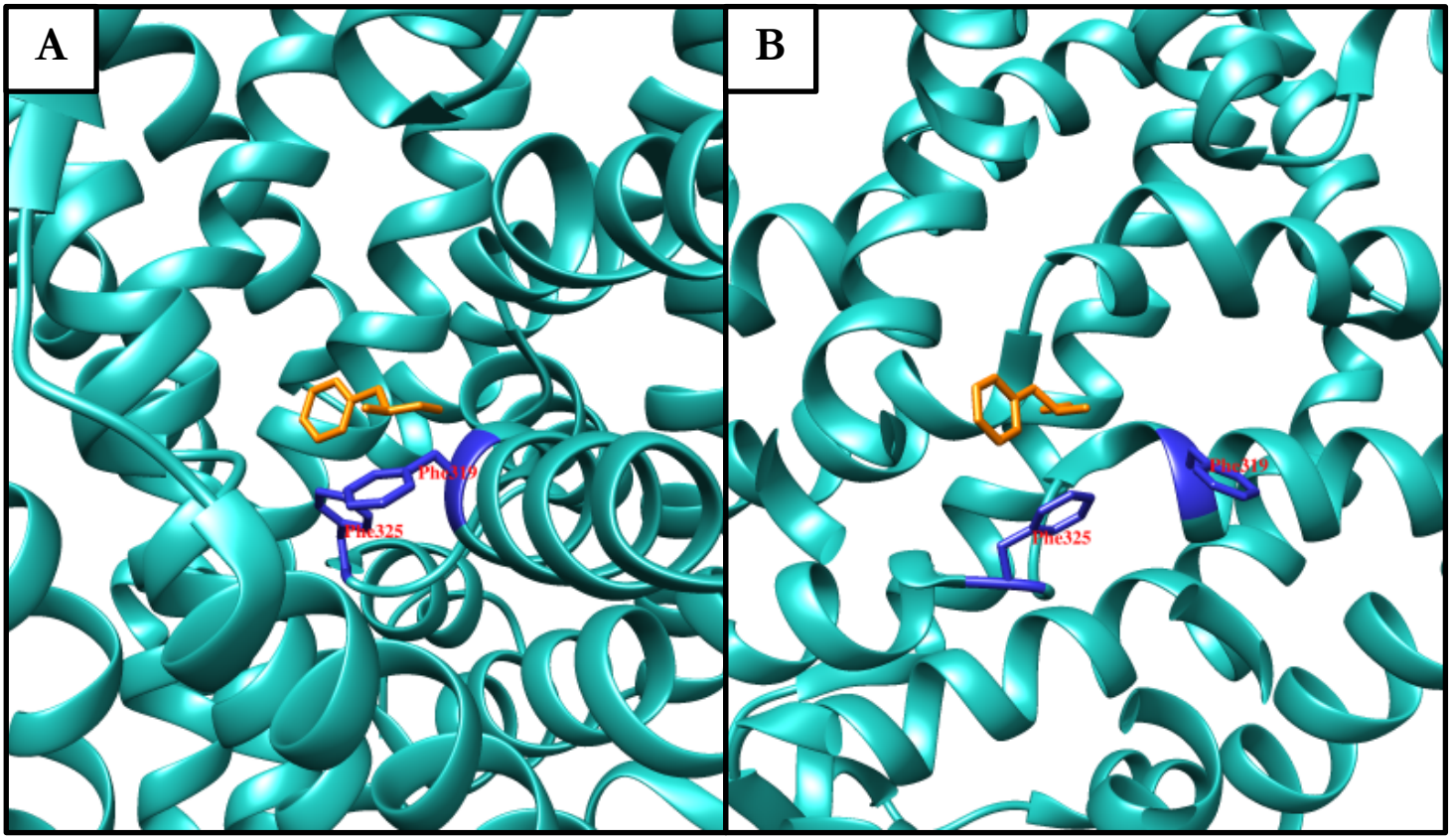

Figure 8. Crystal Structure of dDAT with Conserved Phenylalanines. Panel **A)** The crystal structure of dDAT (blue) with methamphetamine (orange) bound to the S1 site (pdb:4XP6) in an outward-open conformation. Conserved Phe319 and Phe325 are shown in dark blue (labelled in red). These correspond to Phe335 and Phe341 in hSERT. Panel **B)** Same as A, but rotated y=90˚ to demonstrate how in the outward-open state of the transporter, Phe319 is moved away from the S1. In the occluded state, which was typical of substrate bound LeuT structures, the corresponding phenylalanine moves toward the relative position of methamphetamine.

1.8 Central Hypothesis & Specific Aims

This work seeks to identify specific structural features that contribute to 3,4-methylenedioxypyrovalerone's (MDPV) high potency inhibition of the human dopamine transporter (hDAT). As described in Introduction sections 1.5-1.7, MDPV is selective for hDAT and is a low potency inhibitor of the human serotonin transporter (hSERT). Structural studies described in section 1.7 reveal the transporters to have a central binding pocket, the S1 site, with conserved residues that coordinate co-crystalized small molecules. Also described in section 1.7 was the fact that *Drosophila* DAT (dDAT) has a hybrid pharmacological behavior between hDAT and hSERT; it prefers substrates of hDAT, but high potency inhibitors of hSERT that are weak at hDAT are also strong at dDAT. The **Central Hypothesis** of this study is that MDPV binds to the S1 site in monoamine transporters (MATs) and that specific, non-conserved residues there govern MDPV's high affinity interaction with hDAT. The **General Approach** taken to test this hypothesis was to determine residues in hDAT's S1 that may contribute to MDPV binding, introduce them into dDAT's S1 site via mutagenesis, and test MDPV's ability to block DA induced calcium signals in a new calcium/MAT assay. The General Approach was broken into a number of **Specific Aims**. In **Specific Aim I**, we sought to determine if MDPV is a low potency inhibitor of dDAT as would be predicted from previously published pharmacological data. **Specific Aim II** was broken into Aim II A and Aim II B. In **Specific Aim II A** we sought to use a novel deductive approach for determining which residues to mutate in dDAT's S1 site based on 2D alignments of

hDAT, hSERT, and dDAT, as well as 3D structural comparisons between dDAT and hSERT crystals and an hDAT homology model. In **Specific Aim II B** we docked S-MDPV into the S1 site of one of the dDAT crystal structures as well as the hDAT homology model to determine potential roles for our candidate mutations. Finally, In **Specific Aim III** we introduced the candidate mutations in dDAT and expressed them in HEK-293 cells and tested MDPV's ability to inhibit dopamine induced Ca^{2+} signals in these mutant constructs.

METHODS

2.1 Generation of Mutant Constructs

The dDAT gene was supplied by Dr. Satinder Singh (Yale) and ligated intothe commercial vector pGEM 7Zf(+) from Promega Corporation. The C terminal end was found to lack a stop codon, so the gene was cut into two halves at a HincII restriction site at approximately the middle of the gene and each half was ligated nto a pGEM 3zf(+) vector. To repair the C terminal end, a custom oligo was ordered, it's complementary strands annealed, and then ligated into the C terminal end, confirmed by Sanger sequencing provided by Genewiz, and then cut and ligated back into pGEM 7Zf(+). Simultaneously, the dDAT A and dDAT B mutations were created via PCR on the N terminal half of the dDAT gene in pGEM 3zf(+). Each of these mutations were confirmed by Sanger sequencing, then ligated back into pGEM 7Zf(+) yielding dDAT A (D121G) and dDAT B (P323V) each in pGEM 7Zf(+) with the C terminal stop codon repaired. The dDAT C (A117S) and dDAT E (F318C) mutations were produced by PCR in pGEM 7Zf(+), and confirmed via Sanger sequencing. The double mutant dDAT AC (D121G/A117S) was created by obtaining new primers for the dDAT C mutation and performing PCR on the already mutated dDAT A pGEM 7Zf(+). The dDAT EB (F318C/P323V) was created by obtaining new primers for the dDAT E mutation and performing PCR on the already mutated dDAT B pGEM 7Zf(+). New primers were necessary as the primers for each of the A and C mutations and the E and B mutations overlap. Once these mutations were confirmed by Sanger sequencing from Genewiz, the entire dDAT X genes were cut and ligated into the pcDNA5/FRT/TO vector for transfection in the Flp-In T-REx HEK 293 system. This strategy simplified the

confirmation of our mutations, as sequencing only needed to be performed on the coding sections of the gene, as it was ligated out of the pGEM vectors in which PCR was conducted and into the of pcDNA5/FRT/TO vector. A summary of the primers and mutation strategies are summarized in Table 1. All primers were ordered from IDT. PCR was performed using the Quick Change II Site-Directed Mutagenesis Kit from Agilent on a miniPCR™ thermocycler. Thermocycles were set to 95˚C for 30s for an initial melting step, then 15 cycles of 95˚C for 30s/ 55˚C for 60s/ 68˚C for 300s after which they were returned to room temperature.

The double mutants dDAT AB (D121G/P323V) and dDAT CB (A117S/P323V) were created by ligating the pcDNA5/FRT/TO-dDAT B C-terminal half onto either the pcDNA5/FRT/TO-dDAT A or pcDNA5/FRT/TO-dDAT C-N Terminal half of dDAT. Similarly, dDAT ABC was created by ligating the pcDNA5/FRT/TO-dDAT B-C terminal half onto pcDNA5/FRT/TO-dDAT AC-N terminal half. Finally the dDAT ABCE construct was created by ligating the C terminal half of pcDNA5/FRT/TO-dDAT BE onto the N terminal half of of pcDNA5/FRT/TO-dDAT AC. These engineering strategies are summarized in Table 2.

All of pcDNA5/FRT/TO-dDAT constructs were confirmed for a second time by Sanger sequencing via Genewiz before transfection in the Flp-In T-REx HEK 293 system.

CONSTRUCT	APPROACH*	PRIMER (5'-3')	T_M(˚C)
dDAT A (D121G)	1. PCR on pGEM-3Z(+)-dDAT-NTerm$^{1/2}$ 2. Ligated onto pGEM-7Zf(+)-dDAT^{R}-CTerm$^{1/2}$ 3. Ligated into pcDNA5/FRT/TO	5'-ctgatagccttctatgtgggcttctattacaatgtg-3'	78
dDAT B (P323V)	1. PCR on pGEM-3Z(+)-dDAT-NTerm$^{1/2}$ 2. Ligated onto pGEM-7Zf(+)-dDAT^{R}-CTerm$^{1/2}$ 3. Ligated into pcDNA5/FRT/TO/TO	5'-gtgtttttctcattgggtgtaggatttggagtgctgctg-3'	77
dDAT C (A117S)	1. PCR on pGEM-7Zf(+)-dDAT^{R} 2. Ligated into pcDNA5/FRT/TO	5'-cgtggtgctgatatccttctatgtggacttctattac-3'	78
dDAT E (F318C)	1. PCR on pGEM-7Zf(+)-dDAT^{R} 2. Ligated into pcDNA5/FRT/TO	5'-ctgccacccaggtgtgtttctcattgggtc-3'	80
dDAT AC (D121G/A117S)	1. PCR on pGEM-7Zf(+)-dDAT^{R}A 2. Ligated into pcDNA5/FRT/TO	5'-cgtggtgctgatatccttctatgtgggcttctattac-3'	79
dDAT EB (P323/F318C)	1. PCR on pGEM-7Zf(+)-dDAT^{R}B 2. Ligated into pcDNA5/FRT/TO	5'-ctgccacccaggtgtgttcattgggtgtaggattt-3'	78

Table 1. Summary of Mutations produced by PCR.

*Sanger Sequencing performed after each PCR reaction as well as after each ligation into the pcDNA5/FRT/TO vector to confirm mutant construct.

Red Letters indicate mutated base(s). Blue Letters indicate previously mutated bases on the targeted vector.

CONSTRUCT	APPROACH*
dDAT AB (D121G/P323V)	pcDNA5/FRT/TO-dDAT B-CTerm$^{1/2}$ ligated onto pcDNA5/FRT/TO-dDAT A-NTerm$^{1/2}$
dDAT CB (A117S/P323V)	pcDNA5/FRT/TO-dDAT B-CTerm$^{1/2}$ ligated onto pcDNA5/FRT/TO-dDAT C- NTerm$^{1/2}$
dDAT ABC (D121G/P323V/A117S)	pcDNA5/FRT/TO-dDAT B-CTerm$^{1/2}$ ligated onto pcDNA5/FRT/TO-dDAT AC-NTerm$^{1/2}$
dDAT ACBE (D121G/P323V/A117S/F318C)	pcDNA5/FRT/TO-dDAT EB-CTerm$^{1/2}$ ligated onto pcDNA5/FRT/TO-dDAT AC-NTerm$^{1/2}$

Table 2. Summary of Mutations produced by Restriction and Ligation of Existing Constructs.
*Sanger Sequencing performed after each ligation into the pcDNA5/FRT/TO vector to confirm mutant construct.

2.2 Flp-In T-REx HEK-293 Transfection and Maintenance, and Imagining Experiment Preparation

Generation of Mutant dDAT Flp-In TREx HEK-293 Cell Lines: Naïve Flp-In T-REx HEK-293 cells were grown in Dulbecco's Modified Eagle Medium (DMEM) with 10% fetal bovine serum (FBS, Hyclone),1% penicillin/streptomycin (final concentration: 100 μg/ml and 100 units/ml respectively), and Zeocin (100 μg/ml) until ~90% confluent in 100mm dish. A transfection mixture was prepared from 400μl of DMEM and 12μl of FuGENE, 3μG of each of pcDNA5/FRT/TO-dDAT constructs, and 3μG of pOG44 and left to sit for 20mins. It was then added to the dish of cells and allowed to sit

Maintenance of Hek-293 Cell Lines: Flp-In T-REx HEK-293 cells permanently transfected with wild-type dDAT and mutant dDAT genes were stored in 1 ml cryotubes (Nalgene) and submerged in liquid nitrogen until use. Cells were thawed and immediately placed in Dulbecco's Modified Eagle Medium (DMEM) with 10% fetal bovine serum (FBS, Hyclone),1% penicillin/streptomycin (final concentration: 100 μg/ml and 100 units/ml respectively), and hygromycin B (final concentration: 80μg/ml) and incubated at 37˚C. Cells were passaged no more than 12 times, at ~3 day intervals to avoid overgrowth.

Cell Plating, Transfection with Ca^{2+} Channel Subunits, and Transporter Expression: Cells were plated into 96-well plates containing Dulbecco's Modified Eagle Medium (DMEM) with 10% fetal bovine serum (FBS, Hyclone),1% penicillin/streptomycin (final concentration: 100 μg/ml and 100 units/ml respectively) 96 hours prior to an experiment. 24 hrs later, cells were transfected with 12μl/well of a transfection mixture consisting of 440μl DMEM, 8μl FuGENE transfection agent (Promega Corporation), calcium channel components (1.0μg of CaV1.2, 1.0μg of $\alpha 2\delta$, and 0.5 μg β3), 0.25μg EGFP, and incubated at 37˚C for 4hrs. After 4 hours of incubation, the DMEM including the transfection mixture was aspirated and replaced with fresh DMEM containing 1% penicillin/streptomycin (final concentration: 100 μg/ml and 100 units/ml respectively) and doxycycline (1μg/ml) to induce transporter expression. Cells were incubated for approximately another 68 hours before an experiment.

2.3 Two-Electrode Voltage Clamp and Calcium Imaging Experiments

Oocyte Preparation: Oocytes were prepared as described in reference 79. Stage V-VI oocytes were selected and injected with 32nL of dDAT wild-type cRNA (1ng/nl) transcribed from the p oocyte transcription vector cDNA with the T7 message Kit (Ambion Inc.). Oocytes were incubated in Ringers solution containing 5% dialyzed horse serum, tetracycline (50 μg/mL), streptomycin (100 μg/ml) and NaPyruvate (550 μg/ml) for 3-4 days at 16˚C before experiments.

Two-Electrode Voltage Clamp: TEVC was conducted as described in reference 79. Electrodes were pulled to have 1-5 MΩ resistance and filled with 3M KCl. Oocytes were clamped to -60mV using a Gene Clamp 500 Amplifier in conjunction with a 16 bit A/D converter (Digidata 1320A, Axon Instruments). A stable baseline was maintained in an extracellular buffer solution containing 120nM NaCl, 5.4mM Kgluconate, 1.2mM Ca^{2+} gluconate, and 7.5mM HEPES at pH 7.4 before recordings were taken. Recordings were analyzed using Clampfit 10.2.

Imaging solution: Imaging solution (IS) for dye loading and experimental solutions was prepared and contained 135mM NaCl, 4mM KCl, 2mM $CaCl_2$, 1mM $MgCl_2$, 10mM HEPES, and 10mM glucose and was alkalinized to pH ≈ 7.4 with concentrated NaOH.

Fura-2 Cell Loading: Ca^{2+} imaging experiments were prepared 96 hours post plating. A stock solution of fura-2 AM was prepared by dissolution of 50μg Fura-2 AM (mw = 1001) into 30μl of Pluronic F-127 in DMSO (10% w/v). A 3.3μM working solution of Fura-2 AM was prepared by addition of 4μl of the stock to 2ml of IS. Each well containing cells cultured in DMEM was aspirated and replaced with 50μl of the Fura-2 AM working solution. Cells were incubated for 15 minutes at 37˚C, 20 minutes at room temperature (RT) and then aspirated and replaced with fresh IS lacking Fura-2 and left at RT for 20 minutes before initiating an experiment.

MDPV and Dopamine Solutions: Drug solutions were prepared from 10mM stock solutions of racemic MDPV and dopamine (DA) by serial dilution into IS. In an initial step, the range of concentrations of MDPV to be tested were prepared alone by serial dilution in 50ml Falcon tubes. A small amount (~1/3 of the total volume) of each concentration was separated into a 15mL Falcon tube and DA was added into this volume to a final concentration of 10μM. A 10μM DA control solution was prepared separately in a 50ml Falcon tube.

Microscopy and Perfusion: Cells were imaged with a pco.edge 4.2 Lightning Camera (Horiba Scientific sCMOS) on an Olympus IX70 microscope using a 0.80NA 20X objective. The PTI EasyRatioPro imaging system and a monochromator (Horiba Scientific) were used for rapid excitation wavelength switching. PTI EasyRatioPro Software was used to record imagining sessions on a PC running Microsoft Windows.

Perfusion was maintained at ~35˚C using an automated pressurized system and temperature clamp (both from Automate Scientific). Clampex 10.2.0.12 (MDX Analytical Technologies) was used to control the automated perfusion system on a separate Windows PC from the one running EasyRatioPro.

Selection Criteria for Imaging Within a Well: Cells are plated to be around 60% confluent for the day of an experiment. Regions that have healthy cells with characteristic HEK-293 shapes (smoothened rhomboidal with processes; i.e. not round or circular) are selected in an initial step. Secondly, regions with a visible monolayer of cells that contain spaces for background subtraction are utilized. In a third selection step, cells are excited at 490nM to illuminate cells with high EGFP expression. EGFP expression is taken as a marker for Ca^{2+}-channel transfection, as the EGFP plasmid was co-transfected with the calcium channel subunits. The ideal imaging field would therefore contain a monolayer of healthy, characteristically shaped cells with good transfection and some space for background subtraction. Additionally, it is typical that some cells within a field have little to no EGFP expression and accordingly do not generate intracellular Ca^{2+} signals, which serves as a negative control, as presumably almost all of the cells are expressing monoamine transporters. Importantly, each well was only used once for an imaging run, and if cells were not sufficiently responsive, or a perfusion artefact was generated, that well was not incorporated into the analyzed data.

MDPV Competition Perfusion Protocol: Once a viable field was found, the vacuum and perfusion lines were positioned into the well, with the perfusion rod directly over the field of cells. The perfusion was initiated for ~5-10s to allow cells to equilibrate to the ~40μl/s perfusion rate. The height of the vacuum rod was positioned at ~1/2 of the overall height of the well and the perfusion liquid level was checked for the absence of level oscillation prior to initiating the recording. Once initiated, the perfusion was programmed to perfuse IS for 10s, IS with 10μM DA for 5s as a control pulse, which was followed by a 30s washout by IS alone; next, a 30s perfusion of IS containing varying concentrations of MDPV was followed by a 5s pulse of IS containing MDPV at the same concentration as well as 10μM DA. In a final step, the well is perfused with IS for a 30s washout.

Replication: Each construct was tested for a minimum of 3 experimental days (typically 4). For each day, 3-4 wells/runs per concentration were collected. From each well 5-12 separate cells were included in the data set. In general, this yielded 60-100 cells per concentration per construct.

2.4 Analysis

Analysis I. Cell Selection and Background Subtraction: Cells that exhibited rapid and strong responses to the control DA pulse were selected for subsequent analysis. No attention was given to the magnitude or kinetics of second pulse as a criterion for including a given cell, as the second responses were influenced by the concentration dependent effects of MDPV; however, the entire trace was examined for baseline stability and noise. A small area of the well where cells were absent was selected as a measure of background emission. The background emission at 510nm was subtracted from emissions at 510nm due to excitations at 340nm and 380nm, and the ratio of emissions from 340nM and 380nM excitations was calculated for the entire run and exported as a text document.

Analysis II. Automated Unix Shell Script for Baseline Correction: A Unix shell script was developed using AWK operations and the shell command 'column' to process raw output text files from PTI's EasyRatio Pro program. EasyRatio Pro generates text files with a number of excess header lines, a column for the background emission, and a time column for each ratio (i.e. each cell). While the perfusion system tightly controls the timing of the solution changes once a session is initiated, terminating the recording requires manual input via PTI's Warp Drive tactile controller module. This results in columns of varying length at the end of the text file. Additionally, modifying each output file, which corresponds to one well containing 8-12 cells, is time consuming. The shell script was therefore developed to recursively trim errantly long data columns, remove

excess header lines, remove “bonus” time columns, and to perform an initial normalization on the data. In this manner, all of the output files from a given day could be fed into the script, truncated, and neatly returned in new modified output files. Most advantageously, the script also stitched all of columns (e.g. cells) for a given concentration together into one file beset at the left with a singular time column, yielding only as many files as there were concentrations for the day. Each column was also divided by its baseline, which was defined as the average of the ratio value in the first 5 seconds of the recording. Therefore, all of the data from a single concentration from a single day could be imported into a template Microsoft Excel file and tabulated in separate sheets. Concentration-days from subsequent experiments are then added to the corresponding sheet in the Excel file for each construct.

Analysis III. Determination of Relative Responses: Relative responses were determined by dividing the second DA peak by the control peak for each cell. Each peak value was determined as the average of 7 time points at the onset of the peak. These values were averaged, and the standard deviation and standard error about the mean (SEM) were determined for each MDPV concentration in each construct. This data was then tabulated and exported to Prism for curve fitting. Additionally, the data from each cell was normalized by its maximal ratio value (0 to 1 scale), and these normalized ratio columns were averaged and the SEM was calculated for each concentration at each time point. These traces were then generated in Origin.

2.5 Docking, Homology Models, and Molecular Representations

Docking was performed using AutoDock Vina as ported in UCSF Chimera using default settings and a Grid box of the same size about the S1 site in the hDAT homology model and the dDAT crystal (pdb:4XP6).[138,139] The hDAT homology model was built using the web based SWISS-MODEL server and utilized the originally published dDAT crystal (pdb:4M48) and the alignment in that publication as a target.[124,126,136]

RESULTS

3.1 Specific Aim I: Determine MDPV's Potency at dDAT

3,4-Methylenedioxypyrovalerone (MDPV) is known to be a potent inhibitor of the human dopamine transporter (hDAT). We first tested MDPV's ability to inhibit DA induced currents in *Xenopus laevis* oocytes expressing dDAT (**Figure 9.A**). At the high concentration of 10μM, MDPV weakly inhibited a 5μM pulse of dopamine (DA), and a subsequent DA pulse showed little to no decay in magnitude, indicating MDPV was fully washed out and no longer interacting with the transporter.

We next sought to test MDPV at hDAT in the MAT/Ca^{2+} assay, as it had not be previously evaluated in that assay. Flp-In T-Rex HEK293 cells stably expressing hDAT were previously prepared in the Eltit lab. We determined that MDPV inhibited DA signals at hDAT with a potency of 85±7 nM in our assay (**Figure 1**). Our initial dDAT gene lacked a stop codon. To repair the gene we custom ordered an oligo and inserted the stop codon and introduced an Xho1 cut site after the stop codon to facilitate moving this gene into the pcDNA5/FRT vector for the creation of Flp-In T-Rex HEK 293 cells expressing dDAT constructs (See Methods). The C terminal modifications were confirmed by Sanger sequencing. We then created wild-type dDAT Flp-In T-Rex HEK-293 cells and tested MDPV's ability to inhibit DA signals in our MAT/Ca^{2+} assay. MDPV displayed a much weaker ability to inhibit DA signals in dDAT, with a determined potency of 29,180±1,724 nM. The normalized traces and dose response for MDPV at dDAT as well as a comparison to the dose response for MDPV at hDAT can be seen in

Figure 9 Panels A & B. MDPV at dDAT is therefore ~340 times less potent at inhibiting DA-induced Ca^{2+} signals in our assay.

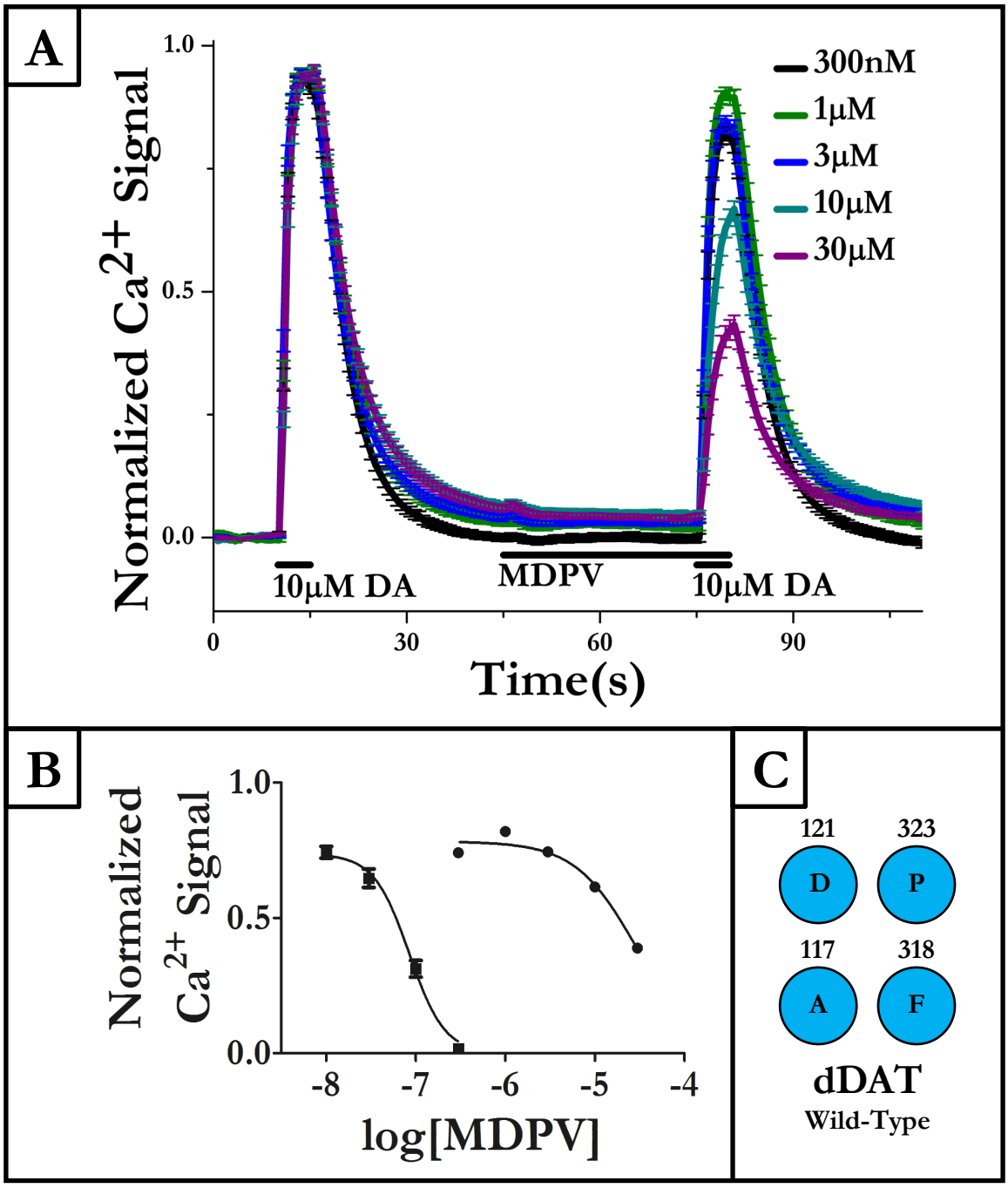

Figure 9. MDPV is More Potent at hDAT than at dDAT. Panel A) The normalized Ca^{2+} signals in dDAT expressing HEK-293 cells are shown. Panel B) The MDPV-dDAT dose response curve for the normalized traces in A are shown in the curve to the right (circles, IC_{50} = 29,180±1,724 nM). The dose-response for MDPV at hDAT is shown at

the left for comparison (squares, IC_{50} = 85±7 nM). Panel C) A schematic representation of the four mutations that were investigated in this study. Numbers indicate the residue position in dDAT. Letters indicate the identity of the residue at that position. The color of the circles indicates whether the residue is endogenous to hDAT (yellow) or dDAT (blue). Since the dDAT construct shown here is wild-type dDAT, all circles are colored blue. For hDAT: n=34, 29, 39, 34 for 10nM, 30nM, 100nM, and 300nM respectively. For dDAT: n=87, 77, 82, 105 ,86 for 300nM, 1μM, 3 μM, 10 μM, and 30 μM respectively.

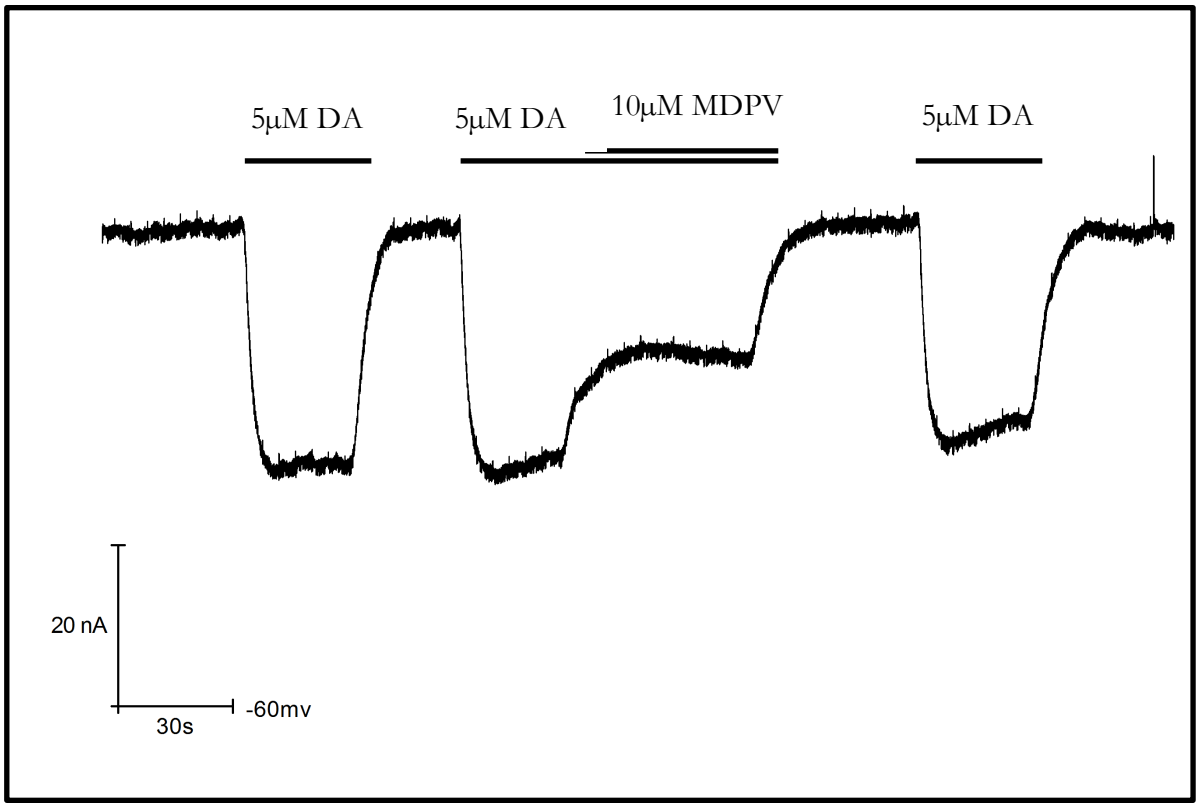

Figure 9.A Two Electrode Voltage Clamp traces of *Xenopus laevis* Oocytes Expressing dDAT. Oocytes were clamped to -60mV. MDPV is unable to completely block DA induced currents at the relatively high concentration of 10*μ*M. A subsequent pulse of DA returns control magnitude.

3.2 Specific Aim II A: Determine Candidate Residues in the dDAT S1 Site

We next sought to determine residues that may underlie the observed differences in MDPV potency at dDAT and hDAT. It is known that dDAT has good affinity for inhibitors of the human serotonin transporter (hSERT), and conversely prefers substrates of hDAT. Similarly, the hDAT selective inhibitor bupropion has low potency at dDAT. We therefore sought residues within the S1 that were shared between hSERT and dDAT, but unique in hDAT. We compared the 2D sequences that line the S1 between these transporters and selected residues that were homologous (e.g identical) between dDAT and hSERT, but unique in hDAT. We next used the 3D crystal structure to locate these residues in the S1 of dDAT. These residues are highlighted yellow in **Figure 10**. In Figure 10, residues conserved between all three transporters are colored dark blue, while those shared between dDAT and hDAT or outside the S1 are shown in light blue. We further reduced this list by selecting residues that are near to or face the inside of the S1 pocket. Interestingly, one other residue (colored orange in Figure 2) was found that is unique to dDAT. This yielded five total target residues, four that are shared between hSERT and dDAT (A117, Y123, P323, and F318), and the one residue unique to dDAT (D121). We chose to investigate four of these, and did not include Y123 in this work. We chose to mutate the dDAT residues to the those found in hDAT and create dDAT/hDAT point chimeras in an effort to recreate MDPV's high

affinity binding in dDAT. Therefore, four total residues were found from our deductive approach, and correspond to the following mutations: A117S, D121G, F318C and P323V.

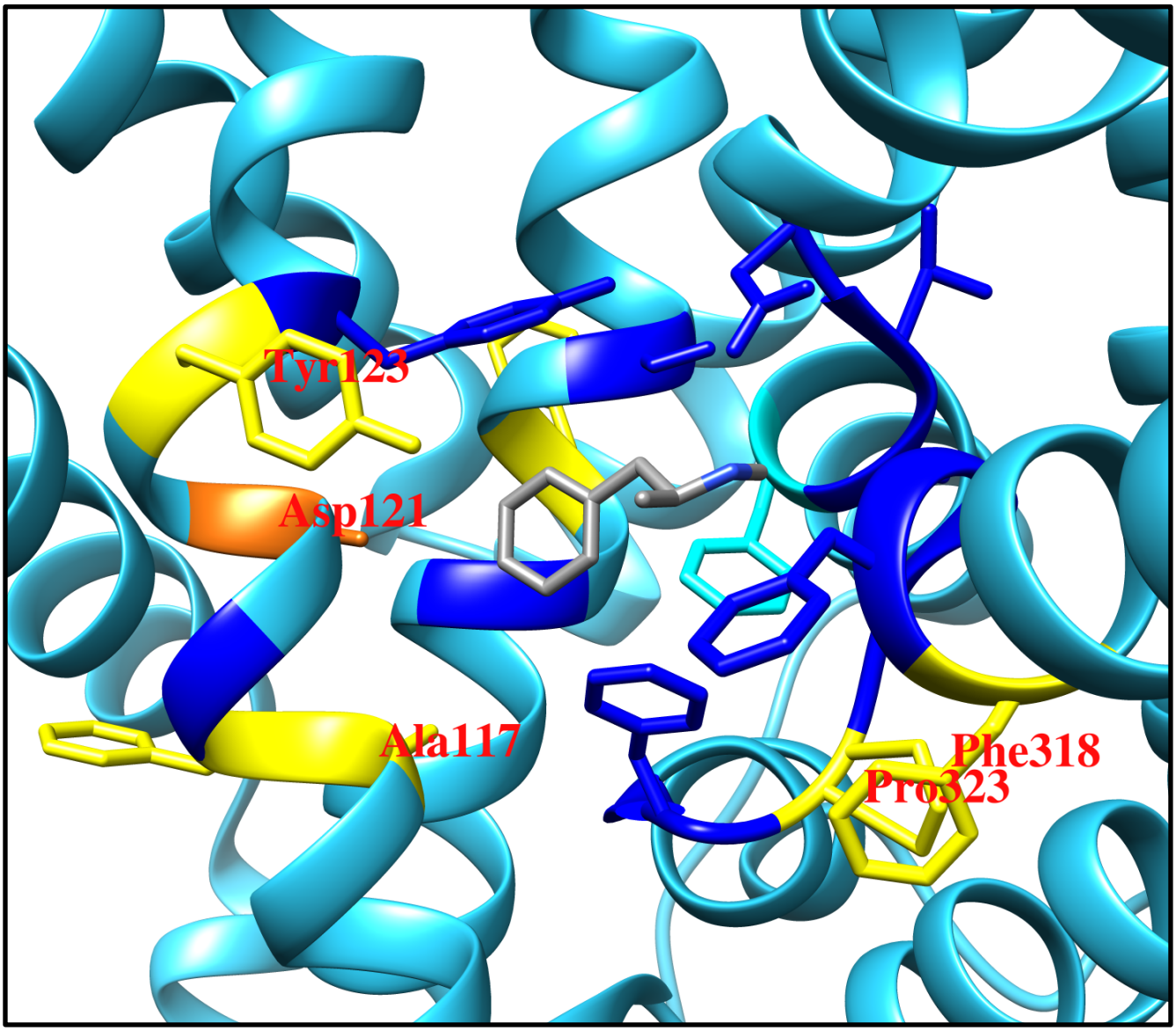

Figure 10. Target Residues Identified in the S1 Site of dDAT. The methamphetamine bound dDAT crystal 4XP6 S1 site is shown. Methamphetamine is displayed for reference to the center of the S1. Residues that are shared between dDAT and hDAT, or are outside of the S1 site are colored cyan. Residues that are within the S1 site and are homologous between dDAT, hDAT, and hSERT are shown in dark blue. Residues in the S1 site that are homologous between hSERT and dDAT but unique in

hDAT are highlighted in yellow. The five residues identified by our comparative approach that also met the criterion of facing or being near to the inner face of the S1 are labeled in red (A117, D121, Y123, F318, P323). From these five, four were selected, and Y123 was not investigated.

3.3 Specific Aim II B: Dock MDPV into dDAT Crystal and hDAT Homology Model S1 Site

To assess potential roles for the target residues identified in the previous section, a homology model for hDAT was developed using SWISS-MODEL's online homology model server. The overall structure of the homology model was quite similar to that of the dDAT crystal it was based upon, but the conserved Phe320, which corresponds to F319 in dDAT, was moved out over the S1 site. In the dDAT crystal, this residue is moved out of the pocket in what has previously been described as an "outward-open" conformation. Autodock Vina was then used as ported in UCSF Chimera version 1.13.1 (build 41949) to dock MDPV into the S1 binding site of hDAT and the dDAT crystal (pdb: 4XP6). S(+)MDPV was docked as it is the active enantiomer of MDPV. The top five docking poses for S(+)MDPV docked at the dDAT crystal are shown in **Figures 11-15** along with their corresponding binding scores**.** The top five binding poses of S(+)MDPV at the S1 of the hDAT homology model are shown in **Figures 16-20** along with their corresponding scores. The conserved phenylalanines on transmembrane (TM) domains 6a and 6b as well as the conserved aspartic acid in TM1 are shown for reference while the four target residues are highlighted in each set of figures. The unitless Autodock Vina binding scores, which approximate binding energy, are summarized in **Table 3.**

Overall, the top scores for the hDAT homology model are lower than those for dDAT, indicating a more energetically favorable interaction. The docking results for

S(+)MDPV at both hDAT and dDAT contain poses with the amine group oriented toward the conserved Asp on transmembrane helix 1 (Asp46 in dDAT and Asp79 in hDAT). These include the S(+)MDPV-dDAT poses seen in Figures 11, 12, 14 and 15 and the S(+)MDPV-hDAT poses seen Figures 17, 19 and 20. See the Discussion section for more information about the relevance of this orientation. In the top hDAT-MDPV pose (**Figure 16**, Score= -8.2) the amine group is seen oriented toward the conserved double phenethylamine motif that sits at the TM 6a-6b interface, while the alkyl tail of MDPV is oriented toward the conserved Asp79 on TM1. No such pose is observed for S(+)MDPV docked at dDAT's S1 site. S(+)MDPV at hDAT is also seen with the methylenedioxy motif oriented at the TM 6a/6b interface, with the amine group oriented toward the back side of the binding pocket (**Figure 18**, Score= -7.6). The poses in Figures 16 and 18 share an alkyl tail orientation toward TM1, with the amine and methylenedioxy groups rotated about the chiral center of MDPV. The poses observed in Figures 17, 19 and 20 for MDPV at hDAT are slight variants of one another, with each of the alkyl, methylenedioxy, and amine groups in similar orientations in these poses. The alkyl tail is seen between the conserved phenylalanines, with the amine group oriented toward TM1 and the methylenedioxy group toward TMs 3 and 8.

In the S(+)MDPV-dDAT there is a notable shift toward the rightward, TM1/TM6 face, whereas the S(+)MDPV-hDAT poses are positioned more toward the leftward TM3/TM8 interface. Additionally, the conserved Phe320 in hDAT, which is shifted toward the S1 relative to its corresponding pose in dDAT (Phe319), is observed over MDPV, sandwiching it down into the S1 site. In the dDAT-MDPV binding poses, this

phenylalanine is shifted out of the pocket and toward the nonconserved phenylalanine at position 318. Accordingly, S(+)MDPV is less buried in the dDAT bound poses. The nonconserved target residues are not directly seen interacting with MDPV in either dDAT or hDAT, though in the hDAT-MDPV poses the methylenedioxy group is better accommodated between TMs 3 and 8, where Asp121 in dDAT sits (G153 in hDAT.

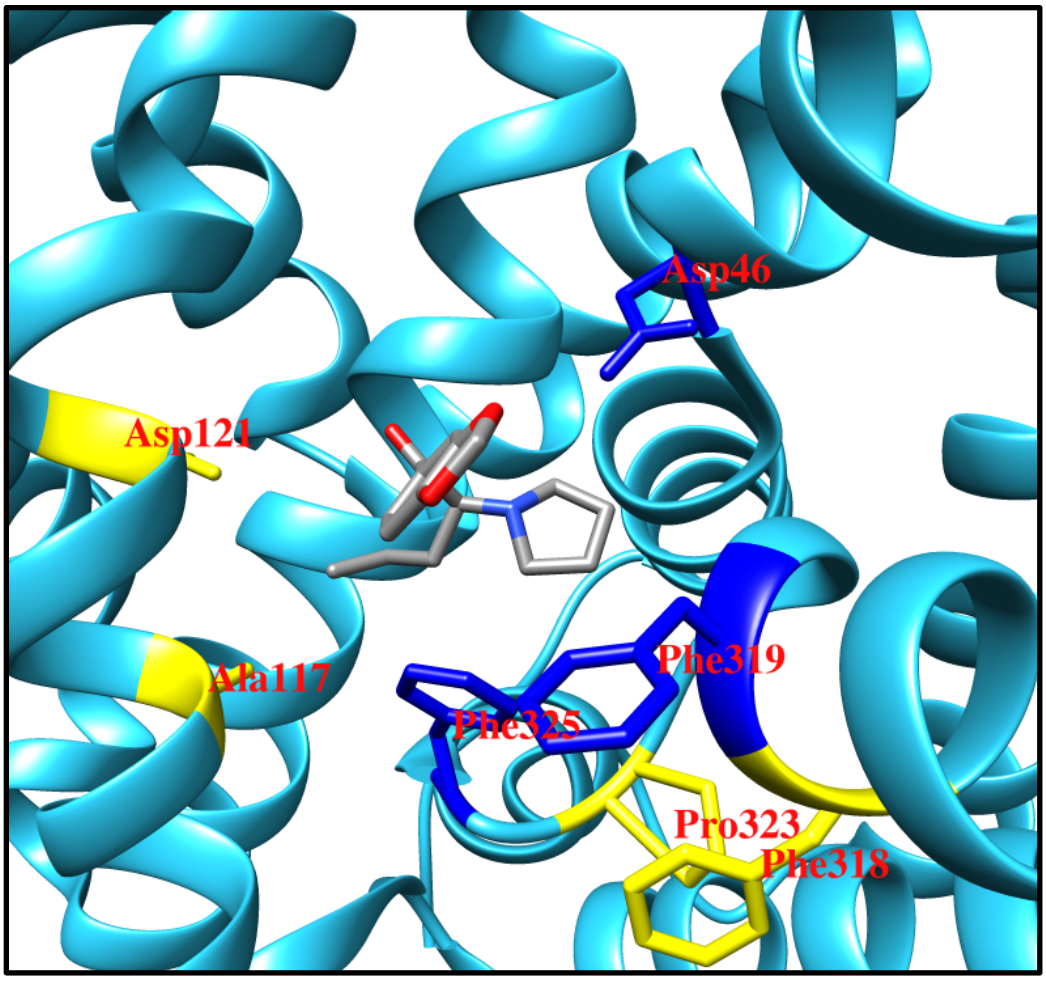

Figure 11. S(+) MDPV at dDAT Pose 1. S(+)MDPV is colored by atom specifier and is bound with an Autodock Vina score of -7.5. The ribbon backbone of dDAT is shown in cyan, with the conserved phenylalanines at TM 6a-6b and the conserved Asp46 on TM1 highlighted in dark blue. The target residues along TMs 3 and 6a-6b are colored yellow. All displayed residues are labelled in red.

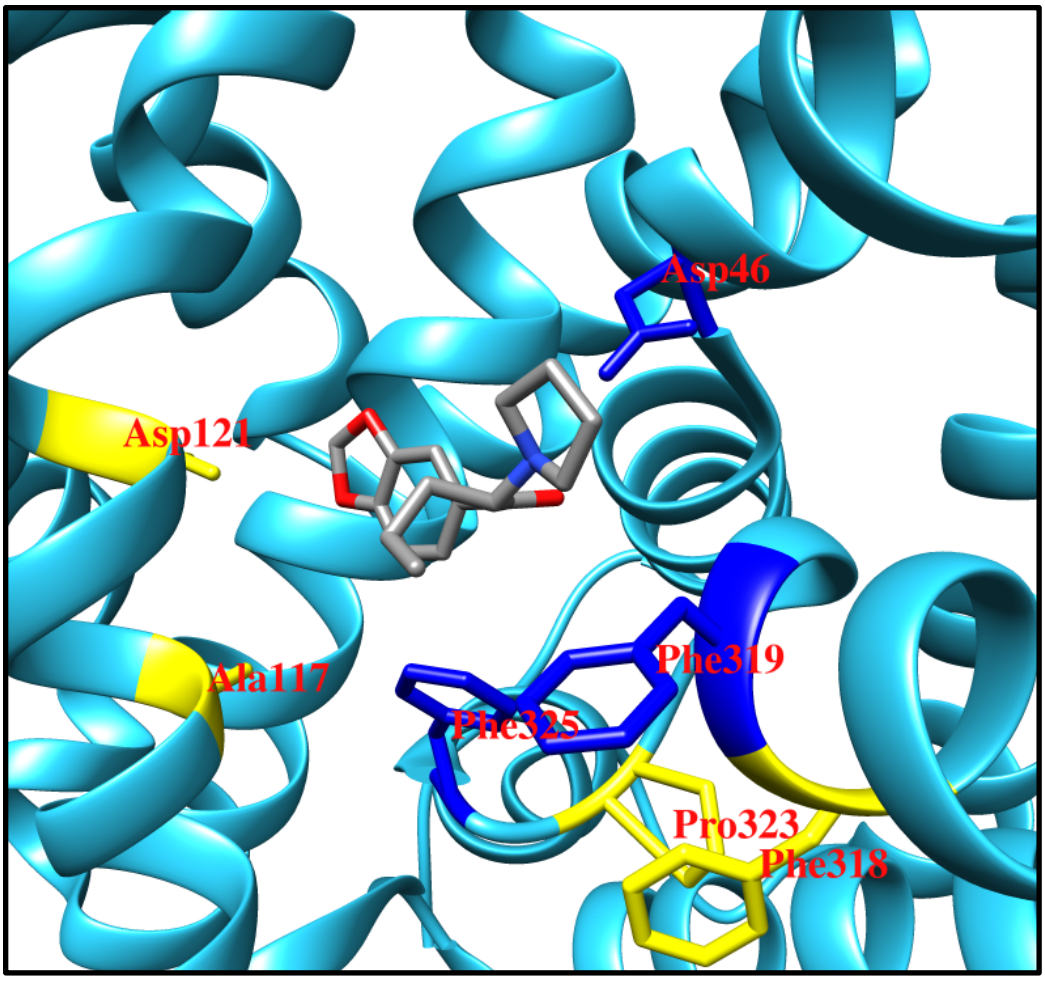

Figure 12. S(+) MDPV at dDAT Pose 2. S(+)MDPV is colored by atom specifier and is bound with an Autodock Vina score of -7.3. The ribbon backbone of dDAT is shown in cyan, with the conserved phenylalanines at TM 6a-6b and the conserved Asp46 on TM1 highlighted in dark blue. The target residues along TMs 3 and 6a-6b are colored yellow. All displayed residues are labelled in red.

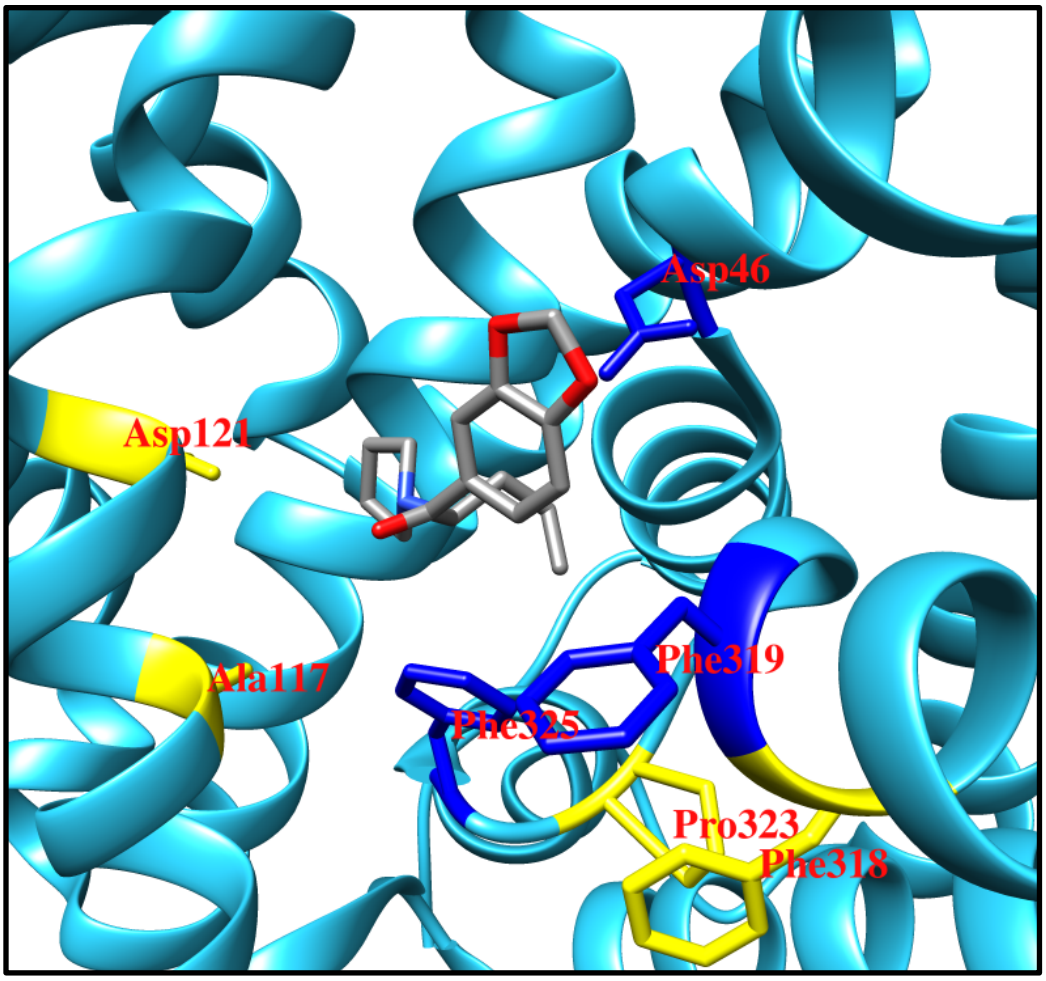

Figure 13. S(+) MDPV at dDAT Pose 3. S(+)MDPV is colored by atom specifier and is bound with an Autodock Vina score of -7.3. The ribbon backbone of dDAT is shown in cyan, with the conserved phenylalanines at TM 6a-6b and the conserved Asp46 on TM1 highlighted in dark blue. The target residues along TMs 3 and 6a-6b are colored yellow. All displayed residues are labelled in red.

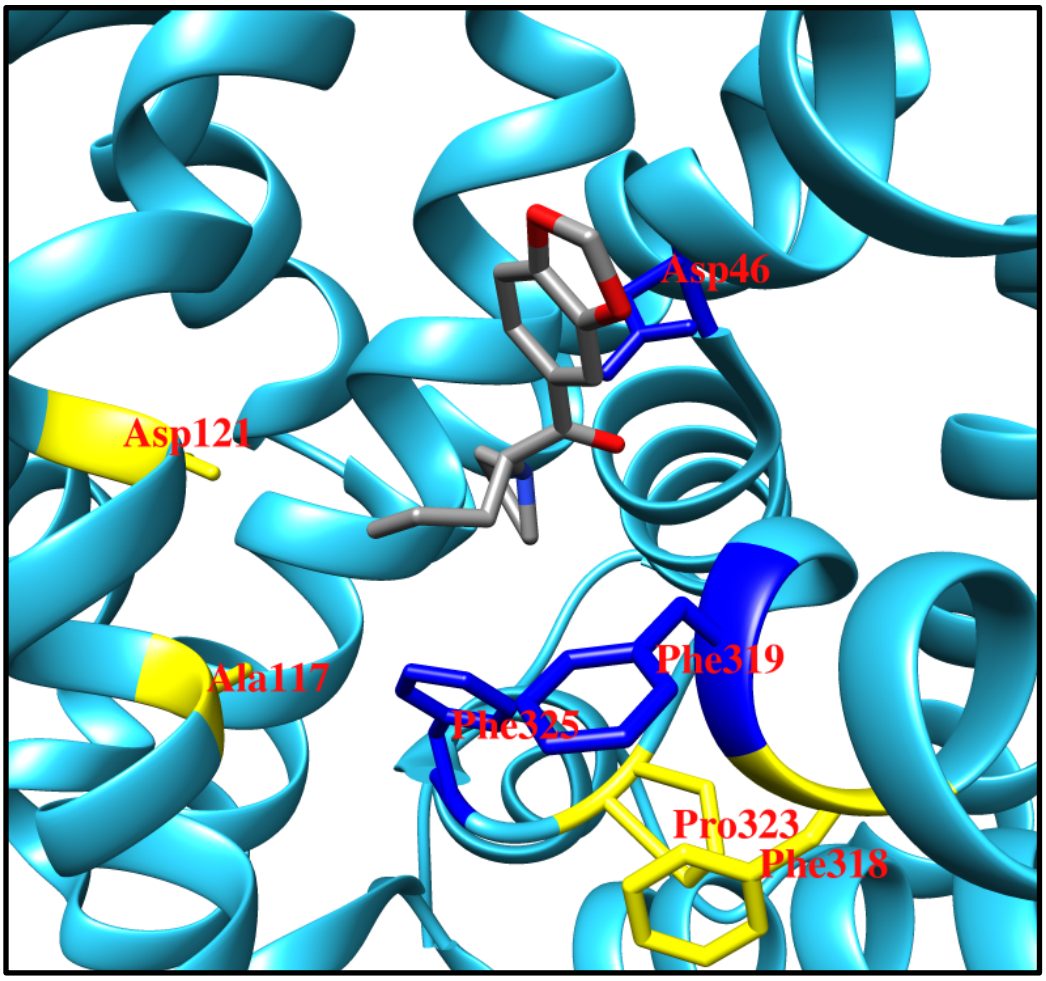

Figure 14. S(+) MDPV at dDAT Pose 4. S(+)MDPV is colored by atom specifier and is bound with an Autodock Vina score of -7.2. The ribbon backbone of dDAT is shown in cyan, with the conserved phenylalanines at TM 6a-6b and the conserved Asp46 on TM1 highlighted in dark blue. The target residues along TMs 3 and 6a-6b are colored yellow. All displayed residues are labelled in red.

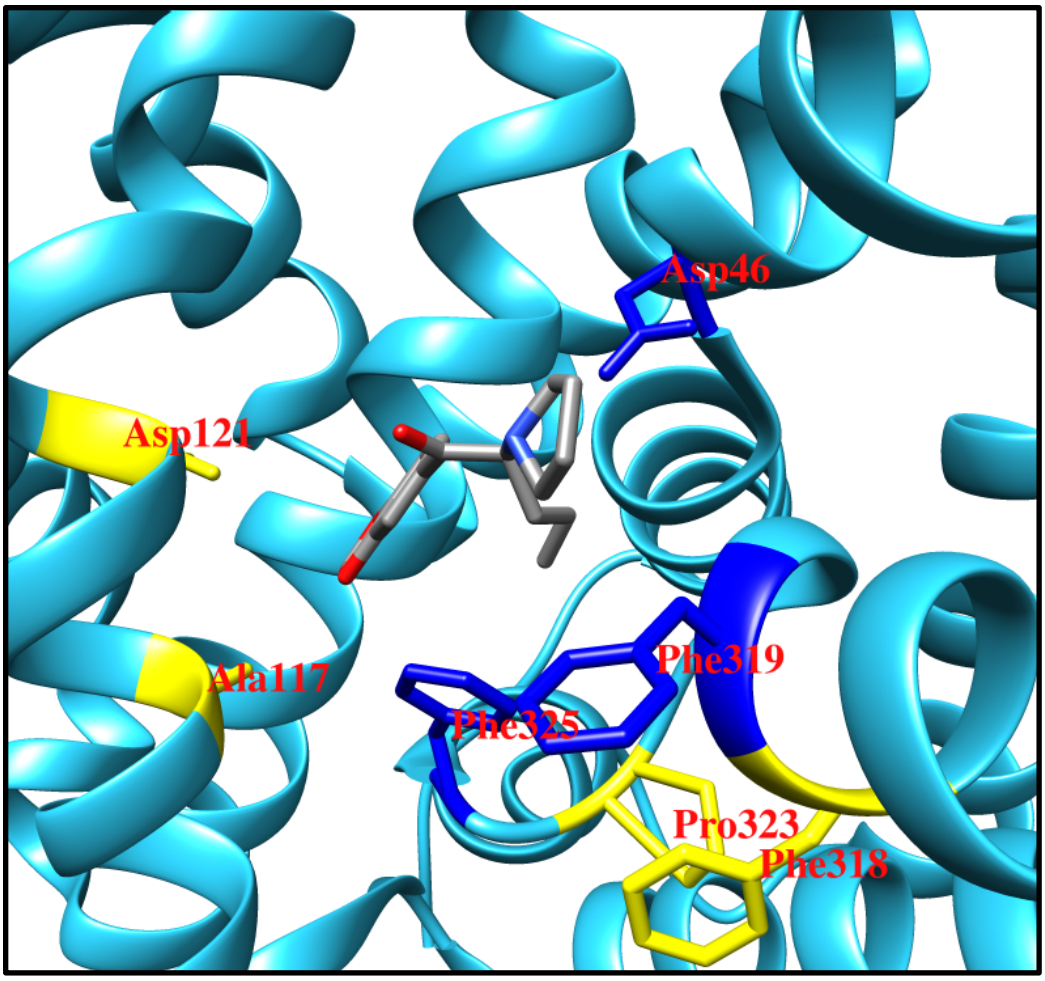

Figure 15. S(+) MDPV at dDAT Pose 5. S(+)MDPV is colored by atom specifier and is bound with an Autodock Vina score of -7.0. The ribbon backbone of dDAT is shown in cyan, with the conserved phenylalanines at TM 6a-6b and the conserved Asp46 on TM1 highlighted in dark blue. The target residues along TMs 3 and 6a-6b are colored yellow. All displayed residues are labelled in red.

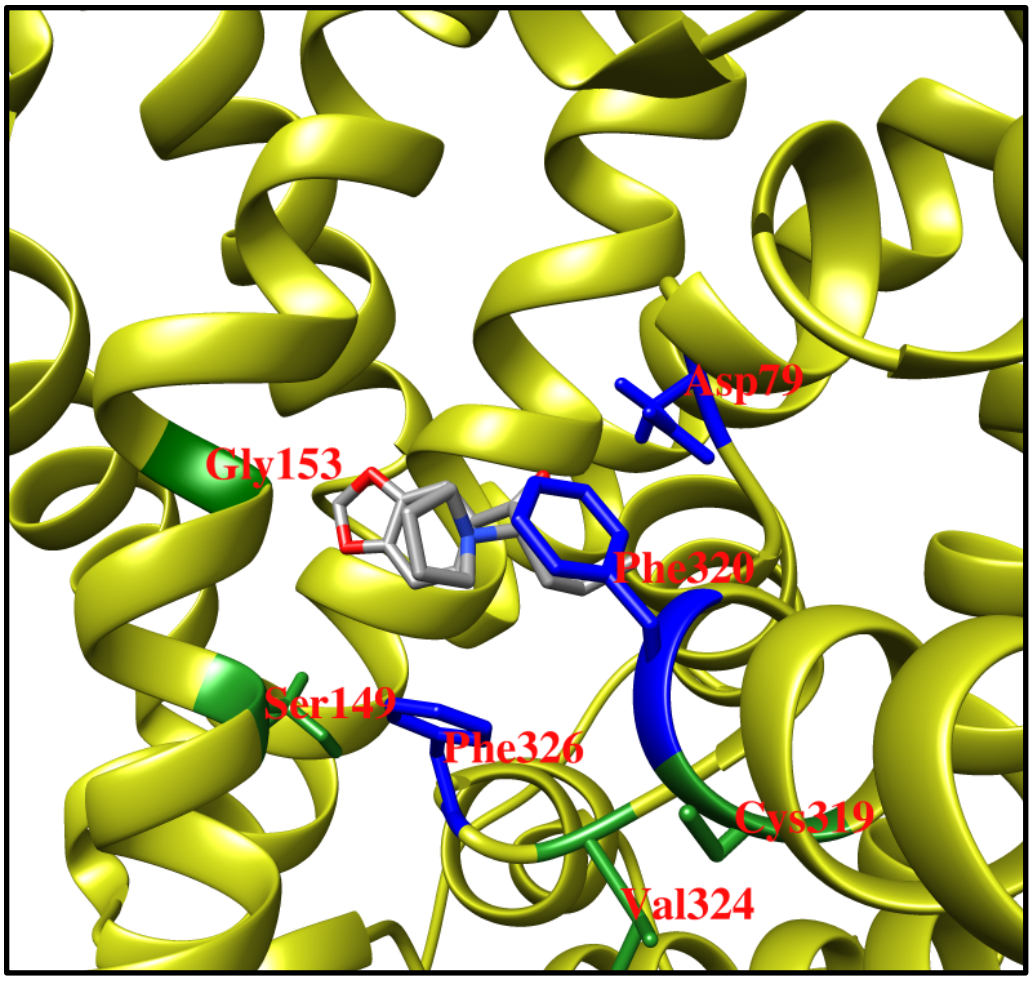

Figure 16. S(+) MDPV at hDAT Pose 1. S(+)MDPV is colored by atom specifier and is bound with an Autodock Vina score of -8.2. The ribbon backbone of hDAT is shown in yellow, with the conserved phenylalanines at TM 6a-6b and the conserved Asp79 on TM1 highlighted in dark blue. The target residues along TMs 3 and 6a-6b are colored green. All displayed residues are labelled in red.

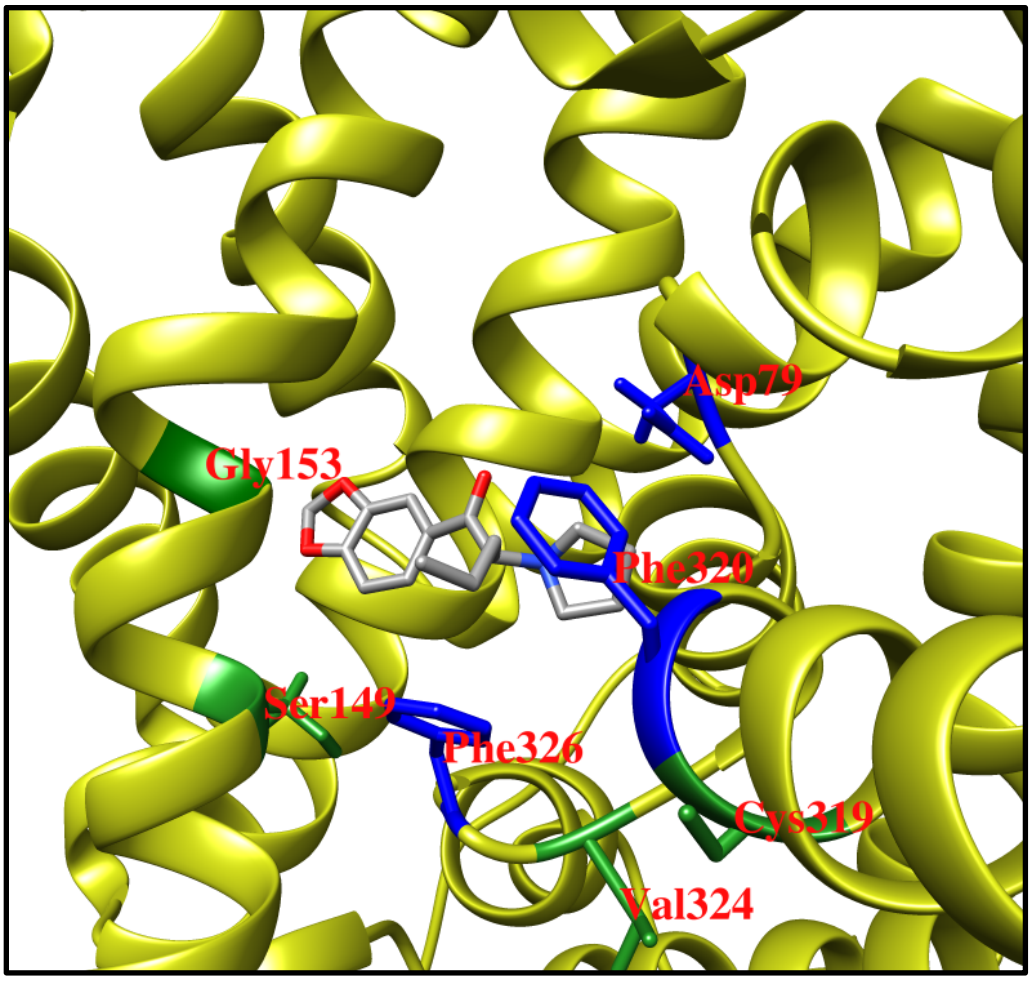

Figure 17. S(+) MDPV at hDAT Pose 2. S(+)MDPV is colored by atom specifier and is bound with an Autodock Vina score of -7.9. The ribbon backbone of hDAT is shown in yellow, with the conserved phenylalanines at TM 6a-6b and the conserved Asp79 on TM1 highlighted in dark blue. The target residues along TMs 3 and 6a-6b are colored green. All displayed residues are labelled in red.

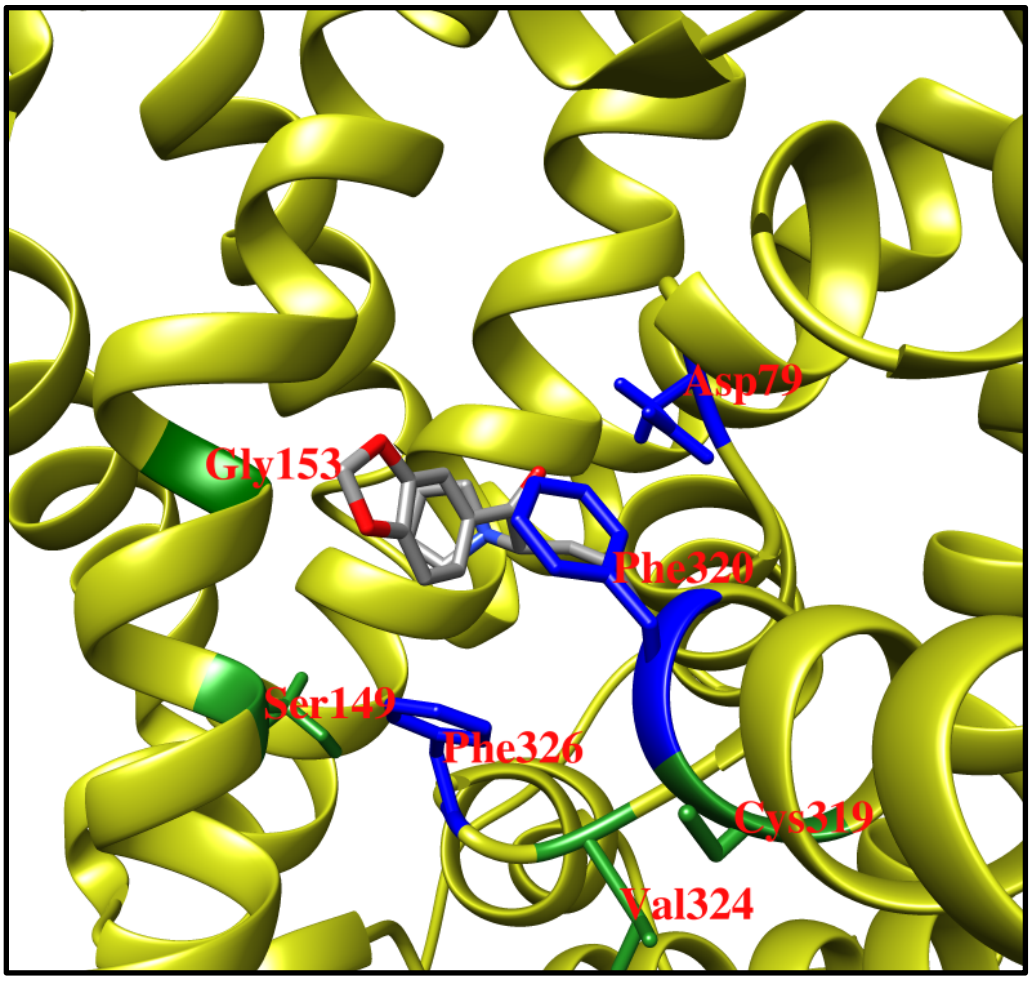

Figure 18. S(+) MDPV at hDAT Pose 3. S(+)MDPV is colored by atom specifier and is bound with an Autodock Vina score of -7.6. The ribbon backbone of hDAT is shown in yellow, with the conserved phenylalanines at TM 6a-6b and the conserved Asp79 on TM1 highlighted in dark blue. The target residues along TMs 3 and 6a-6b are colored green. All displayed residues are labelled in red.

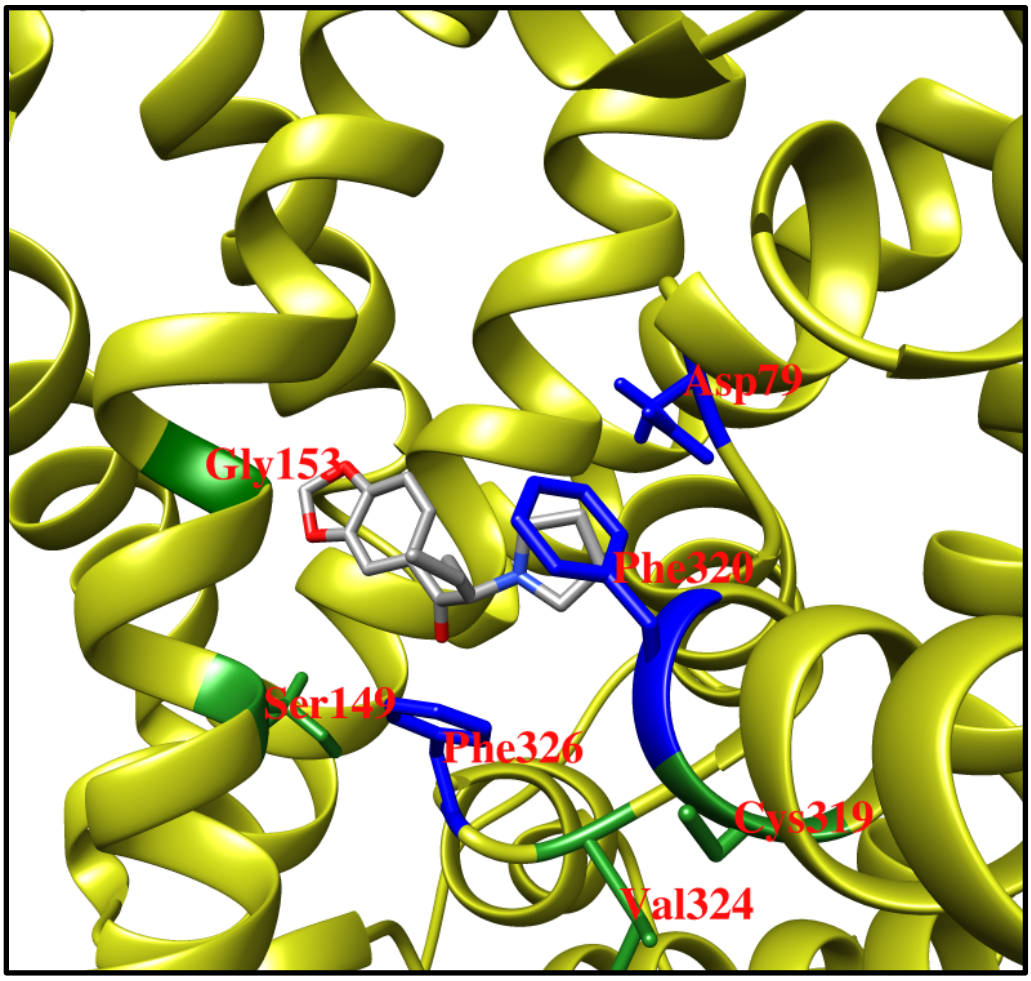

Figure 19. S(+) MDPV at hDAT Pose 4. S(+)MDPV is colored by atom specifier and is bound with an Autodock Vina score of -7.1. The ribbon backbone of hDAT is shown in yellow, with the conserved phenylalanines at TM 6a-6b and the conserved Asp79 on TM1 highlighted in dark blue. The target residues along TMs 3 and 6a-6b are colored green. All displayed residues are labelled in red.

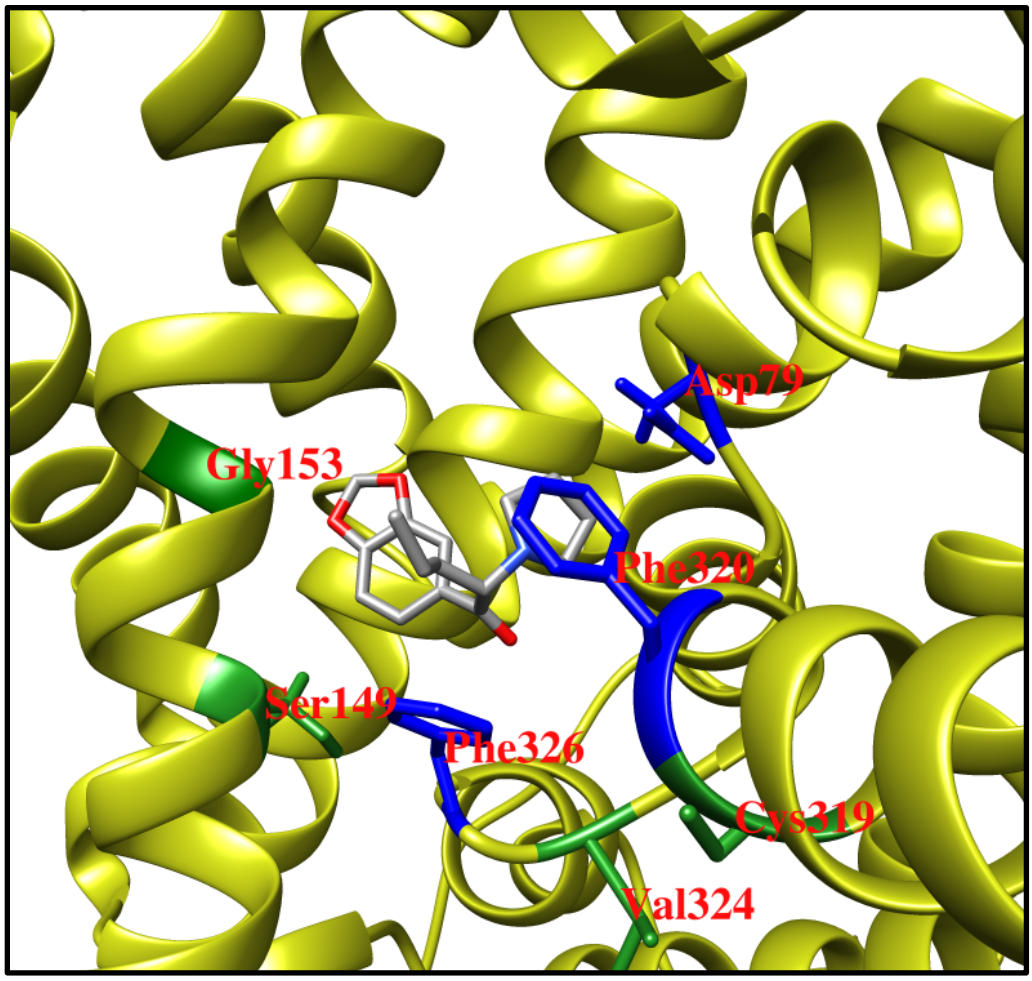

Figure 20. S(+) MDPV at hDAT Pose 5. S(+)MDPV is colored by atom specifier and is bound with an Autodock Vina score of -7.0. The ribbon backbone of hDAT is shown in yellow, with the conserved phenylalanines at TM 6a-6b and the conserved Asp79 on TM1 highlighted in dark blue. The target residues along TMs 3 and 6a-6b are colored green. All displayed residues are labelled in red.

Construct	Autodock Vina Score
dDAT	-7.5
	-7.3
	-7.3
	-7.2
	-7.0
hDAT	-8.2
	-7.9
	-7.6
	-7.1
	-7.0

Table 3. Summary of Autodock Vina Scores at the dDAT Crystal and hDAT Homology Model.

3.4 Specific Aim III: Test MDPV in HEK-293 Cells Expressing Chimeric dDAT

We next sought to make the chimeric dDAT mutations identified in Aim II and express them in HEK-293 Flp-In T-REx cells. The Methods section describes the approach for generating each construct in detail. All constructs were confirmed by Sanger sequencing in their finalized pcDNA5/FRT form prior to transfection in the Flp-In T-REx HEK293 cells. In all, four single mutants, three double mutants, and a triple and quadruple mutant were created.

Upon successful selection, MDPV was tested for its ability to inhibit Ca^{2+} signals in cells expressing each construct in our Ca^{2+}/ monoamine transporter (MAT) assay. Initially, we tested a single 10μM MDPV concentration at each of the four single mutation constructs. We found that only mutations A, B, and C, (dDAT D121G, P323V, and A117S) showed appreciable increases in MDPV potency as compared to wild-type dDAT. For the purposes of this analysis, we defined “appreciable” as an inhibition of DA signals greater than or equal to 50% for the 10μM spot test. dDAT F318C (“dDAT E”) displayed minimal difference with wild-type at the 10μM MDPV spot test. For that reason, we proceeded with determining the full dose-response for MDPV at each of these constructs, but not dDAT F318C. The dose responses for the single mutations dDAT D121G, P323V, and A117S can be found in **Figures 21**, **22**, and **23**, respectively. The wild-type dDAT MDPV inhibition curve is shown for reference in these figures (IC_{50}=29,180±1,724). For dDAT D121G (“dDAT A”, **Figure 21**) an appreciable increase in potency in MDPV action was observed (Ic_{50}= 4,727 ± 421). Similarly, MDPV had an

increased potency to inhibit dopamine (DA) induced Ca^{2+} signals at dDAT P323V ("dDAT B", **Figure 22**) and dDAT A117S ("dDAT C", **Figure 23**) as compared to wild-type dDAT, though to a lesser degree than was observed in dDAT D121G (dDAT A, **Figure 21**). The potencies for MDPV inhibition of DA induced Ca^{2+} signals at constructs dDAT B and dDAT C were, 9,121 ± 684 nM and 7,410 ± 682 nM, respectively.

Due to the fact that the increased MDPV potency observed in the three single mutations (dDAT A, B, and C) did not approximate the observed MDPV potency in hDAT, three double mutant constructs were created (dDAT AB, dDAT AC, and dDAT CB). Two of these constructs did not function properly in the Ca^{2+} assay. One of these, dDAT AB (dDAT D121G/P323V) seemed to have little transporter expression as very few cells produced measurable changes in intracellular Ca^{2+} levels upon exposure to DA. The few cells that did produce Ca^{2+} signals did not return to baseline normally, and this resulted in second, experimental pulses that exceeded the magnitude of the first, control peak. As a result, the dose response curve is shifted toward 1.0, whereas in all other cell lines, the second pulse decays to around 80% (0.8) in the presence of low concentrations of MDPV (**Figure 27**). Conversely, dDAT CB (dDAT A117S/P323V) cells responded to DA, and these responses were potently inhibited by MDPV (IC_{50}≈300nM). However, the dose-response curve for this inhibition was flat across a series of MDPV concentrations, suggesting a biphasic dose-response curve (**Figure 27**). Cells expressing the third double mutant, dDAT AC (dDAT D121G/P323V), displayed typical responses to 10μM DA and MDPV was able to inhibit these signals in a normal sigmoidal fashion (**Figure 24**). In HEK293 cells expressing this construct,

MDPV inhibited DA induced signals with a potency of 2,092 ± 166 nM. This increase in potency over the cells expressing single mutant constructs dDAT A (dDAT D121G) and dDAT C (dDAT A117S) is seemingly additive and not cooperative.

A triple mutant construct, dDAT ABC (dDAT D121G/P323V/A117S) was made and expressed in HEK293 Flp-In T-REx cells. MDPV was slightly more potent at inhibiting DA induced Ca^{2+} signals in these cells than in the double mutant dDAT AC cells, suggesting again, a roughly additive increase in potency. The dose response for these cells can be seen in **Figure 25** (IC_{50}= 1,126 ± 54 nM). Finally, a quadruple mutant construct, dDAT ABCE (dDAT D121G/P323V/A117S/F318C) was created and expressed in HEK-293 Flp-In T-REx cells and MDPV's ability to inhibit DA induced Ca^{2+} signals was assessed. In this construct, MDPV showed a considerable jump in potency over the triple mutant construct (**Figure 26**, IC_{50}= 229 ± 18 nM). Given that a full dose-response for MDPV inhibition of DA signals at the dDAT F318C construct was not determined, it cannot be definitively determined if the increase in potency in the quadruple mutant is additive or cooperative (See the Discussion section for a more thorough examination of this idea.) A summary of the IC_{50} values for MDPV inhibition at each of the constructs can be found in **Table 5.**

We next sought to determine if the apparent increases in MDPV potency across the series of constructs outlined in **Table 6** were due to actual increases in MDPV's inhibition of DA induced Ca^{2+} signals or if they were due to a loss of DA potency to elicit Ca^{2+} signals. While the Ca^{2+} signals induced from 10μM DA control pulses did not seem to vary in magnitude across the mutant constructs, a subset of constructs was selected

and the dose-response of DA elicited signals was determined. Only slight deviations in DA potency were observed between dDAT wild-type, dDAT ABC, dDAT ABCE, and hDAT wild-type (**Table 6**). Furthermore, the inhibitory constant, K_i was calculated using the IC_{50} of MDPV and the EC_{50} of DA at each of these four constructs via the Cheng-Prusoff equation. These values are summarized in **Table 6**. The calculated K_i values for MDPV improve similarly to the IC_{50} values across the dDAT wild-type, triple, and quadruple mutants as would be expected for minimal changes in DA EC_{50} values.

In summary, four candidate mutations were selected from a deductive 2D and 3D comparison of dDAT, hDAT, and hSERT. These chimeric mutations were made in dDAT where the cognate hDAT residue was inserted. MDPV was tested in single mutant constructs and a subset of these four single mutant constructs were selected for the creation of double and triple mutants. A quadruple mutant was also made, combining all four of these chimeric mutations. A seemingly additive increase in potency was observed for MDPV's inhibition of DA induced Ca^{2+} signals across the series of mutants. Finally, the apparent increase in MDPV potency observed in the final quadruple mutant, which approximates MDPV potency in hDAT, is not due to a loss of DA potency.

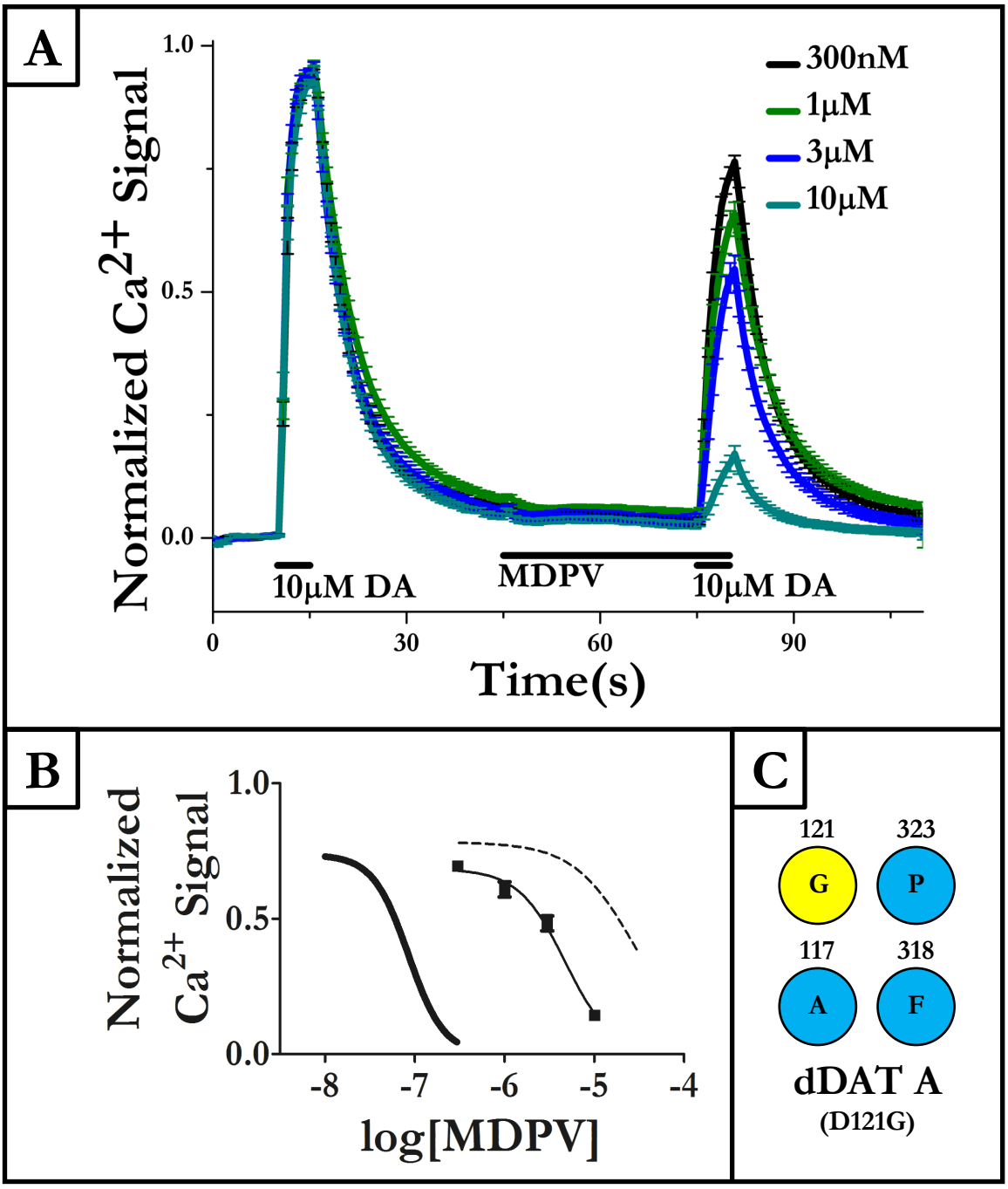

Figure 21. MDPV inhibits DA Induced Signals at dDAT A (D121G) Expressing HEK-293 Cells. Panel A) The normalized Ca^{2+} signals in dDAT A (D121G) expressing HEK-293 cells are shown. Panel B) The MDPV-dDAT A dose response curve for the normalized traces in Panel A are shown in the middle curve (squares, IC_{50} = 4,727 ±

421 nM). For comparison, the dose-response for MDPV at hDAT is shown at the left (solid line) and the dose-response for MDPV at dDAT wild type is shown at the right (dashed line). Panel C) A schematic representation of the construct presented in this Figure. The four circles represent the four individual mutations that were investigated in this study. Numbers indicate the residue position in dDAT. Letters indicate the identity of the residue at that position. The color of the circles indicates whether the residue is endogenous to hDAT (yellow) or dDAT (blue). dDAT A: n = 79, 78, 62, and 78 for 300nM, 1μM, 3μM and 10μM respectively.

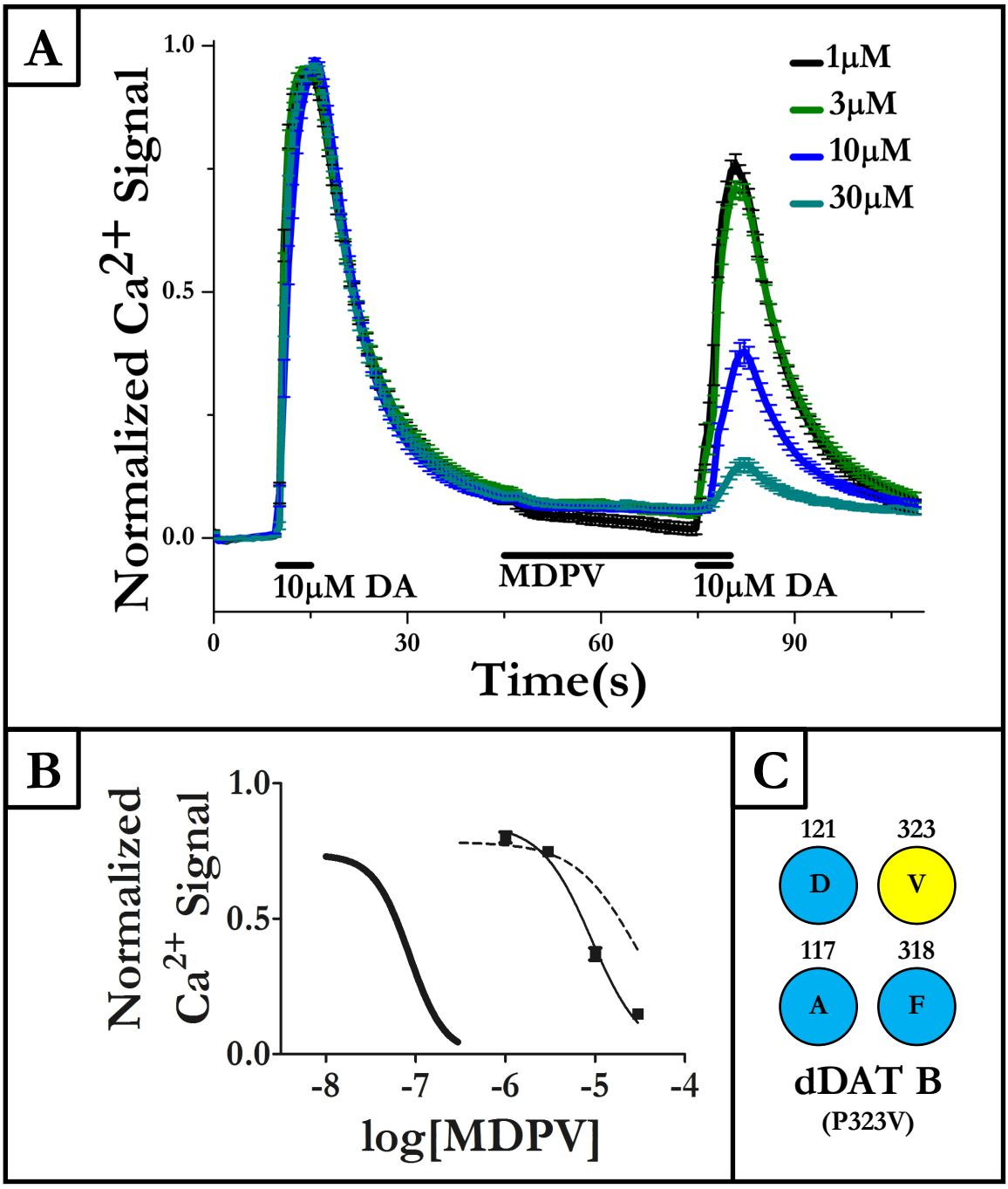

Figure 22. MDPV inhibits DA Induced Signals at dDAT B (P323V) Expressing HEK-293 Cells. Panel A) The normalized Ca^{2+} signals in dDAT B (P323V) expressing HEK-293 cells are shown. Panel B) The MDPV-dDAT B dose response curve for the normalized traces in Panel A are shown in the middle curve (squares, IC_{50} = 9,121 ±

684 nM). For comparison, the dose-response for MDPV at hDAT is shown at the left (solid line) and the dose-response for MDPV at dDAT wild-type is shown at the right (dashed line). Panel C) A schematic representation of the construct presented in this figure. The four circles represent the four individual mutations that were investigated in this study. Numbers indicate the residue position in dDAT. Letters indicate the identity of the residue at that position. The color of the circles indicates whether the residue is endogenous to hDAT (yellow) or dDAT (blue). dDAT B: n= 63, 73, 78, 58 for 1μM, 3μM, 10μM and 30 μM respectively.

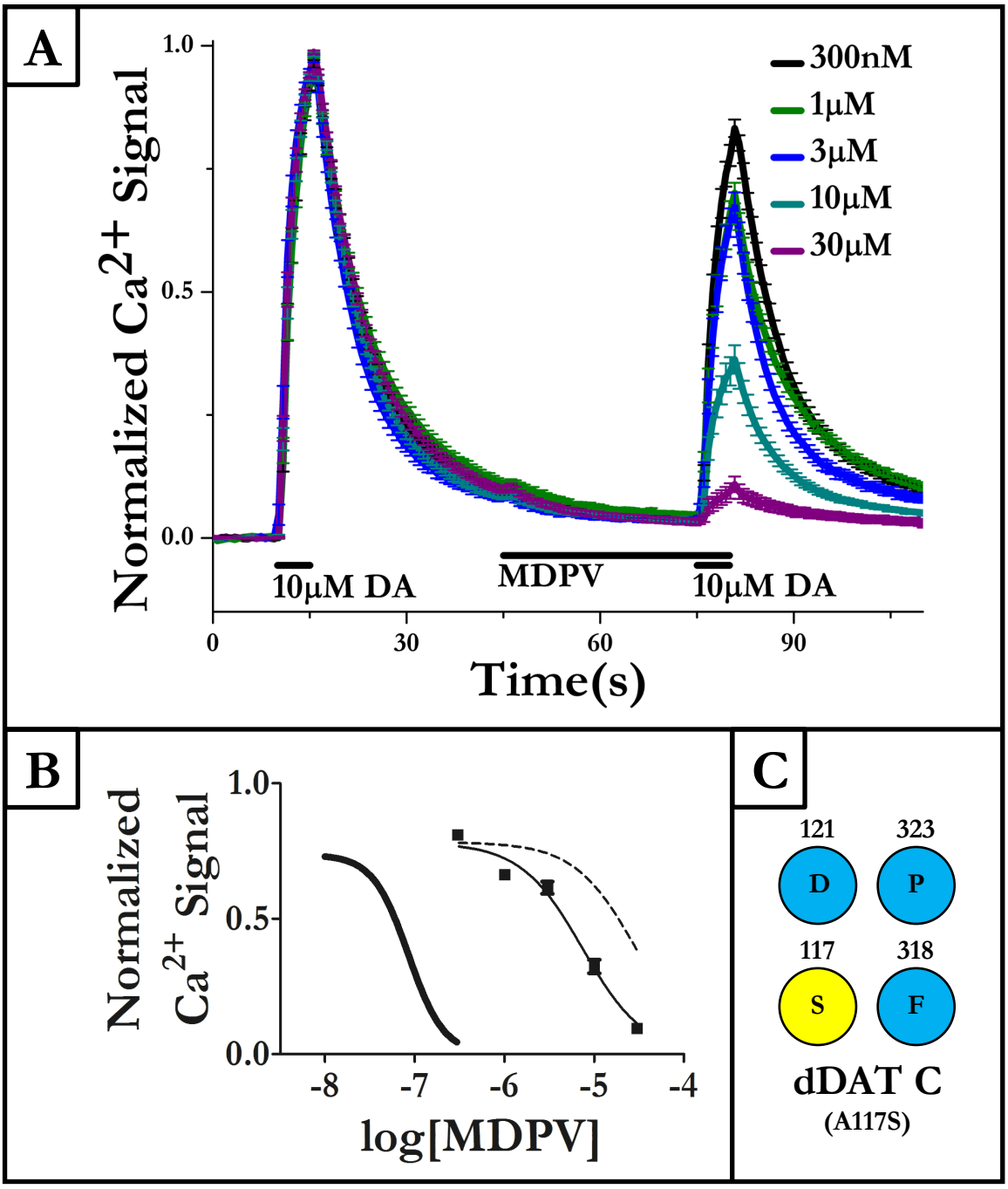

Figure 23. MDPV inhibits DA Induced Signals at dDAT C (A117S) Expressing HEK-293 Cells. Panel A) The normalized Ca^{2+} signals in dDAT C (A117S) expressing HEK-293 cells are shown. Panel B) The MDPV-dDAT C dose response curve for the normalized traces in Panel A are shown in the middle curve (squares, IC_{50} = 7,410 ±

682 nM). For comparison, the dose-response for MDPV at hDAT is shown at the left (solid line) and the dose-response for MDPV at dDAT wild-type is shown at the right (dashed line). Panel C) A schematic representation of the construct presented in this figure. The four circles represent the four individual mutations that were investigated in this study. Numbers indicate the residue position in dDAT. Letters indicate the identity of the residue at that position. The color of the circles indicates whether the residue is endogenous to hDAT (yellow) or dDAT (blue). dDAT C: n= 60, 65, 58, 84, 69 for 300nM, 1μM, 3μM, 10μM, and 30μM, respectively.

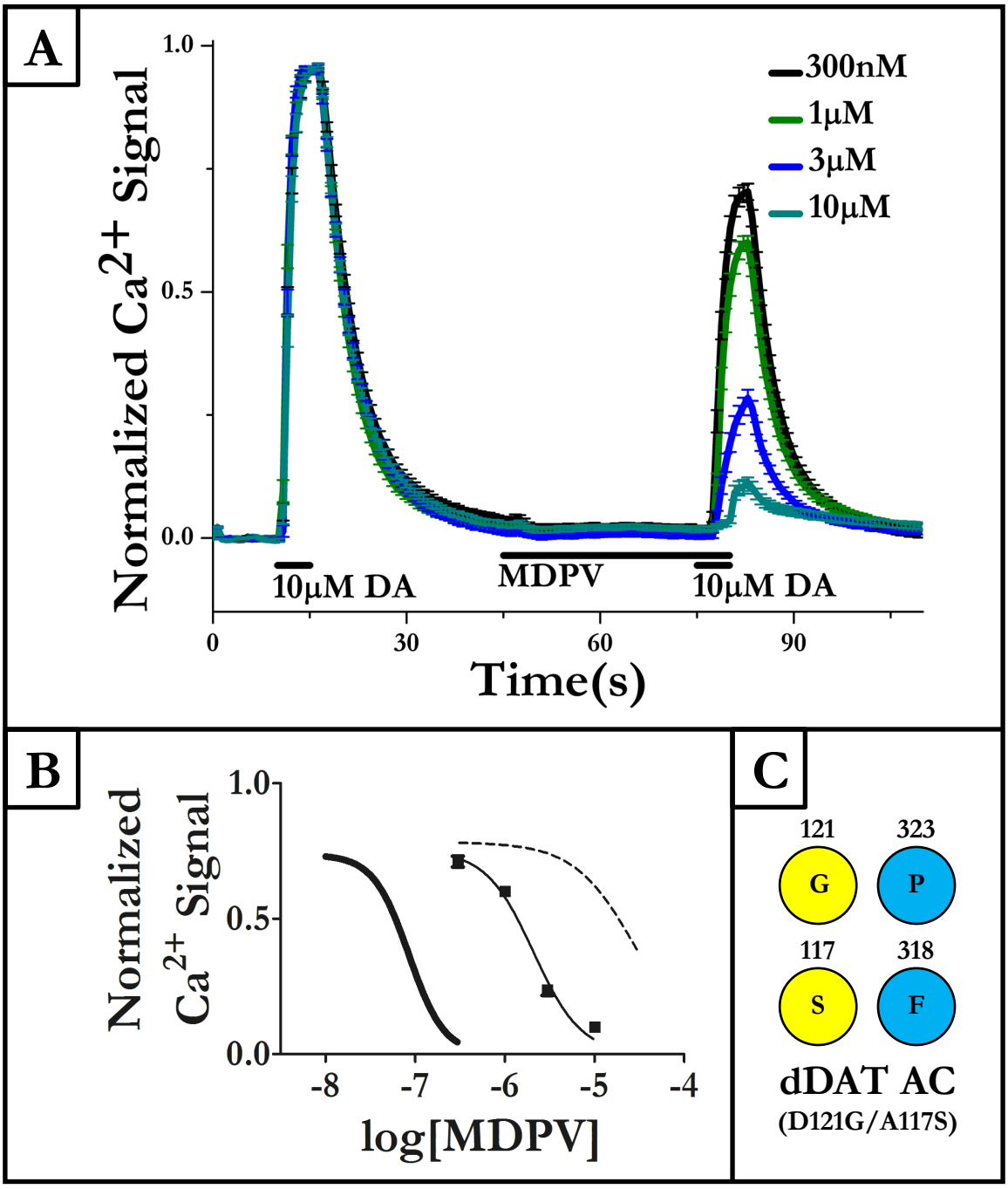

Figure 24. MDPV inhibits DA Induced Signals at dDAT AC (D121G/A117S) Expressing HEK-293 Cells. Panel A) The normalized Ca^{2+} signals in dDAT AC (D121G/A117S) expressing HEK-293 cells are shown. Panel B) The MDPV-dDAT AC dose response curve for the normalized traces in Panel A are shown in the middle curve

(squares, IC_{50} = 2,092 ± 166 nM). For comparison, the dose-response for MDPV at hDAT is shown at the left (solid line) and the dose-response for MDPV at dDAT wild-type is shown at the right (dashed line). Panel C) A schematic representation of the construct presented in this figure. The four circles represent the four individual mutations that were investigated in this study. Numbers indicate the residue position in dDAT. Letters indicate the identity of the residue at that position. The color of the circles indicates whether the residue is endogenous to hDAT (yellow) or dDAT (blue). dDAT AC: n= 109, 118, 102, 105 for 300nM, 1μM, 3μM and 10μM, respectively.

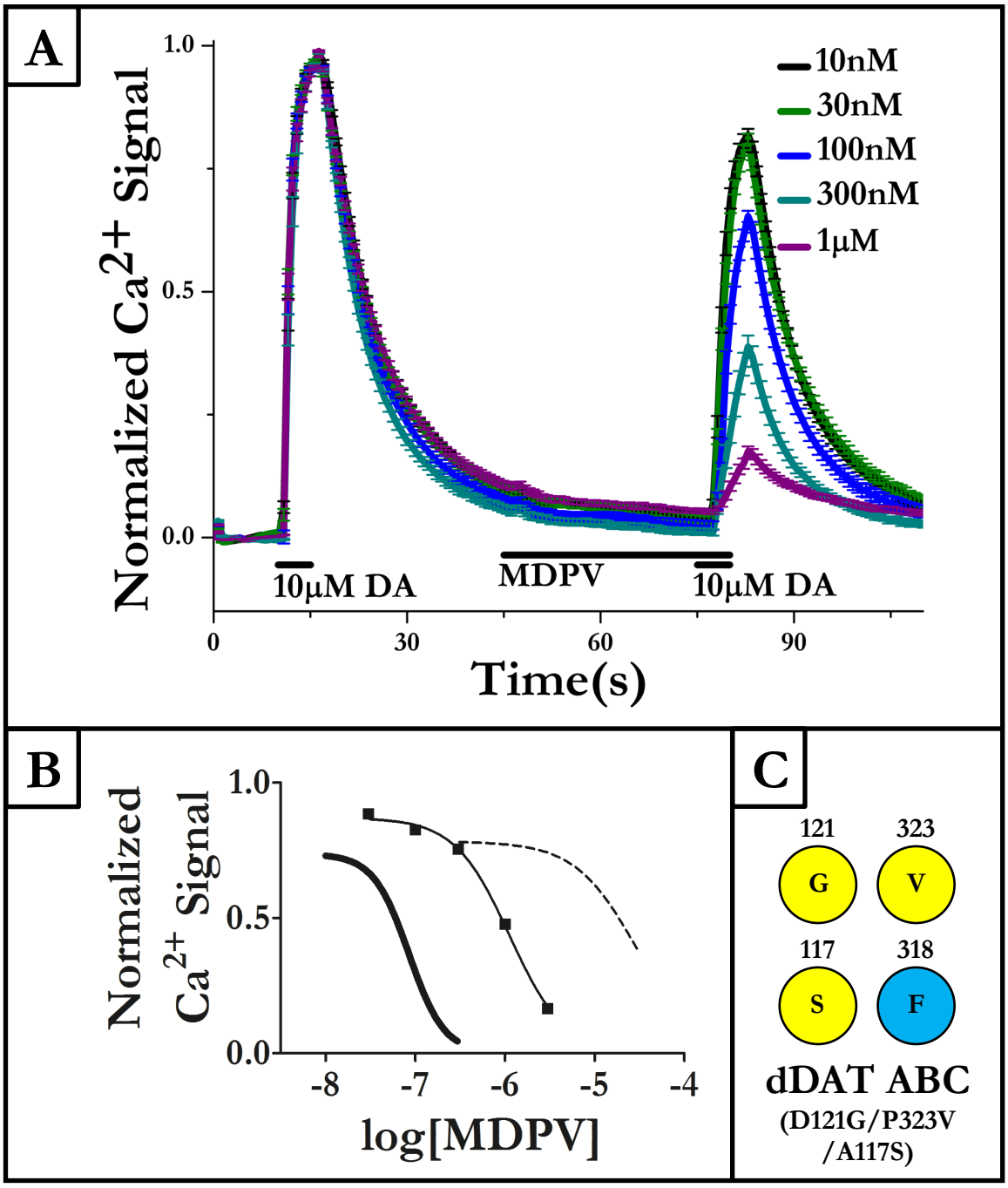

Figure 25. MDPV inhibits DA Induced Signals at dDAT ABC (D121G/P323V/A117S) Expressing HEK-293 Cells. Panel A) The normalized Ca^{2+} signals in dDAT ABC (D121G/P323V/A117S) expressing HEK-293 cells are shown. Panel B) The MDPV-dDAT ABC dose response curve for the normalized traces in Panel A are shown in the

middle curve (squares, IC_{50} = 1,126 ± 54 nM). For comparison, the dose-response for MDPV at hDAT is shown at the left (solid line) and the dose-response for MDPV at dDAT wild-type is shown at the right (dashed line). Panel C) A schematic representation of the construct presented in this figure. The four circles represent the four individual mutations that were investigated in this study. Numbers indicate the residue position in dDAT. Letters indicate the identity of the residue at that position. The color of the circles indicates whether the residue is endogenous to hDAT (yellow) or dDAT (blue). dDAT ABC: n= 121, 163, 187, 139, 137 for 30nM, 100nM, 300nM, 1μM, and 3μM, respectively.

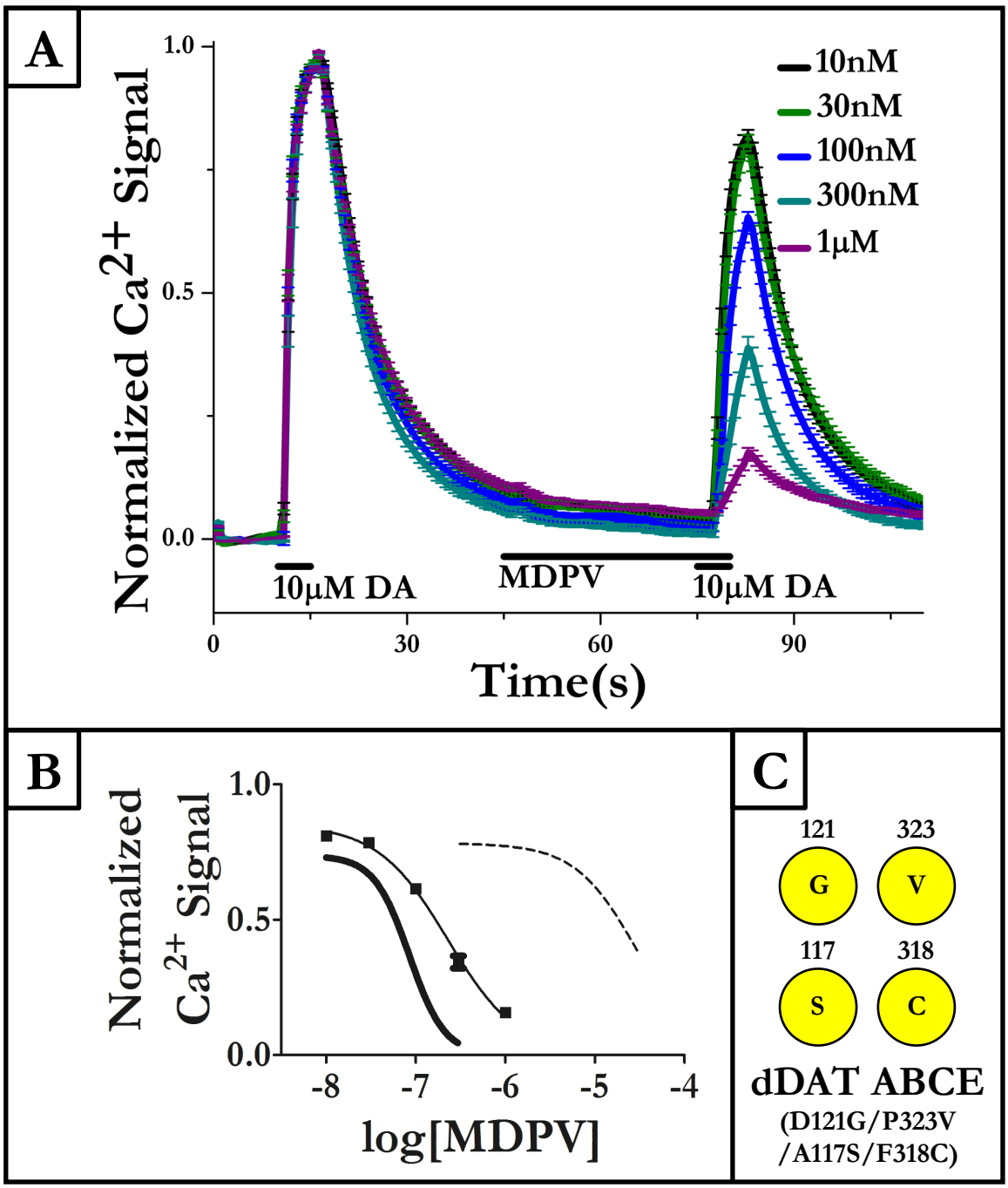

Figure 26. MDPV inhibits DA Induced Signals at dDAT ABCE (D121G/P323V/A117S/F318C) Expressing HEK-293 Cells. Panel A) The normalized Ca^{2+} signals in dDAT ABCE (D121G/P323V/A117S/F318C) expressing HEK-293 cells are shown. Panel B) The MDPV-dDAT ABC dose response curve for the normalized traces in Panel A are shown in the middle curve (squares, IC_{50} = 229 ± 18nM). For

comparison, the dose-response for MDPV at hDAT is shown at the left (solid line) and the dose-response for MDPV at dDAT wild-type is shown at the right (dashed line). Panel C) A schematic representation of the construct presented in this figure. The four circles represent the four individual mutations that were investigated in this study. Numbers indicate the residue position in dDAT. Letters indicate the identity of the residue at that position. The color of the circles indicates whether the residue is endogenous to hDAT (yellow) or dDAT (blue). dDAT ABCE: n = 81, 100, 83, 95, 100 for 10nM, 30nM, 100nM, 300nM, and 1μM, respectively.

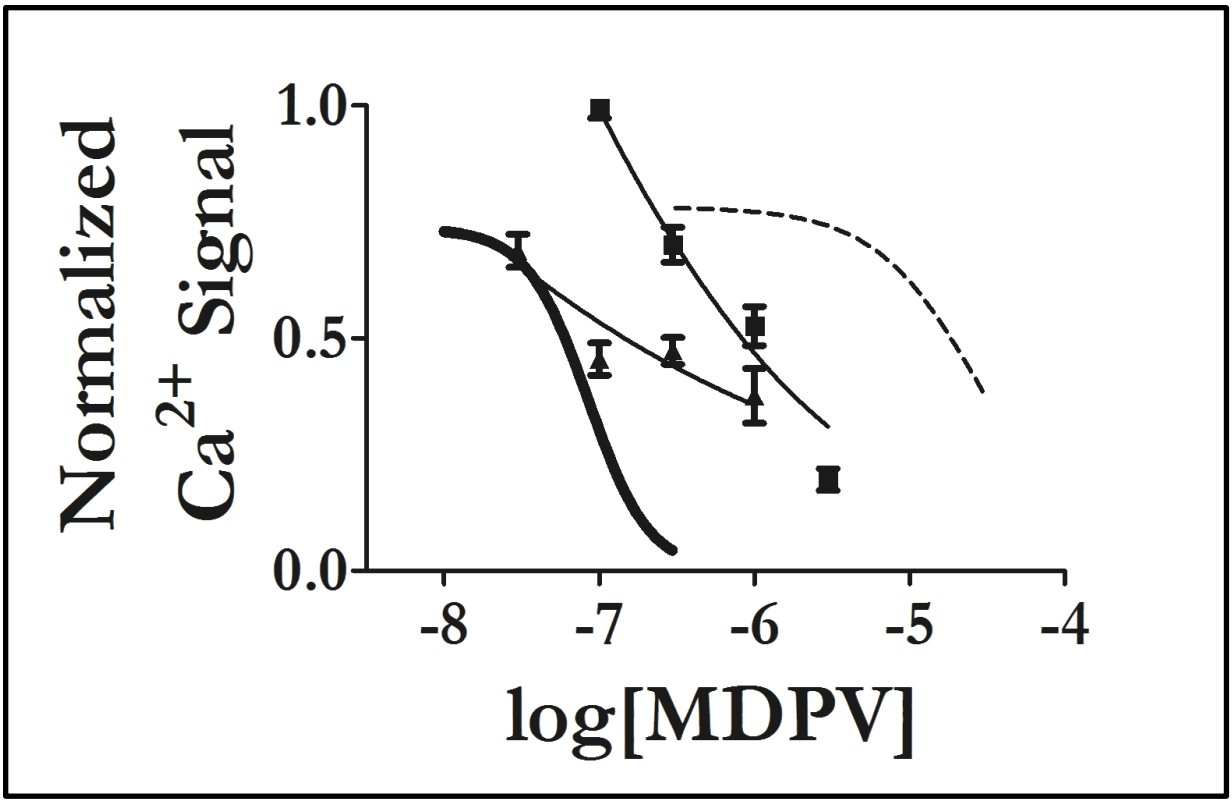

Figure 27. Dose Response Curves for MAT Induced Ca^{2+} Signal Inhibition by MDPV at dDAT AB and dDAT CB Mutants. MDPV dose response at dDAT AB HEK-293 cells in squares. MDPV dose response at dDAT CB HEK-293 cells in triangles. Solid line and dashed line are MDPV dose-responses at hDAT and dDAT wild-type, respectively.

Construct	MDPV IC_{50} (log IC_{50})	n
dDAT wt	-4.535 ± 0.02567	437
dDAT B	-5.040 ± 0.03254	272
dDAT C	-5.130 ± 0.03995	336
dDAT A	-5.325 ± 0.03872	297
dDAT AC	-5.679 ± 0.03451	434
dDAT ABC	-5.949 ± 0.0207	747
dDAT ABCE	-6.641 ± 0.03351	459
hDAT wt	-7.072 ± 0.03759	136

Table 4. Summary of MDPV IC_{50} values in log Scale at hDAT and dDAT Wild-type and Mutant Expressing HEK-293 Cells. A one way ANOVA determined group means to be statistically significant at the $P \leq 0.0001$ level. A post hoc Tukey's HSD test found that all values were significantly different at the $P \leq 0.001$ level, with the exception

of dDAT A vs dDAT C, which was found to be significant at the P≤ 0.01 level. dDAT B vs dDAT C was not significantly different.

Construct	MDPV IC_{50} (nM)
dDAT wt	29,180 ± 1,724
dDAT B	9,121 ± 684
dDAT C	7,410 ± 682
dDAT A	4,727 ± 421
dDAT AC	2,092 ± 166
dDAT ABC	1,126 ± 54
dDAT ABCE	229 ± 18
hDAT wt	85 ± 7

Table 5. Summary of MDPV IC_{50} values in Linear Scale at hDAT and dDAT Wild-type and Mutant Expressing HEK-293 Cells.

Transporter	DA EC_{50} (μM)	MDPV IC_{50} (nM)	K_i from CP Eqn (nM)
dDAT wt	1.49	29,180	3,382
dDAT ABC	2.06	1,126	191
dDAT ABCE	3.21	229	55
hDAT	1.2	84	9

Table 6. Summary of MDPV IC_{50} values, DA EC_{50} Values, and Computed K_i Values at hDAT and dDAT Wild-Type, Triple, and Quadruple Mutant Expressing HEK-293 Cells.

DISCUSSION

4.1 Structural Requirements for High Potency MDPV Inhibition at the Dopamine Transporter

3,4-methylenedioxypyrovalerone (MDPV) is a potent and selective inhibitor of dopamine (DA) uptake by the human dopamine transporter (hDAT).[102-104] Accordingly, it has been shown that MDPV entails a significant abuse liability as determined by intracranial self-stimulation (ICSS) studies of rats.[114] MDPV's ability to facilitate ICSS at low frequencies of stimulation is long acting, which is congruent with the fact that in electrophysiological studies of MDPV at hDAT, MDPV has a distinct and prolonged duration of action.[79] In this work, we sought to understand the structural underpinnings of hDAT's affinity for MDPV. Previous studies of monoamine transporter (MAT) structure using x-ray crystallography highlighted the importance of the central binding site, the S1 site, for inhibitor binding in both the *Drosophila melanogaster* dopamine transporter (dDAT) and the human serotonin transporter (hSERT).[124-127] In an earlier study, dDAT was demonstrated to behave in a pharmacologically intermediate manner between that of hDAT and serotonin transporters (hSERT).[131] Specifically, dDAT was potently inhibited by blockers that also potently inhibited hSERT, which are weak hDAT inhibitors. Conversely, substrates of hDAT that are poorly transported by hSERT, such as amphetamine (AMPH) and DA, are good dDAT substrates. We hypothesized that specific residues within hDAT's S1 were governing MDPV's potent inhibition of hDAT associated currents and uptake. We first determined that MDPV is weak at dDAT (Results, **Figure 9**), as might be presumed from the previously published

pharmacological data discussed above. We then examined the primary sequences of dDAT, hDAT, and hSERT and determined a number of residues that line the S1 that are identical in dDAT and hSERT, but unique in hDAT. The logic underpinning this approach was that shared structural features in the S1 make MDPV weak at hSERT and dDAT, but in hDAT unique residues contribute to strong MDPV binding at the S1. A number of residues resulted from this analysis (Results, **Figure 10**), and a subset was selected that were positioned on the inner face of the S1. We then mutated these residues in dDAT to the corresponding hDAT residues, and recapitulated high potency MDPV inhibition in the fly dopamine transporter.

4.2 The S1 is the Primary Recognition Site in Monoamine Transporters for Inhibitors but not Substrates

The results of this work fit with a previous study that took a similar approach. In that study, it was determined that nonconserved residues in the primary, S1, binding site of hDAT could recapitulate hDAT selective inhibitor binding in the human norepinephrine transporter (hNET).[132] However, the converse was not shown to be true: altering hDAT's S1 site with nonconserved residues from hNET did not confer a hNET-inhibitor selectivity profile to hDAT. Two of the four residues identified by our analysis were identified in that study. In dDAT these correspond to F318 and A117, which are also shared by hNET, implicating these residues' roles in coordinating a number of different inhibitors at MATs. However, in that study, the role of the S2 site and EL4 loops, were investigated for their roles in driving inhibitor selectivity at hNET and hDAT.[132] The nonconserved residues in each of these three areas were swapped en masse between hNET and hDAT. In our work, we investigated the individual contributions of these nonconserved residues alone within the S1. In a similar study, the same group compared residues in hNET and hSERT, but focused on the S1 site.[133] Only one mutation in that study overlapped with alterations to a position in our study and corresponds to the D121 in dDAT, which will be discussed more in depth below. In this investigation, five mutations to hNET to nonconserved hSERT residues recapitulated R- and S-citalopram binding in hNET. The same was not true for the hNET selective inhibitor talopram at hSERT modified with hNET residues.[133] Combined with

our results these studies suggest that inhibitor recognition by MATs occurs primarily in the S1, but not exclusively. Interestingly, in dDAT, our mutations to the S1 did not significantly alter DA recognition. This fits with the emerging view that conserved residues within the S1 are important for substrate transport by MATs, but the structural features that drive substrate selectivity lie outside the S1, or somewhere that has not yet been eluicidated.[134] However, at least one study has suggested that S1 residues may be responsible for governing hDAT and hSERT selectivity for para substituted methcathinone derivatves.[135] In the context of our MDPV results, the fact that DA's potency was only slightly altered from wild-type dDAT through dDAT ABC to ABCE bolsters the idea that these mutations are specifically pertinent to MDPV 's action at the dopamine transporter.

4.3 Docking Results Suggest Potential Differences in dDAT's and hDAT's S1 Sites

The docking results indicate some potential differences between S(+)MDPV binding in dDAT and hDAT. The hDAT homology model was based on dDAT (pdb:4M48) and made using SWISS-MODEL.[136] Since the docking protocol used through AutoDock Vina is rigid body docking, the protein structure is not allowed to reorient itself around the ligand, though the ligand is conformationally flexible. Consequently, the conserved phenylalanine in position 320 in hDAT that is observed over the S1and seen "trapping" S(+) MDPV in the binding pocket is a feature of the homology model before S(+)MDPV was docked. This position for Phe320, which corresponds to Phe319 in dDAT, is associated with the "occluded" state crystal structures with substrates bound.[124-127] SWISS-MODEL uses a template structure and a target sequence to build homology models, and then performs an energy minimization to find the optimal position for side chain rotamers.[136] It is possible that the presence of the neighboring cysteine in hDAT at position 319, which is occupied by a second phenylalanine in dDAT, allows more conformational flexibility to Phe320. Phenylalanine rings are often seen interacting at angles of ~90˚ in crystal structures of proteins, and the replacement of Phe318 in dDAT with Cys319 in hDAT may allow the Phe320 in hDAT to reorient about its rotamer more easily.[137] In other words, in dDAT the Phe318-Phe319 interaction may keep Phe319 oriented away from the S1, whereas in hDAT the

Cys319-Phe320 allows Phe320 more conformational freedom to move over the S1 as the favorable interaction between phenylalanine rings is absent. Furthermore, a second conserved phenylalanine (Phe325 in dDAT and Phe326 in hDAT) is seen slightly shifted in the hDAT homology model. It is possible that the replacement of Pro323 in dDAT with Val324 in hDAT at the center of the transmembrane (TM) 6a-6b interface allows a reorientation of this residue. Proline is notorious for its unique structure, which introduces conformational rigidity to the protein backbone. With Val324 in hDAT, this rigidity is abolished, which may allow the scaffold along the TM 6a-6b linker more conformational flexibility. The changes in 6a-6b brought about by our mutations in dDAT (F318C and P323V) may therefore allow the reorienting of these two conserved phenylalanines (Phe320 and Phe325) in a way that better accommodates MDPV.

In the docking poses of S(+)MDPV at hDAT and dDAT where the methylenedioxy moiety of MDPV is oriented into the TM3 TM8 interface (**Fig 11** for dDAT; **Figs 16** and **18** for hDAT), an obvious difference arises. In the hDAT-S(+)MDPV poses, the methylenedioxy group is seen more deeply positioned into the TM3-TM8 interface. This is likely due to the removal of steric bulk from D121 in dDAT to G153 in hDAT. In our dDAT mutant constructs containing the change D121G, MDPV may be able orient more deeply into this pocket than when binding to wild-type dDAT. D121 is the one residue we investigated that is unique to dDAT, whereas in hSERT this residue is an alanine. However, it is possible that the steric bulk afforded by both aspartate and alanine residues preclude the deep positioning of the methylenedioxy moiety into the TM3-TM8 interface in dDAT and hSERT. In hDAT the glycine at that position would be more

accommodating than either alanine in hSERT or aspartate in dDAT. Also, it is worth noting in MAT crystals the that the amine groups are oriented toward TM1's conserved aspartate residue.[124-127] This interaction is presumed to be essential for transport as mutations to that residue break create non-functional MATs. Therefore, despite the docking scores, the poses that preserve this orientation for the amine group may be more realistic.

No obvious role for the A117S mutation in dDAT is apparent from the docking poses. However, it should be noted that in dDAT and hSERT, a hydrophobic façade is created between TM3 and TM6b. In dDAT, this would include Val120 and Ala117 on TM3 and Phe325 on TM6b. In hSERT, the valine is occupied instead by Ile172, but Ala169 and Phe341 are identical to the dDAT residues. In hDAT, however, a serine occupies the position corresponding to the alanines in dDAT and hSERT. In hDAT, this constitutes a polar punctuation to the continuous hydrophobic façade seen in dDAT and hSERT. It is therefore possible that the A117S in dDAT allows for more favorable interactions with MDPV by orienting MDPV through repulsive interactions with the non-polar regions of MDPV.

It should be noted that the docking only captures snapshots of potential interactions, and dynamical simulations may be needed to fully understand how MDPV orients in the S1 site. Molecular dynamics may also be used to understand how residues such as the conserved phenylalanines on TMs 6a and 6b reorient in MATs and how their conformational distribution may change as a result of mutated neighbors. Furthermore, while the amine-aspartate interaction is considered essential for transport

of substrates, it is possible that multiple binding modes are accommodated in the transport cycle, or for inhibitors specifically. One view offered in this study is that the S1 is in part a space with conserved residues whose conformational ensemble is dictated by nonconserved neighbors as in the 6a-6b region. Conversely, nonconserved residues may contribute directly to differences in binding for MDPV and other inhibitors, such as in the case of the residues along TM3. To probe these differences dynamical simulations will surely be useful, however ongoing research is also pursuing how the mutations investigated here affect the ability inhibitors related to MDPV to inhibit DA induced currents.

REFERENCES CITED

1. Schloss, P., & Williams, D. C. (1998). The serotonin transporter: A primary target for antidepressant drugs. *Journal of Psychopharmacology*, *12*(2), 115–121. https://doi.org/10.1177/026988119801200201

2. Stahl, S. M. (1998). Basic psychopharmacology of antidepressants, part 1: antidepressants have seven distinct mechanisms of action. *Journal of Clinical Psychiatry*, *59*(suppl 4), 5–14.

3. Coppen, A., Shaw, D., Herzberg, B., & Maggs, R. (1967). TRYPTOPHAN IN THE TREATMENT OF DEPRESSION. *The Lancet*, *290*(7527), 1178–1180. https://doi.org/10.1016/S0140-6736(67)91894-6

4. Vaswani, M., Linda, F. K., & Ramesh, S. (2003). Vaswani03, *27*, 1–18. Retrieved from papers://40ab18b2-d275-4dd1-ab17-808c82b9f3da/Paper/p415

5. Vaswani, M., & Kalra, H. (2004). Selective serotonin re-uptake inhibitors in anorexia nervosa. *Expert Opinion on Investigational Drugs*, *13*(4), 349–357. https://doi.org/10.1517/13543784.13.4.349

6. Sghendo, L., & Mifsud, J. (2012). Understanding the molecular pharmacology of the serotonergic system: Using fluoxetine as a model. *Journal of Pharmacy and Pharmacology*, *64*(3), 317–325. https://doi.org/10.1111/j.2042-7158.2011.01384.x

7. Ozaki, N., Goldman, D., Kaye, W. H., Plotnicov, K., Greenberg, B. D., Lappalainen, J., … Murphy, D. L. (2003). Serotonin transporter missense mutation associated with a complex neuropsychiatric phenotype. *Molecular Psychiatry*, *8*(11), 933–936. https://doi.org/10.1038/sj.mp.4001365

8. Kilic, F. (2003). A Human Serotonin Transporter Mutation Causes Constitutive Activation of Transport Activity. *Molecular Pharmacology*, *64*(2), 440–446. https://doi.org/10.1124/mol.64.2.440

9. Lesch, K.-P., Bengel, D., Heils, A., Sabol, S. Z., Greenberg, B. D., Petri, S., … Murphy, D. L. (1996). Association of Anxiety-Related Traits with a Polymorphism in the Serotonin Transporter Gene Regulatory Region. *Science*, *274*(5292), 1527–1531. https://doi.org/10.1126/science.274.5292.1527

10. Wilkie, M. J. V., Smith, G., Day, R. K., Matthews, K., Smith, D., Blackwood, D., … Wolf, C. R. (2009). Polymorphisms in the SLC6A4 and HTR2A genes influence treatment outcome following antidepressant therapy. *Pharmacogenomics Journal*, *9*(1), 61–70. https://doi.org/10.1038/sj.tpj.6500491

11. Torres, G. E., Gainetdinov, R. R., & Caron, M. G. (2003). Plasma membrane monoamine transporters: Structure, regulation and function. *Nature Reviews Neuroscience*, *4*(1), 13–25. https://doi.org/10.1038/nrn1008

12. Gainetdinov, R. R., & Caron, M. G. (2003). Monoamine Transporters: From Genes to Behavior. *Annual Review of Pharmacology and Toxicology*, *43*(1), 261–284. https://doi.org/10.1146/annurev.pharmtox.43.050802.112309

13. Bozzi, Y., & Borrelli, E. (2006). Dopamine in neurotoxicity and neuroprotection: What do D2 receptors have to do with it? *Trends in Neurosciences*, *29*(3), 167–174. https://doi.org/10.1016/j.tins.2006.01.002

14. Di Chiara, G., & Imperato, A. (1988). Drugs abused by humans preferentially increase synaptic dopamine concentrations in the mesolimbic system of freely moving rats. *Proceedings of the National Academy of Sciences of the United States of America*, *85*(14), 5274–5278. Retrieved from http://www.ncbi.nlm.nih.gov/pubmed/2899326%0Ahttp://www.pubmedcentral.nih.gov/articlerender.fcgi?artid=PMC281732

15. Hyman, S. E., Malenka, R. C., & Nestler, E. J. (2006). NEURAL MECHANISMS OF ADDICTION: The Role of Reward-Related Learning and Memory. *Annual Review of Neuroscience*, *29*(1), 565–598. https://doi.org/10.1146/annurev.neuro.29.051605.113009

16. Sulzer, D. (2011). How Addictive Drugs Disrupt Presynaptic Dopamine Neurotransmission. *Neuron*, *69*(4), 628–649. https://doi.org/10.1016/j.neuron.2011.02.010

17. Amara, S. G., & Sonders, M. S. (1998). Neurotransmitter transporters as molecular targets for addictive drugs. *Drug and Alcohol Dependence*, *51*(1–2), 87–96. https://doi.org/10.1016/S0376-8716(98)00068-4

18. Bédard, A.-C., Schulz, K. P., Cook, E. H., Fan, J., Clerkin, S. M., Ivanov, I., … Newcorn, J. H. (2010). Dopamine transporter gene variation modulates activation of striatum in youth with ADHD. *NeuroImage*, *53*(3), 935–942. https://doi.org/10.1016/j.neuroimage.2009.12.041

19. Froehlich, T. E., Epstein, J. N., Nick, T. G., Melguizo Castro, M. S., Stein, M. A., Brinkman, W. B., … Kahn, R. S. (2011). Pharmacogenetic predictors of methylphenidate dose-response in attention-deficit/hyperactivity disorder. *Journal of the American Academy of Child and Adolescent Psychiatry*, *50*(11), 1129-1139.e2. https://doi.org/10.1016/j.jaac.2011.08.002

20. Mazei-Robison, M. S., Bowton, E., Holy, M., Schmudermaier, M., Freissmuth, M., Sitte, H. H., … Blakely, R. D. (2008). Anomalous Dopamine Release Associated with a Human Dopamine Transporter Coding Variant. *Journal of Neuroscience*, *28*(28), 7040–7046. https://doi.org/10.1523/JNEUROSCI.0473-08.2008

21. Tellioglu, T., & Robertson, D. (2001). Genetic or acquired deficits in the norepinephrine transporter: current understanding of clinical implications. *Expert*

Reviews in Molecular Medicine, *3*(29), 1–10. https://doi.org/10.1017/s1462399401003878

22. Yehuda, R., Siever, L. J., Teicher, M. H., Levengood, R. A., Gerber, D. K., Schmeidler, J., & Yang, R. K. (1998). Plasma norepinephrine and 3-methoxy-4-hydroxyphenylglycol concentrations and severity of depression in combat posttraumatic stress disorder and major depressive disorder. *Biological Psychiatry*, *44*(1), 56–63. https://doi.org/10.1016/S0006-3223(98)80007-3

23. Lake, C. R., Pickar, D., Ziegler, M. G., Lipper, S., Slater, S., & Murphy, D. L. (1982). High plasma norepinephrine levels in patients with major affective disorder. *American Journal of Psychiatry*, *139*(10), 1315–1318. https://doi.org/10.1176/ajp.139.10.1315

24. Goekoop, J. G., de Winter, R. F. p., Wolterbeek, R., Van Kempen, G. M. j., & Wiegant, V. M. (2012). Increased plasma norepinephrine concentration in psychotic depression. *Therapeutic Advances in Psychopharmacology*, *2*(2), 51–63. https://doi.org/10.1177/2045125312436574

25. Shannon, J. R., Flattem, N. L., Jordan, J., Jacob, G., Black, B. K., Biaggioni, I., … Robertson, D. (2000). Orthostatic Intolerance and Tachycardia Associated with Norepinephrine-Transporter Deficiency. *New England Journal of Medicine*, *342*(8), 541–549. https://doi.org/10.1056/NEJM200002243420803

26. Perland, E., & Fredriksson, R. (2017). Classification Systems of Secondary Active Transporters. *Trends in Pharmacological Sciences*, *38*(3), 305–315. https://doi.org/10.1016/j.tips.2016.11.008

27. Ramamoorthy, S., Baumant, A. L., Mooret, K. R., Han4, H., Yang-Feng, T., Chang, A. S., … Blakelyt, R. D. (1993). Antidepressant-and cocaine-sensitive human serotonin transporter: Molecular cloning, expression, and chromosomal localization

28. Kawarai, T., Kawakami, H., Yamamura, Y., & Nakamura, S. (1997). Structure and organization of the gene encoding human dopamine transporter. *Gene*, *195*(1), 11–18. https://doi.org/10.1016/S0378-1119(97)00131-5

29. Pörzgen, P., Bonisch, H., & Bruss, M. (1995). Molecular Cloning and Organization of the Coding Region of the Human Norepinephrine Transporter Gene. *Biochemical and Biophysical Research Communications*. https://doi.org/10.1006/bbrc.1995.2582

30. Pörzgen, P., Bönisch, H., Hammermann, R., & Brüss, M. (1998). The human noradrenaline transporter gene contains multiple polyadenylation sites and two alternatively spliced C-terminal exons. *Biochimica et Biophysica Acta - Gene Structure and Expression*, *1398*(3), 365–370. https://doi.org/10.1016/S0167-4781(98)00072-4

31. Morón, J. A., Brockington, A., Wise, R. A., Rocha, B. A., & Hope, B. T. (2002). Dopamine uptake through the norepinephrine transporter in brain regions with low levels of the dopamine transporter: evidence from knock-out mouse lines. *The Journal of Neuroscience : The Official Journal of the Society for Neuroscience*, *22*(2), 389–395. Retrieved from http://www.ncbi.nlm.nih.gov/pubmed/11784783

32. Hoffman, B. J., Hansson, S. R., Mezey, É., & Palkovits, M. (1998). Localization and dynamic regulation of biogenic amine transporters in the mammalian central nervous system. *Frontiers in Neuroendocrinology*, *19*(3), 187–231. https://doi.org/10.1006/frne.1998.0168

33. Giros, B., Jaber, M., Jones, S. R., Wightman, R. M., & Caron, M. G. (1996). Hyperlocomotion and indifference to cocaine and amphetamine in mice lacking the dopamine transporter. *Nature*, *379*(6566), 606–612. https://doi.org/10.1038/379606a0

34. Jones, S. R., Gainetdinov, R. R., Wightman, R. M., & Caron, M. G. (1998). Mechanisms of Amphetamine Action Revealed in Mice Lacking the Dopamine Transporter. *The Journal of Neuroscience*, *18*(6), 1979–1986. https://doi.org/10.1523/JNEUROSCI.18-06-01979.1998

35. Gainetdinov, R. R. (2008). Dopamine transporter mutant mice in experimental neuropharmacology. *Naunyn-Schmiedeberg's Archives of Pharmacology*, *377*(4–6), 301–313. https://doi.org/10.1007/s00210-007-0216-0

36. Bengel, D., Murphy, D. L., Andrews, A. M., Wichems, C. H., Feltner, D., Heils, A., … Lesch, K. P. (1998). Altered brain serotonin homeostasis and locomotor insensitivity to 3, 4-methylenedioxymethamphetamine ("Ecstasy") in serotonin transporter-deficient mice. *Molecular Pharmacology*, *53*(4), 649–655.

37. Rudnick S. C., G. . W. (1993). Non-neurotoxic amphetamine derivatives release serotonin through serotonin transporters. *Mol Pharmacol*, *43*(2), 271–276.

38. Fox, M. A., Jensen, C. L., French, H. T., Stein, A. R., Huang, S. J., Tolliver, T. J., & Murphy, D. L. (2008). Neurochemical, behavioral, and physiological effects of pharmacologically enhanced serotonin levels in serotonin transporter (SERT)-deficient mice. *Psychopharmacology*, *201*(2), 203–218. https://doi.org/10.1007/s00213-008-1268-7

39. Caron, M. G., Xu, F., Gainetdinov, R. R., Wetsel, W. C., Jones, S. R., Bohn, L. M., … Wang, Y.-M. (2000). Mice lacking the norepinephrine transporter are supersensitive to psychostimulants. *Nature Neuroscience*, *3*(5), 465–471. https://doi.org/10.1038/74839

40. Jardetzky, O. (1966). Simple Allosteric Model for Membrane Pumps. *Nature*, *211*(5052), 969–970. https://doi.org/10.1038/211969a0

41. Rudnick, G. (1998). Bioenergetics of neurotransmitter transport. *Journal of Bioenergetics and Biomembranes*, *30*(2), 173–185. https://doi.org/10.1023/A:102057332

42. Rudnick, G. (1998). Ion-coupled neurotransmitter transport: Thermodynamic vs. kinetic determinations of stoichiometry. *Methods in Enzymology*, *296*, 233–247. https://doi.org/10.1016/S0076-6879(98)96018-9

43. Rudnick, G., & Clark, J. (1993). From synapse to vesicle: The reuptake and storage of biogenic amine neurotransmitters. *BBA - Bioenergetics*, *1144*(3), 249–263. https://doi.org/10.1016/0005-2728(93)90109-S

44. Gu, H., Wall, S. C., & Rudnick, G. (1994). Stable expression of biogenic amine transporters reveals differences in inhibitor sensitivity, kinetics, and ion dependence. *Journal of Biological Chemistry*, *269*(10), 7124–7130.

45. Sonders, M. S., & Amara, S. G. (1996). Channels in transporters. *Current Opinion in Neurobiology*, *6*(3), 294–302. https://doi.org/10.1016/S0959-4388(96)80111-5

46. Mager, S., Min, C., Henry, D. J., Chavkintt, C., Hoffman, B. J., Davidson, N., & Lester, H. A. (1994). Conducting states of a mammalian serotonin transporter. *Neuron*, *12*(4), 845–859. https://doi.org/10.1016/0896-6273(94)90337-9

47. Galli, A., DeFelice, L. J., Duke, B. J., Moore, K. R., & Blakely, R. D. (1995). Sodium-dependent norepinephrine-induced currents in norepinephrine-transporter-transfected HEK-293 cells blocked by cocaine and antidepressants. *The Journal of Experimental Biology*, *198*(Pt 10), 2197–2212. Retrieved from http://www.ncbi.nlm.nih.gov/pubmed/7500004

48. Sonders, M. S., Zhu, S. J., Zahniser, N. R., Kavanaugh, M. P., & Amara, S. G. (1997). Multiple ionic conductances of the human dopamine transporter: the actions of dopamine and psychostimulants. *The Journal of Neuroscience : The Official Journal of the Society for Neuroscience*, *17*(3), 960–974. Retrieved from http://www.ncbi.nlm.nih.gov/pubmed/8994051

49. DeFelice, L. J., & Blakely, R. D. (1996). Pore models for transporters? *Biophysical Journal*, *70*(2), 579–580. https://doi.org/10.1016/S0006-3495(96)79604-2

50. DeFelice, L. J., & Goswami, T. (2007). Transporters as Channels. *Annual Review of Physiology*, *69*(1), 87–112. https://doi.org/10.1146/annurev.physiol.69.031905.164816

51. Adams, S. V., & DeFelice, L. J. (2002). Flux coupling in the human serotonin transporter. *Biophysical Journal*, *83*(6), 3268–3282. https://doi.org/10.1016/S0006-3495(02)75328-9

52. Adams, S. V., & DeFelice, L. J. (2003). Ionic currents in the human serotonin transporter reveal inconsistencies in the alternating access hypothesis. *Biophysical Journal*, *85*(3), 1548–1559. https://doi.org/10.1016/S0006-3495(03)74587-1

53. Ramsey, I. S., & DeFelice, L. J. (2002). Serotonin Transporter Function and Pharmacology Are Sensitive to Expression Level. *Journal of Biological Chemistry*, *277*(17), 14475–14482. https://doi.org/10.1074/jbc.m110783200

54. DeFelice, L. J. (2004). Going against the flow. *Nature*, *432*(7015), 279. https://doi.org/10.1038/432279a

55. Borre, L., Andreassen, T. F., Shi, L., Weinstein, H., & Gether, U. (2014). The second sodium site in the dopamine transporter controls cation permeation and is regulated by chloride. *Journal of Biological Chemistry*, *289*(37), 25764–25773. https://doi.org/10.1074/jbc.M114.574269

56. Carvelli, L., McDonald, P. W., Blakely, R. D., & DeFelice, L. J. (2004). Dopamine transporters depolarize neurons by a channel mechanism. *Proceedings of the National Academy of Sciences*, *101*(45), 16046–16051. https://doi.org/10.1073/pnas.0403299101

57. Ingram, S. L., Prasad, B. M., & Amara, S. G. (2002). Dopamine transporter-mediated conductances increase excitability of midbrain dopamine neurons. *Nature Neuroscience*, *5*(10), 971–978. https://doi.org/10.1038/nn920

58. De Felice, L. J. (2017). Monoamine Transporters as Ionotropic Receptors. *Trends in Neurosciences*, *40*(4), 195–196. https://doi.org/10.1016/j.tins.2017.02.003

59. Aversa, D., Martini, A., Guatteo, E., Pisani, A., Mercuri, N. B., & Berretta, N. (2018). Reversal of dopamine-mediated firing inhibition through activation of the dopamine transporter in substantia nigra pars compacta neurons. *British Journal of Pharmacology*, *175*(17), 3534–3547. https://doi.org/10.1111/bph.14422

60. Schicker, K., Uzelac, Z., Gesmonde, J., Bulling, S., Stockner, T., Freissmuth, M., … Sandtner, W. (2012). Unifying concept of serotonin transporter-associated currents. *Journal of Biological Chemistry*, *287*(1), 438–445. https://doi.org/10.1074/jbc.M111.304261

61. Niello, M., Cintulova, D., Hellsberg, E., Jäntsch, K., Holy, M., Ayatollahi, L. H., … Sitte, H. H. (2019). para-Trifluoromethyl-methcathinone is an allosteric modulator of the serotonin transporter. *Neuropharmacology*, (April), 1–12. https://doi.org/10.1016/j.neuropharm.2019.04.021

62. Sitte, H. H., & Freissmuth, M. (2015). Amphetamines, new psychoactive drugs and the monoamine transporter cycle. *Trends in Pharmacological Sciences*, *36*(1), 41–50. https://doi.org/10.1016/j.tips.2014.11.006

63. Naftalin, R. J. (2018). A critique of the alternating access transporter model of uniport glucose transport. *Biophysics Reports*, *4*(6), 287–299. https://doi.org/10.1007/s41048-018-0076-9

64. Naftalin, R. J. (2010). Reassessment of models of facilitated transport and cotransport. *Journal of Membrane Biology*, *234*(2), 75–112. https://doi.org/10.1007/s00232-010-9228-7

65. Naftalin, R. J. (2008). Alternating carrier models of asymmetric glucose transport violate the energy conservation laws. *Biophysical Journal*, *95*(9), 4300–4314. https://doi.org/10.1529/biophysj.108.136366

66. Cameron, K. N., Solis, E., Ruchala, I., De Felice, L. J., & Eltit, J. M. (2015). Amphetamine activates calcium channels through dopamine transporter-mediated depolarization. *Cell Calcium*, *58*(5), 457–466. https://doi.org/10.1016/j.ceca.2015.06.013

67. Rothman, R. B., & Baumann, M. H. (2003). Monoamine transporters and psychostimulant drugs. *European Journal of Pharmacology*, *479*(1–3), 23–40. https://doi.org/10.1016/j.ejphar.2003.08.054

68. Sulzer, D., Chen, T. K., Lau, Y. Y., Kristensen, H., Rayport, S., & Ewing, A. (1995). Amphetamine redistributes dopamine from synaptic vesicles to the cytosol and promotes reverse transport. *The Journal of Neuroscience : The Official Journal of the Society for Neuroscience*, *15*(5 Pt 2), 4102–4108. Retrieved from http://www.ncbi.nlm.nih.gov/pubmed/7751968

69. Seiden, L. S., Sabol, K. E., & Ricaurte, G. A. (1993). Amphetamine: effects on catecholamine systems and behavior. *Annual Review of Pharmacology and Toxicology*, *33*, 639–677. https://doi.org/10.1146/annurev.pa.33.040193.003231

70. Ritz, M. C., Lamb, R. J., Goldberg, S. R., & Kuhar, M. J. (1987). Cocaine receptors on dopamine transporters are related to self-administration of cocaine. *Science*, *237*(4819), 1219–1223. https://doi.org/10.1126/science.2820058

71. Carboni, E., Tanda, G. L., Frau, R., & Chiara, G. Di. (1990). Blockade of the Noradrenaline Carrier Increases Extracellular Dopamine Concentrations in the Prefrontal Cortex: Evidence that Dopamine Is Taken up In Vivo by Noradrenergic Terminals. *Journal of Neurochemistry*, *55*(3), 1067–1070. https://doi.org/10.1111/j.1471-4159.1990.tb04599.x

72. Rothman, R. B., Lewis, B., Dersch, C., Xu, H., Radesca, L., De Costa, B. R., … Pert, A. (1993). Identification of a GBR12935 homolog, LR1111, which is over 4,000-fold selective for the dopamine transporter, relative to serotonin and norepinephrine transporters. *Synapse*, *14*(1), 34–39. https://doi.org/10.1002/syn.890140106

73. Rothman, R. B., Baumann, M. H., Dersch, C. M., Romero, D. V., Rice, K. C., Carroll, F. I., & Partilla, J. S. (2001). Amphetamine-type central nervous system stimulants release norepinephrine more potently than they release dopamine and serotonin. *Synapse*, *39*(1), 32–41. https://doi.org/10.1002/1098-2396(20010101)39:1<32::AID-SYN5>3.0.CO;2-3

74. Rothman, R. B. (2003). In Vitro Characterization of Ephedrine-Related Stereoisomers at Biogenic Amine Transporters and the Receptorome Reveals Selective Actions as Norepinephrine Transporter Substrates. *Journal of Pharmacology and Experimental Therapeutics*, *307*(1), 138–145. https://doi.org/10.1124/jpet.103.053975

75. Scholze, P., Zwach, J., Kattinger, A., Pifl, C., Singer, E. A., & Sitte, H. H. (2000). Transporter-mediated release: a superfusion study on human embryonic kidney cells stably expressing the human serotonin transporter. *The Journal of Pharmacology and Experimental Therapeutics*, *293*(3), 870–878. Retrieved from http://www.ncbi.nlm.nih.gov/pubmed/10869387

76. Rothman, R. B., Partilla, J. S., Baumann, M. H., Lightfoot-Siordia, C., & Blough, B. E. (2012). Studies of the Biogenic Amine Transporters. 14. Identification of Low-Efficacy “Partial” Substrates for the Biogenic Amine Transporters. *Journal of Pharmacology and Experimental Therapeutics*, *341*(1), 251–262. https://doi.org/10.1124/jpet.111.188946

77. Cameron, K., Kolanos, R., Verkariya, R., De Felice, L., & Glennon, R. A. (2013). Mephedrone and methylenedioxypyrovalerone (MDPV), major constituents of “bath salts,” produce opposite effects at the human dopamine transporter. *Psychopharmacology*, *227*(3), 493–499. https://doi.org/10.1007/s00213-013-2967-2

78. Solis, E., Partilla, J. S., Sakloth, F., Ruchala, I., Schwienteck, K. L., De Felice, L. J., … Baumann, M. H. (2017). N-Alkylated Analogs of 4-Methylamphetamine (4-MA) Differentially Affect Monoamine Transporters and Abuse Liability. *Neuropsychopharmacology*, *42*(10), 1950–1961. https://doi.org/10.1038/npp.2017.98

79. Cameron, K. N., Kolanos, R., Solis, E., Glennon, R. A., & De Felice, L. J. (2013). Bath salts components mephedrone and methylenedioxypyrovalerone (MDPV) act synergistically at the human dopamine transporter. *British Journal of Pharmacology*, *168*(7), 1750–1757. https://doi.org/10.1111/bph.12061

80. Steele, T. W. E., & Eltit, J. M. (2018). Using Ca 2+ -channel biosensors to profile amphetamines and cathinones at monoamine transporters: electro-engineering cells to detect potential new psychoactive substances. *Psychopharmacology*. https://doi.org/10.1007/s00213-018-5103-5

81. Ruchala, I., Cabra, V., Solis, E., Glennon, R. A., De Felice, L. J., & Eltit, J. M. (2014). Electrical coupling between the human serotonin transporter and voltage-

gated Ca(2+) channels. *Cell Calcium*, *56*(1), 25–33. https://doi.org/10.1016/j.ceca.2014.04.003

82. Battisti, U. M., Sitta, R., Harris, A., Sakloth, F., Walther, D., Ruchala, I., … Eltit, J. M. (2018). Effects of N-Alkyl-4-Methylamphetamine Optical Isomers on Plasma Membrane Monoamine Transporters and Abuse-Related Behavior. *ACS Chemical Neuroscience*, *9*(7), 1829–1839. research-article. https://doi.org/10.1021/acschemneuro.8b00138

83. Moerke, M. J., Ananthan, S., Banks, M. L., Eltit, J. M., Freitas, K. C., Johnson, A. R., … Negus, S. S. (2018). Interactions between Cocaine and the Putative Allosteric Dopamine Transporter Ligand SRI-31142. *Journal of Pharmacology and Experimental Therapeutics*, *367*(2), 222–233. https://doi.org/10.1124/jpet.118.250902

84. Sulzer, D., Sonders, M. S., Poulsen, N. W., & Galli, A. (2005). Mechanisms of neurotransmitter release by amphetamines: A review. *Progress in Neurobiology*, *75*(6), 406–433. https://doi.org/10.1016/j.pneurobio.2005.04.003

85. Gettig, J. P., Grady, S. E., & Nowosadzka, I. (2006). Methamphetamine: putting the brakes on speed. *The Journal of School Nursing : The Official Publication of the National Association of School Nurses*, *22*(2), 66–73.

86. Melega, W. P., Williams, A. E., Schmitz, D. A., DiStefano, E. W., & Cho, A. K. (1995). Pharmacokinetic and pharmacodynamic analysis of the actions of D-amphetamine and D-methamphetamine on the dopamine terminal. *The Journal of Pharmacology and Experimental Therapeutics*, *274*(1), 90–96.

87. Goodwin, J. S., Larson, G. A., Swant, J., Sen, N., Javitch, J. A., Zahniser, N. R., … Khoshbouei, H. (2009). Amphetamine and methamphetamine differentially affect dopamine transporters in vitro and in vivo. *Journal of Biological Chemistry*, *284*(5), 2978–2989. https://doi.org/10.1074/jbc.M805298200

88. Shoblock, J. R., Maisonneuve, I. M., & Glick, S. D. (2003). Differences between d-methamphetamine and d-amphetamine in rats: Working memory, tolerance, and extinction. *Psychopharmacology*, *170*(2), 150–156. https://doi.org/10.1007/s00213-003-1522-y

89. Shoblock, J. R., Sullivan, E. B., Maisonneuve, I. M., & Glick, S. D. (2003). Neurochemical and behavioral differences between d-methamphetamine and d-amphetamine in rats. *Psychopharmacology*, *165*(4), 359–369. https://doi.org/10.1007/s00213-002-1288-7

90. Baumann, M. H., Solis, E., Watterson, L. R., Marusich, J. A., Fantegrossi, W. E., & Wiley, J. L. (2014). Baths Salts, Spice, and Related Designer Drugs: The Science Behind the Headlines. *Journal of Neuroscience*, *34*(46), 15150–15158. https://doi.org/10.1523/JNEUROSCI.3223-14.2014

91. Madras, B. K. (2016). The Growing Problem of New Psychoactive Substances (NPS) (pp. 1–18). https://doi.org/10.1007/7854_2016_34

92. Baumann, M. H., & Volkow, N. D. (2016). Abuse of New Psychoactive Substances: Threats and Solutions. *Neuropsychopharmacology*, *41*(3), 663–665. https://doi.org/10.1038/npp.2015.260

93. Shulgin S, Shulgin A. (1991) PiHKAL:A Chemical Love Story. Berkeley: Transform Press

94. Shulgin S, Shulgin A. (1997) TiHKAL:The Continuation. Berkeley: Transform Press

95. Nugteren-van Lonkhuyzen, J. J., van Riel, A. J. H. P., Brunt, T. M., & Hondebrink, L. (2015). Pharmacokinetics, pharmacodynamics and toxicology of new psychoactive substances (NPS): 2C-B, 4-fluoroamphetamine and benzofurans. *Drug and Alcohol Dependence*, *157*, 18–27. https://doi.org/10.1016/j.drugalcdep.2015.10.011

96. Bernschneider-Reif, S., Öxler, F., & Freudenmann, R. W. (2006). The origin of MDMA ("Ecstasy") - Separating the facts from the myth. *Pharmazie*, *61*(11), 966–972.

97. De Felice, L. J., Glennon, R. A., & Negus, S. S. (2014). Synthetic cathinones: Chemical phylogeny, physiology, and neuropharmacology. *Life Sciences*, *97*(1), 20–26. https://doi.org/10.1016/j.lfs.2013.10.029

98. Marinetti, L. J., & Antonides, H. M. (2013). Analysis of Synthetic Cathinones Commonly Found in Bath Salts in Human Performance and Postmortem To.pdf. *Journal of Analytical Toxicology*, (2), 1–12.

99. Shanks, K. G., Dahn, T., Behonick, G., & Terrell, A. (2012). Analysis of first and second generation legal highs for synthetic cannabinoids and synthetic stimulants by ultra-performance liquid chromatography and time of flight mass spectrometry. *Journal of Analytical Toxicology*, *36*(6), 360–371. https://doi.org/10.1093/jat/bks047

100. Baumann, M. H., Partilla, J. S., Lehner, K. R., Thorndike, E. B., Hoffman, A. F., Holy, M., … Schindler, C. W. (2013). Powerful cocaine-like actions of 3,4-methylenedioxypyrovalerone (MDPV), a principal constituent of psychoactive "bath salts" products. *Neuropsychopharmacology*, *38*(4), 552–562. https://doi.org/10.1038/npp.2012.204

101. Glennon, R. A., & Dukat, M. (2016). Structure-Activity Relationships of Synthetic Cathinones (pp. 19–47). https://doi.org/10.1007/7854_2016_41

102. Kolanos, R., Solis, E., Sakloth, F., De Felice, L. J., & Glennon, R. A. (2013). "deconstruction" of the abused synthetic cathinone methylenedioxypyrovalerone

(MDPV) and an examination of effects at the human dopamine transporter. *ACS Chemical Neuroscience*, *4*(12), 1524–1529. https://doi.org/10.1021/cn4001236

103. Marusich, J. A., Antonazzo, K. R., Wiley, J. L., Blough, B. E., Partilla, J. S., & Baumann, M. H. (2014). Pharmacology of novel synthetic stimulants structurally related to the "bath salts" constituent 3,4-methylenedioxypyrovalerone (MDPV). *Neuropharmacology*, *87*, 206–213. https://doi.org/10.1016/j.neuropharm.2014.02.016

104. Kolanos, R., Sakloth, F., Jain, A. D., Partilla, J. S., Baumann, M. H., & Glennon, R. A. (2015). Structural Modification of the Designer Stimulant α-Pyrrolidinovalerophenone (α-PVP) Influences Potency at Dopamine Transporters. *ACS Chemical Neuroscience*, *6*(10), 1726–1731. https://doi.org/10.1021/acschemneuro.5b00160

105. Bonano, J. S., Banks, M. L., Kolanos, R., Sakloth, F., Barnier, M. L., Glennon, R. A., … Negus, S. S. (2015). Quantitative structure-activity relationship analysis of the pharmacology of para-substituted methcathinone analogues. *British Journal of Pharmacology*, *172*(10), 2433–2444. https://doi.org/10.1111/bph.13030

106. Saha, K., Li, Y., Holy, M., Lehner, K. R., Bukhari, M. O., Partilla, J. S., … Baumann, M. H. (2018). The synthetic cathinones, butylone and pentylone, are stimulants that act as dopamine transporter blockers but 5-HT transporter substrates. *Psychopharmacology*. https://doi.org/10.1007/s00213-018-5075-5

107. Nutt, D. J., King, L. A., & Nichols, D. E. (2013). Effects of Schedule I drug laws on neuroscience research and treatment innovation. *Nature Reviews Neuroscience*, *14*(8), 577–585. https://doi.org/10.1038/nrn3530

108. Nestler, E. J. (2013). Cellular basis of memory for addiction. *Dialogues in Clinical Neuroscience*, *15*(4), 431–443.

109. Olds, J., & Milner, P. (1954). Positive reinforcement produced by electrical stimulation of septal area and other regions of rat brain. *Journal of Comparative and Physiological Psychology*, *47*(6), 419–427.

110. Wise, R. A. (1996). Addictive Drugs and Brain Stimulation Reward. *Annual Review of Neuroscience*, *19*(1), 319–340. https://doi.org/10.1146/annurev.neuro.19.1.319

111. Vlachou, S., & Markou, A. (2011). Intracranial Self-Stimulation (pp. 3–56). https://doi.org/10.1007/978-1-60761-934-5_1

112. Bauer, C. T., Banks, M. L., Blough, B. E., & Negus, S. S. (2013). Use of intracranial self-stimulation to evaluate abuse-related and abuse-limiting effects of monoamine releasers in rats. *British Journal of Pharmacology*, *168*(4), 850–862. https://doi.org/10.1111/j.1476-5381.2012.02214.x

113. Suyama, J. A., Sakloth, F., Kolanos, R., Glennon, R. A., Lazenka, M. F., Negus, S. S., & Banks, M. L. (2015). Abuse-Related Neurochemical Effects of Para-Substituted Methcathinone Analogs in Rats: Microdialysis Studies of Nucleus Accumbens Dopamine and Serotonin. *Journal of Pharmacology and Experimental Therapeutics*, *356*(1), 182–190. https://doi.org/10.1124/jpet.115.229559

114. Bonano, J. S., Glennon, R. A., De Felice, L. J., Banks, M. L., & Negus, S. S. (2014). Abuse-related and abuse-limiting effects of methcathinone and the synthetic "bath salts" cathinone analogs methylenedioxypyrovalerone (MDPV), methylone and mephedrone on intracranial self-stimulation in rats. *Psychopharmacology*, *231*(1), 199–207. https://doi.org/10.1007/s00213-013-3223-5

115. Yamashita, A., Singh, S. K., Kawate, T., Jin, Y., & Gouaux, E. (2005). Crystal structure of a bacterial homologue of Na+/Cl--dependent neurotransmitter transporters. *Nature*, *437*(7056), 215–223.https://doi.org/10.1038/nature03978

116. Singh, S. K. (2008). LeuT: A prokaryotic stepping stone on the way to a eukaryotic neurotransmitter transporter structure. *Channels*, *2*(5), 380–389. https://doi.org/10.4161/chan.2.5.6904

117. Pacholczyk T, Blakely RD, A. S. (1991). Expression cloning of an antidepressant-sensitive noradrenaline transporter. *Letters To Nature*, *350*(March), 350.

118. Chen, J. G., Liu-Chen, S., & Rudnick, G. (1998). Determination of external loop topology in the serotonin transporter by site-directed chemical labeling. *Journal of Biological Chemistry*, *273*(20), 12675–12681. https://doi.org/10.1074/jbc.273.20.12675

119. Zhou, Z., Zhen, J., Karpowich, N. K., Goetz, R. M., Law, C. J., Reith, M. E. A., & Wang, D.-N. (2007). LeuT-Desipramine Structure Reveals How Antidepressants Block Neurotransmitter Reuptake. *Science*, *317*(5843), 1390–1393. https://doi.org/10.1126/science.1147614

120. Singh, S. K., Yamashita, A., & Gouaux, E. (2007). Antidepressant binding site in a bacterial homologue of neurotransmitter transporters. *Nature*, *448*(7156), 952–956. https://doi.org/10.1038/nature06038

121. Singh, S. K., Piscitelli, C. L., Yamashita, A., & Gouaux, E. (2008). A Competitive Inhibitor Traps LeuT in an Open-to-Out Conformation. *Science*, *322*(5908), 1655–1661. https://doi.org/10.1126/science.1166777

122. Jørgensen, A. M., Tagmose, L., Jørgensen, A. M. M., Topiol, S., Sabio, M., Gundertofte, K., … Peters, G. H. (2007). Homology modeling of the serotonin

transporter: Insights into the primary escitalopram-binding site. *ChemMedChem*, *2*(6), 815–826. https://doi.org/10.1002/cmdc.200600242

123. Beuming, T., Kniazeff, J., Bergmann, M. L., Shi, L., Gracia, L., Raniszewska, K., … Loland, C. J. (2008). The binding sites for cocaine and dopamine in the dopamine transporter overlap. *Nature Neuroscience*, *11*(7), 780–789. https://doi.org/10.1038/nn.2146

124. Penmatsa, A., Wang, K. H., & Gouaux, E. (2013). X-ray structure of dopamine transporter elucidates antidepressant mechanism. *Nature*, *503*(7474), 85–90. https://doi.org/10.1038/nature12533

125. Wang, H., Goehring, A., Wang, K. H., Penmatsa, A., Ressler, R., & Gouaux, E. (2013). Structural basis for action by diverse antidepressants on biogenic amine transporters. *Nature*, *503*(7474), 141–145. https://doi.org/10.1038/nature12648

126. Wang, K. H., Penmatsa, A., & Gouaux, E. (2015). Neurotransmitter and psychostimulant recognition by the dopamine transporter. *Nature*, *521*(7552), 322–327. https://doi.org/10.1038/nature14431

127. Coleman, J. A., Green, E. M., & Gouaux, E. (2016). X-ray structures and mechanism of the human serotonin transporter. *Nature*, *532*(7599), 334–339. https://doi.org/10.1038/nature17629

128. Henry, L. K., Field, J. R., Adkins, E. M., Parnas, M. L., Vaughan, R. A., Zou, M. F., … Blakely, R. D. (2006). Tyr-95 and Ile-172 in transmembrane segments 1 and 3 of human serotonin transporters interact to establish high affinity recognition of antidepressants. *Journal of Biological Chemistry*, *281*(4), 2012–2023. https://doi.org/10.1074/jbc.M505055200

129. Andersen, J., Olsen, L., Hansen, K. B., Taboureau, O., Jørgensen, F. S., Marie, A., … Kristensen, A. S. (2010). Mutational Mapping and Modeling of the Binding Site for (S) -Citalopram in the Human Serotonin Transporter * □, *285*(3), 2051–2063. https://doi.org/10.1074/jbc.M109.072587

130. Coleman, J. A., Yang, D., Zhao, Z., Wen, P. C., Yoshioka, C., Tajkhorshid, E., & Gouaux, E. (2019). Serotonin transporter–ibogaine complexes illuminate mechanisms of inhibition and transport. *Nature*. https://doi.org/10.1038/s41586-019-1135-1

131. Pörzgen, P., Park, S. K., Hirsh, J., Sonders, M. S., & Amara, S. G. (2001). The antidepressant-sensitive dopamine transporter in Drosophila melanogaster: a primordial carrier for catecholamines. *Molecular Pharmacology*, *59*(1), 83–95. Retrieved from http://www.ncbi.nlm.nih.gov/pubmed/11125028

132. Andersen, J., Ringsted, K. B., Bang-Andersen, B., Strømgaard, K., & Kristensen, A. S. (2015). Binding site residues control inhibitor selectivity in the human

norepinephrine transporter but not in the human dopamine transporter. *Scientific Reports*, *5*(October), 1–12. https://doi.org/10.1038/srep15650

133. Andersen, J., Stuhr-Hansen, N., Zachariassen, L., Toubro, S., Hansen, S. M. R., Eildal, J. N. N., … Stromgaard, K. (2011). Molecular determinants for selective recognition of antidepressants in the human serotonin and norepinephrine transporters. *Proceedings of the National Academy of Sciences*, *108*(29), 12137–12142. https://doi.org/10.1073/pnas.1103060108

134. Andersen, J., Ladefoged, L. K., Kristensen, T. N. B., Munro, L., Grouleff, J., Stuhr-Hansen, N., … Strømgaard, K. (2016). Interrogating the Molecular Basis for Substrate Recognition in Serotonin and Dopamine Transporters with High-Affinity Substrate-Based Bivalent Ligands. *ACS Chemical Neuroscience*, *7*(10), 1406–1417. https://doi.org/10.1021/acschemneuro.6b00164

135. Seddik, A., Geerke, D. P., Stockner, T., Holy, M., Kudlacek, O., Cozzi, N. V., … Ecker, G. F. (2017). Combined Simulation and Mutation Studies to Elucidate Selectivity of Unsubstituted Amphetamine-like Cathinones at the Dopamine Transporter. *Molecular Informatics*, *36*(5), 1–8. https://doi.org/10.1002/minf.201600094

136. Waterhouse, A., Bertoni, M., Bienert, S., Studer, G., Tauriello, G., Gumienny, R., … Schwede, T. (2018). SWISS-MODEL: Homology modelling of protein structures and complexes. *Nucleic Acids Research*, *46*(W1), W296–W303. https://doi.org/10.1093/nar/gky427

137. Singh, J., & Thornton, J. M. (1985). The interaction between phenylalanine rings in proteins. *FEBS Letters*, *191*(1), 1–6. https://doi.org/10.1016/0014-5793(85)80982-0

138. Trott, O., & Olson, A. J. (2009). AutoDock Vina: Improving the speed and accuracy of docking with a new scoring function, efficient optimization, and multithreading. *Journal of Computational Chemistry*, *31*(2), NA-NA. https://doi.org/10.1002/jcc.21334

139. Pettersen, E. F., Goddard, T. D., Huang, C. C., Couch, G. S., Greenblatt, D. M., Meng, E. C., & Ferrin, T. E. (2004). UCSF Chimera--a visualization system for exploratory research and analysis. *Journal of Computational Chemistry*, *25*(13), 1605–1612. https://doi.org/10.1002/jcc.20084